



THE HONG KONG  
POLYTECHNIC UNIVERSITY

香港理工大學

Pao Yue-kong Library

包玉剛圖書館

---

## Copyright Undertaking

This thesis is protected by copyright, with all rights reserved.

**By reading and using the thesis, the reader understands and agrees to the following terms:**

1. The reader will abide by the rules and legal ordinances governing copyright regarding the use of the thesis.
2. The reader will use the thesis for the purpose of research or private study only and not for distribution or further reproduction or any other purpose.
3. The reader agrees to indemnify and hold the University harmless from and against any loss, damage, cost, liability or expenses arising from copyright infringement or unauthorized usage.

### IMPORTANT

If you have reasons to believe that any materials in this thesis are deemed not suitable to be distributed in this form, or a copyright owner having difficulty with the material being included in our database, please contact [lbsys@polyu.edu.hk](mailto:lbsys@polyu.edu.hk) providing details. The Library will look into your claim and consider taking remedial action upon receipt of the written requests.

**OPERATIONAL STABILITY OF A DIRECT  
EXPANSION AIR CONDITIONING SYSTEM  
UNDER VARIABLE SPEED OPERATION AND  
ITS CONTROL APPLICATION**

**XIA YUDONG**

Ph.D  
The Hong Kong  
Polytechnic University  
2017

The Hong Kong Polytechnic University  
Department of Building Services Engineering

**Operational Stability of a Direct Expansion  
Air Conditioning System under Variable  
Speed Operation and its Control  
Application**

**Xia Yudong**

**A thesis submitted in partial fulfillment of the requirements  
for the degree of Doctor of Philosophy**

March 2017

## **Certificate of Originality**

I hereby declare that this thesis is my own work and that, to the best of my knowledge and belief, it reproduces no material previously published or written, nor material that has been accepted for the award of any other degree or diploma, except where due acknowledgement has been made in the text.

Xia Yudong

Department of Building Services Engineering

The Hong Kong Polytechnic University

Hong Kong SAR, China

March, 2017

## **Abstract**

In comparison to chilled water-based large-scale central air conditioning (A/C) systems, direct expansion (DX) A/C systems are simpler in configuration, more energy efficient and generally cost less to own and maintain. Therefore, for the last few decades, DX A/C systems have found increased applications in buildings, especially in small to medium-scale buildings. A DX A/C system is made up of a DX refrigeration plant and an air-distribution sub-system. In the DX refrigeration plant, there exists an expansion valve (EV)-evaporator control loop to regulate the refrigerant mass flow rate entering the evaporator in response to the degree of refrigerant superheat (DS) at the evaporator's exit. Fundamentally, a DX A/C system can be classified as a special kind of refrigeration system, and the issue of operational instability often encountered in a refrigeration system would also occur in a DX A/C system.

The issue of operational instability in a refrigeration system has been extensively studied. There have been two different views on the possible causes for the operational instability, or hunting, namely, the inherent operational characteristics of an evaporator and the operational characteristics of an EV. While hunting has been widely observed in both thermostatic expansion valve (TEV) and electronic expansion valve (EEV) controlled refrigeration systems, limited numbers of studies on investigating the operational characteristics of an EEV on the operational stability of the EEV-controlled refrigeration system may be identified.

On the other hand, the wide application of variable-speed (VS) technology has made the continuous control of compressor speed and supply fan speed in a DX A/C system more practical, paving the way for achieving simultaneous control of indoor air temperature and relative humidity (RH) using DX A/C systems. Previous extensive studies on the inherent operational characteristics of a VS DX A/C system expressed in terms of the inherent correlation between its output total cooling capacity (TCC) and equipment sensible heat ratio (E SHR) were carried out, with the issue of operational stability being ignored when both compressor speed and supply fan speed were simultaneously varied. However, hunting was actually observed in a VS DX A/C system when it was VS operated for simultaneously controlling indoor air temperature and humidity, resulting in a relatively low operational safety and high energy consumption.

Therefore, in this Thesis, a systematic study to investigate the operational stability of an EEV controlled VS DX A/C system under VS operation is reported. The Thesis, first of all, begins with presenting a theoretical and experimental study on the influences of the operational characteristics of a proportional-integral (PI) controlled EEV on the operational stability of the DX A/C system. Using the classical control theory, EEV's PI settings and time constant of EEV's temperature sensor on stability were analyzed. The theoretical analysis results using the classical control theory were further verified experimentally using an EEV-controlled experimental DX A/C system. The study results showed that a larger proportional or integral gain for the PI-controlled EEV would lead to a higher chance for the EEV-evaporator control loop to become unstable, while slowing down the rate of DS signal transfer by increasing EEV's time constant may help mitigate system instability. The study results confirmed

that the operational characteristics of an EV in a refrigeration system could impact its operational stability and further suggested an effective approach to mitigate the instability problem encountered in an EEV-controlled refrigeration system by incorporating a first-order transfer function in its EEV-evaporator control loop to slow down the rate of DS signal transfer.

Secondly, this Thesis reports a study to investigate the inherent operational characteristics of the VS DX A/C system considering its operational stability at different DS settings and inlet air states, which may be regarded as a follow-up to the previous reported studies on the inherent operational characteristics of the VS DX A/C system when the issues of instability were ignored. Using the experimental VS DX A/C system, the inherent correlations between its TCC and E SHR at different combinations of compressor speed and supply fan speed were studied, and the unstable operating points of speed combinations under different DS settings and inlet air states identified. The experimental results suggested while different DS settings may not significantly influence the inherent correlations between TCC and E SHR, but did impact the operational stability. Furthermore, VS operation and different inlet air states to the DX evaporator also influenced the operational stability. A higher compressor speed or a lower supply fan speed, and a lower inlet air temperature or RH level would lead to a higher chance to instability.

Finally, the development of a new capacity controller that is able to not only simultaneously control indoor air temperature and humidity, but also select an optimized DS setting to properly balance the operational safety and efficiency of the VS DX A/C system is reported in this Thesis. The new capacity controller was

developed by adding a control module to a previously developed capacity controller. The core of the control module was an artificial neural network (ANN) based model representing the known relationship between the inherent operational characteristics and operational stability of the VS DX A/C system. The new capacity controller was experimentally tested using the experimental VS DX A/C system. The test results showed that the hunting of the experimental DX A/C system was mitigated and a slight improvement in operational efficiency achieved when using the new capacity controller for simultaneously controlling indoor air temperature and humidity.

The study results reported in this Thesis have provided a better understanding of the operational stability of an EEV-controlled DX A/C system under VS operation. Furthermore, the study has also laid a good basis for developing capacity controllers to address the issues of operational instability for VS DX A/C systems. The outputs from this study can help improve the operational safety and energy efficiency of a VS DX A/C system when it is VS operated for achieving a better indoor thermal environment control.



## Publications Arising from the Thesis

### I. Journal Papers

- **Yudong Xia** and Shiming Deng, The influences of the operating characteristics of an Electronic Expansion Valve (EEV) on the operational stability of an EEV controlled direct expansion air conditioning system, *International Journal of Refrigeration* 69 (2016) 394–406. (Based on Chapter 5)
- **Yudong Xia**, Shiming Deng and Ming-Yin Chan, Inherent operational characteristics and operational stability of a variable speed direct expansion air conditioning system, *Applied Thermal Engineering* 113 (2017) 268-277. (Based on Chapter 6)
- **Yudong Xia**, Huaxia Yan, Shiming Deng and Ming-Yin Chan, A new capacity controller for a direct expansion air conditioning system under variable speed operation for operational safety and efficiency, *Building Services Engineering Research and Technology*, First published date: July-01-2017 (Based on Chapter 7)

## II. Conference papers

- **Xia, Yudong** and Deng, Shiming, A Modeling Study on the Operational Stability of a Variable Speed Direct Expansion Air Conditioning System. In Proceeding of: *16<sup>th</sup> International Refrigeration and Air Conditioning Conference*. Purdue University, USA, July 11-14, 2016

## **Acknowledgements**

I must express my grateful thanks to my Chief Supervisor, Dr. Shiming Deng, Professor, and my Co-Supervisor, Dr. Ming-yin Chan, Assistant Professor, both from the Department of Building Services Engineering (BSE), The Hong Kong Polytechnic University, for their readily available supervision, valuable suggestions, patient guidance, continuous help and encouragement throughout the course of the work.

My special thanks go to The Hong Kong Polytechnic University for financially supporting this project. I would like to also thank Dr. Zhao Li and Mr. Chen Wenjing for their assistance in building the experimental DX A/C system. I am also grateful to my fellow students for their supports and care over the last three years. I also want to thank the technicians in the Heating Ventilation and Air Conditioning Laboratory of the BSE Department for their supports during my experimental work.

Finally, my deepest gratitude goes to my parents, my wife Ms. Zhuang Yingtian and all other family members. I could not have completed my work without their loves and continuous support throughout my life.

# Table of Contents

	Page
<b>Certificate of Originality</b> .....	<b>I</b>
<b>Abstract</b> .....	<b>II</b>
<b>Publications Arising from the Thesis</b> .....	<b>VI</b>
<b>Acknowledgements</b> .....	<b>VIII</b>
<b>Table of Contents</b> .....	<b>IX</b>
<b>List of Figures</b> .....	<b>XIV</b>
<b>List of Tables</b> .....	<b>XIX</b>
<b>Nomenclature</b> .....	<b>XXI</b>
<b>List of Abbreviations</b> .....	<b>XXIII</b>
<b>Chapter 1 Introduction</b> .....	<b>1</b>
<b>Chapter 2 Literature Review</b> .....	<b>6</b>
2.1 Introduction.....	6
2.2 Operational stability in vapor-compression refrigeration systems .....	8
2.2.1 Operational instability in vapor-compression refrigeration systems	10
2.2.2 Possible causes for hunting in refrigeration systems.....	12
2.3 Operation and Control of DX A/C systems.....	30
2.3.1 Control and operational issues for DX A/C systems.....	31
2.3.2 Indoor thermal environment control using DX A/C system .....	42
2.3.3 Operational instability of a DX A/C system under VS operation .....	46
2.4 Conclusions.....	48

<b>Chapter 3 Proposition</b> .....	<b>51</b>
3.1 Background.....	51
3.2 Project title .....	53
3.3 Aims and objectives .....	54
3.4 Research methodologies .....	55
<b>Chapter 4 Description of the Experimental DX A/C System</b> .....	<b>57</b>
4.1 Introduction.....	57
4.2 Descriptions of the experimental system and its major components .....	57
4.2.1 The DX refrigeration plant.....	59
4.2.2 The air-distribution sub-system .....	62
4.3 Computerized instrumentation and data acquisition system .....	63
4.3.1 Sensors/measuring devices for temperatures, pressures and flow rates	
64	
4.3.2 The data acquisition system .....	66
4.4 LabVIEW logging & control supervisory program.....	66
4.5 Conventional control loops in the experimental VS DX A/C system.....	68
4.6 Summary.....	69
<b>Chapter 5 The influences of the operational characteristics of the EEV on the</b>	
<b>operational stability of the EEV-controlled experimental DX A/C</b>	
<b>system</b> .....	<b>71</b>
5.1 Introduction.....	71
5.2 The PI controlled EEV-evaporator control loop in the experimental DX	
A/C system .....	73

5.3	Development of a transfer function for the EEV-evaporator control loop.....	74
5.3.1	Transfer function for each of the four components in the EEV-evaporator control loop.....	76
5.3.2	Identification of transfer function parameters.....	80
5.4	Stability analysis for the EEV-evaporator control loop using the Frequency Response Method .....	83
5.4.1	Nyquist stability criterion .....	84
5.5	Experimental validation .....	91
5.5.1	The influences of EEV's PI settings on the stability of the EEV-evaporator control loop.....	93
5.5.2	The influences of the time constants of EEV's temperature sensor on the stability of the EEV-evaporator control loop .....	95
5.6	Discussions .....	96
5.7	Conclusion.....	98

**Chapter 6 Inherent operational characteristics and operational stability of the experimental VS DX A/C system ..... 100**

6.1	Introduction.....	100
6.2	Experimental conditions, procedures and data interpretation .....	101
6.3	Experimental results.....	105
6.3.1	Experimental results of Case T-25 at 8 °C DS setting .....	107
6.3.2	The ICs_os of the experimental VS DX A/C system at different DS settings .....	110

6.3.3	The IC_os of the experimental VS DX A/C system at different inlet air states .....	112
6.4	Discussions .....	114
6.4.1	The influences of different DS settings on the operation stability of the experimental VS DX A/C system .....	115
6.4.2	The influences of different speed combinations and inlet air states on the operational stability of the experimental VS DX A/C system .....	116
6.5	Conclusions .....	119

**Chapter 7 Development of a new capacity controller for the experimental DX A/C system under VS operation for operational safety and efficiency**

	.....	<b>121</b>
7.1	Introduction .....	121
7.2	Overview of the new capacity controller .....	122
7.3	Development of the DS setting establishment (DSE) module .....	124
7.4	Controllability tests .....	130
7.4.1	Experimental conditions .....	130
7.4.2	Experimental results .....	131
7.5	Discussions .....	139
7.6	Conclusions .....	140

**Chapter 8 Conclusions and Future Work .....** **142**

8.1	Conclusions .....	142
8.2	Proposed future work .....	145

<b>Appendix</b>	.....	<b>148</b>
<b>References</b>	.....	<b>153</b>



## List of Figures

	<b>Page</b>
<b>Chapter 2</b>	
Fig. 2.1	Schematic diagram of a vapor compression refrigeration system 8
Fig. 2.2	Schematic diagrams of the two typical EVs (a) TEV; (b) EEV 10
Fig. 2.3	Hunting observed in a TEV controlled refrigeration system. (a) TEV-bulb pressure, (b) evaporating pressure, (c) pressure differential, (d) refrigerant flow rate [Mithraratne and Wijesundera, 2002] 12
Fig. 2.4	Regions in a horizontal evaporator 13
Fig. 2.5	A typical MSS line proposed by Huelle [1972] 17
Fig. 2.6	The modified MSS line proposed by Chen et al. [Chen et al., 2008] 18
Fig. 2.7	Flow boiling process in an evaporator [Shang et al., 2015] 20
Fig. 2.8	DS responses to a step change in valve's opening at different initial operating DS [Otten, 2010] 25
Fig. 2.9	Nonlinearity of an EEV: (a) Mass flow vs. valve position, and (b) Step responses for low and high flows [Elliott et al., 2010] 28
Fig. 2.10	The variations in TCC and E SHR at different combinations of compressor and supply fan speeds [Li and Deng, 2007c] 39
Fig. 2.11	The IC between TCC and E SHR at different speed combinations of compressor and supply fan for a VS DX A/C system [Xu et al., 2010] 41

Fig. 2.12	The hunting in a VS DX A/C system when both of compressor and supply fan were VS operated for simultaneously controlling indoor air temperature and humidity [Qi et al., 2010a]	47
-----------	---	----

#### **Chapter 4**

Fig. 4.1	Schematic diagram of the DX refrigeration plant	58
Fig. 4.2	Schematic diagram of the complete experimental	59
Fig. 4.3	The details of the DX air cooling and dehumidifying coil used in the experimental DX A/C system	60

#### **Chapter 5**

Fig. 5.1	Schematic diagram of the PI controlled EEV-evaporator control loop in the experimental DX A/C system	73
Fig. 5.2	Block diagram of the PI controlled EEV-evaporator control loop	74
Fig. 5.3	Schematic diagram of the installation of EEV's temperature sensor attached to the refrigerant pipe at evaporator exit and its equivalent thermal circuit	79
Fig. 5.4	The comparison between the predicted and experimental responses for the $DS_m$	83
Fig. 5.5	Nyquist diagrams for $L(s)$ at two different groups of EEV's PI settings	87
Fig. 5.6	Nyquist diagrams for $L'(s)$ at three different groups of time constants of EEV's temperature sensor	91

Fig. 5.7	Block diagram of the PI controlled EEV-evaporator control loop after incorporating $H3(s)$	92
Fig. 5.8	Experimental validation results for the study cases I-1 and I-2	93
Fig. 5.9	Experimental validation results for the study cases II-3 and II-4	94
Fig. 5.10	Experimental validation results for the study cases IV-3, IV-4 and IV-5	95
<b>Chapter 6</b>		
Fig. 6.1	The IC <sub>os</sub> of the experimental VS DX A/C system for Case T-25 at 8 °C DS setting	107
Fig. 6.2	The measured variations in the operating DS after increasing only the compressor speed in Case T-25 and 8 °C DS setting	109
Fig. 6.3	The measured variation in the operating DS after changing only the fan speed in Case T-25 and 8 °C DS setting	109
Fig. 6.4	The ICs <sub>os</sub> of the experimental VS DX A/C system for Case T-25 at three different DS settings	110
Fig. 6.5	The measured variations in the operating DS following a change in the DS setting at an operating point of C80F60 in Case T-25	112
Fig. 6.6	The ICs <sub>os</sub> of the experimental VS DX A/C system for the constant RH group at 8 °C DS setting	112
Fig. 6.7	The ICs <sub>os</sub> of the experimental VS DX A/C system for the constant temperature group at 8 °C DS setting	113

Fig. 6.8	MSS line proposed by Huelle [1972]	115
Fig. 6.9	The evaporator gains at different evaporating temperatures for the experimental VS DX A/C system	118
 <b>Chapter 7</b>		
Fig. 7.1	A schematic diagram of the new capacity controller for the experimental VS DX A/C system	122
Fig. 7.2	The configuration of the DSE module	125
Fig. 7.3	Structure of the selected 5-10-1 network for the ANN based model of the ICs <sub>os</sub>	126
Fig. 7.4	Flowchart of the DSE module for establishing an optimized DS setting	129
Fig. 7.5	Measured variations in the operating parameters in the Test I under the previous capacity controller (a) Temperatures and speeds variations; (b) DS and EEV's opening variations	133
Fig. 7.6	Measured variations in the operating parameters in the Test I under the new capacity controller (a) Temperatures and speeds variations; (b) DS and EEV's opening variations	134
Fig. 7.7	Comparison of the measured DS under both controllers in Test I	135
Fig. 7.8	Comparison of the COP under both controllers in Test I	135
Fig. 7.9	Measured variations in the operating parameters in Test II under the previous capacity controller (a) Temperatures and speeds variations; (b) DS and EEV's opening variations	137

Fig. 7.10	Measured variations in the operating parameters in Test II under the new capacity controller. (a) Temperatures and speeds variations; (b) DS and EEV's opening variations	138
Fig. 7.11	Comparison of the measured DS under both controllers in Test II	139
Fig. 7.12	Comparison of the COP under both controllers in Test II	139

### **Appendix**

Photo 1	Conditioned spaces	148
Photo 2	Control console	148
Photo 3	Air-distribution sub-system	149
Photo 4	DX evaporator in air-distribution sub-system	149
Photo 5	DX refrigeration plant	150
Photo 6	The EEV in the DX refrigeration plant	150
Photo 7	Load generation unit	151
Photo 8	Air sampling device	151
Photo 9	Logging & control supervisory program	152

## List of Tables

	<b>Page</b>
<b>Chapter 4</b>	
Table 4.1 Geometric parameters of the	61
Table 4.2 Details of the VS rotary compressor	62
Table 4.3 Details of the experimental EEV	62
Table 4.4 Details of the VS supply fan	63
<b>Chapter 5</b>	
Table 5.1 Specifications of EEV's temperature sensor used in the experimental DX A/C system	81
Table 5.2 The stability of the EEV-evaporator control loop at two different groups of EEV's PI settings	86
Table 5.3 The stability of the EEV-evaporator control loop at three different groups of time constant of EEV's temperature sensor	89
<b>Chapter 6</b>	
Table 6.1 Measurement/calculation uncertainty of system operating parameters	102
Table 6.2 The experimental cases of inlet air states and DS settings	103
Table 6.3 The experimental compressor and supply fan speeds	103

## Chapter 7

Table 7.1	Measurement/calculation uncertainty of system operating parameters	131
-----------	--	-----

## Nomenclature

Variable	Description	Unit
$e$	relative error	—
$C_p$	specific heat	kJ/kg K
$DS$	degree of refrigerant superheat	°C
$h_a$	air enthalpy	kJ/kg
$K_e$	evaporator gain	°C h/kg
$K_p$	proportional gain	—
$K_i$	integral gain	—
$M_{re}$	refrigerant mass flow rate	kg/h
$M_a$	mass flow rate of air through the evaporator	kg/s
$Q_s$	sensible cooling capacity	kW
$R$	thermal resistance	K/kW
$R_c$	correlation coefficient	—
$R_{DS}$	degree of superheat setting	°C
$T$	temperature	°C
$T_e$	evaporating temperature	°C
$T_i$	integral time	s
$T_{db}$	air dry-bulb temperature	°C
$T_{wb}$	air wet-bulb temperature	°C
$u_e$	EEV control signal	—
$u_c$	compressor speed	%
$u_f$	supply fan speed	%
$V$	volume	m <sup>3</sup>



$S$	operational stability index	—
$t$	target output set	—
$p$	predicted output set	—

### Greek Letters

$\rho$	density	kg /m <sup>3</sup>
$\theta$	time delay	s
$\tau$	time constant	s
$\phi_0$	offset adjustment parameter for a particular EEV	—

### Subscripts

a	air side
e	evaporator
m	measured by the temperature sensor
i	inlet
o	outlet
re	refrigerant side
s	sensible
se	sensor
v	valve

## List of Abbreviations

A/C	air conditioning
ANN	artificial neural network
A SHR	application sensible heat ratio
COP	coefficient of performance
DS	degree of refrigerant superheat
DX	direct expansion
DSE	DS setting establishment
EV	Expansion valve
EEV	electronic expansion valve
E SHR	equipment sensible heat ratio
HVAC	heating, ventilation and air conditioning
IC	inherent correlation
IC_os	inherent correlation considering the operational stability
LGU	load generation unit
MIMO	multiple-input multiple-output
RMSE	root mean square error
RTD	resistance temperature device
PD	proportional-derivative
PI	proportional-integral
PID	proportional-integral-derivative
PFC	PD law based fuzzy logic controller
SPM	self-programming module
TCC	total cooling capacity

TEV	thermostatic expansion valve
RH	relative humidity
VS	variable speed
VSD	variable-speed drive

# Chapter 1

## Introduction

Direct expansion (DX) air conditioning (A/C) has been widely used in small- to medium-scaled buildings. A DX A/C system consists of a DX refrigeration plant and an air-distribution sub-system. The DX refrigeration plant is mainly composed of a DX evaporator, a condenser, an expansion valve (EV) and a compressor. The evaporator in the DX refrigeration plant acts as a DX air cooling coil in the air-distribution sub-system to simultaneously cool and dehumidify the air passing through the coil. The conditioned air is then supplied to a conditioned space through the air distribution sub-system by a supply fan.

In such a vapor-compression refrigeration system, thermostatic expansion valves (TEVs) and electronic expansion valves (EEVs) are two of the most widely used EVs for regulating the refrigerant mass flow rate entering an evaporator in response to the degree of refrigerant superheat (DS) at the evaporator exit. On the other hand, instability in a refrigeration system, conventionally known as hunting, is the phenomena of the oscillation of certain system operational parameters such as DS, refrigerant mass flow rate and evaporating pressure. Hunting has been noticed in not only the refrigeration systems controlled by TEVs, but also those controlled by EEVs. Hunting leads to a lower operational safety, and a higher energy consumption of a refrigeration system, and thus should be avoided as far as possible. There have been two different views on the possible causes for hunting. The first concentrated on the operational characteristics of an EV, as it would take some time for the DS signal to propagate through the EV to adjust the refrigerant mass flow required, which was

considered as the fundamental reason for hunting. The other however tried to explain the causes for hunting based on the inherent operational characteristics of an evaporator. However, there has been no verdict of which view would reflect truly what leads to hunting in a refrigeration system. Moreover, while the hunting in those EEV-controlled refrigeration systems has been widely studied, limited numbers of investigations on studying the influences of the operational characteristics of an EEV on the operational stability of EEV-controlled refrigeration systems may be identified.

With the introduction of variable speed (VS) technology to DX A/C systems, both compressor and supply air fan in a DX A/C system can be simultaneously varied, offering tremendous opportunities for improving indoor thermal control and energy efficiency when using DX A/C systems. For a DX A/C system under VS operation, varying its compressor and supply fan speeds influences its output sensible and latent cooling capacities, which can be regarded as the inherent operational characteristics of a VS DX A/C system. While the inherent operational characteristics of a VS DX A/C system expressed in terms of the inherent correlations between its total cooling capacity (TCC) and equipment sensible heat ratio (E SHR) were extensively studied previously, the issues of operational instability were ignored in these previous studies where the DX A/C system was VS operated at different inlet air states. However, previous studies showed that when an EEV-controlled DX A/C system was VS operated for simultaneous control over indoor air temperature and humidity, its operating DS may fluctuate at certain operating points.

Therefore, it becomes necessary to study the influences of the operational characteristics of an EEV on the operational stability of an EEV controlled DX A/C

system, and to further investigate the inherent operational characteristics of a DX A/C system considering its operational stability when it is VS operated for simultaneously controlling indoor air temperature and humidity.

This Thesis begins in Chapter 2 with a detailed literature review on the various issues related to the operational stability and control of a DX A/C system. The review on the two different views on the possible causes for hunting in a refrigeration system, i.e., the inherent operational characteristics of an evaporator and the operational characteristics of an EV, is firstly presented. This is followed by reviewing various issues related to the operation and control of DX A/C systems, including capacity control, indoor humidity control, inherent operational characteristics of a VS DX A/C system and indoor thermal environment control using DX A/C systems. The issues of operational instability problem identified in a DX A/C system when VS operated are discussed. Finally, the identified further necessary research project on studying the operational stability in an EEV-controlled VS DX A/C system under VS operation is presented.

Chapter 3 presents the research proposal, which covers the background, project title, objectives and research methodologies deployed for the research project reported in this Thesis.

In Chapter 4, descriptions of an available experimental EEV-controlled VS DX A/C system to facilitate the research project reported in this Thesis are presented. Firstly, the experimental VS DX A/C system and its major components are described in detail. This is followed by introducing the computerized measuring devices and a data

acquisition system. Finally, a computer supervisory program used to operate and control the experimental VS DX A/C system is detailed. The availability of the experimental system is expected to be essential in successfully carrying out the research project proposed in Chapter 3.

Chapter 5 reports on a theoretical and experimental study on the influences of the operational characteristics of a proportional-integral (PI) controlled EEV on the operational stability of an EEV-controlled DX A/C system. Using the classical control theory, the influences of both EEV's PI settings and time constant of EEV's temperature sensor on system stability were analyzed. The theoretical analysis results using the classical control theory were further verified experimentally using the experimental EEV-controlled DX A/C system and the experimental results are presented.

In Chapter 6, a follow-up study on the inherent operational characteristics of the experimental VS DX A/C system considering its operational stability at i) different combinations of compressor and supply fan speeds, ii) different DS settings and iii) different inlet air states, is reported. Using the experimental VS DX A/C system, the inherent correlations between its output total cooling capacity (TCC) and equipment sensible heat ratio (E SHR) at different combinations of compressor speed and supply fan speed were studied and the unstable operating points of speed combinations under different DS settings and inlet air states identified. The experimental results suggested while different DS settings may not significantly influence the inherent correlations between TCC and E SHR, but did impact the operational stability. VS operation and different inlet air states to the DX evaporator also influenced the operational stability.

Chapter 7 reports the development of a new capacity controller for the experimental VS DX A/C system that is able to not only simultaneously control indoor air temperature and humidity, but also select an optimized DS setting to properly balance the operational safety and energy efficiency. The new capacity controller was developed by adding a control module to a previously developed capacity controller. The core of the control module was an artificial neural network (ANN) based model representing the known relationship between the inherent operational characteristics and operational stability of the experimental VS DX A/C system obtained in Chapter 6. The new capacity controller was experimentally tested using the experimental VS DX A/C system. The test results showed that the hunting of the experimental DX A/C system was mitigated and a slight improvement in operational efficiency achieved when using the new capacity controller for simultaneously controlling indoor air temperature and humidity.

Finally, the conclusions of this Thesis and the proposed future work are presented in Chapter 8.



## **Chapter 2**

### **Literature Review**

#### **2.1 Introduction**

Air conditioning (A/C) systems are widely used in buildings for indoor thermal environment control, and thus the energy consumption for A/C takes a large share of the total energy use in buildings. A close look at the US energy consumption shows that approximately 40% of all the energy used in the US was by heating, ventilation and air conditioning (HVAC) and refrigeration systems in 2011 [USDOE, 2012]. In China, energy consumption in buildings increased by about 10% every year for the past 20 years since 1984 [Yao and Chen, 2010] and comprised about 19.12% of the total national energy usage by the year 2014 [CABEE, 2016]. In Europe, around 40% of the total energy consumption was by commercial and residential buildings [Balaras et al., 2007]. In Hong Kong, the energy use for space A/C and refrigeration accounted for 36% of the total electricity use in 2013 [EMSD, 2015]. On the other hand, in small- to medium-scale buildings, direct expansion (DX) A/C systems are commonly used due to their advantages of simple configuration, high energy efficiency and low cost to own and maintain [Bansal, 2015; Zhang, 2002]. For example, in Hong Kong, the annual total sale of DX residential air conditioners was around 400,000 units in 2000 [Zhang, 2002]. In the US, packaged rooftop DX A/C systems accounted for approximately 60% of the total installed cooling capacity in commercial buildings [Brodrick and Gilbride, 2002]. Therefore, it is very important to improve the operational efficiency of DX A/C systems to contribute to both environmental protection and sustainable development.

The operational instability, or hunting, and its consequence of a lower operational safety and a higher energy consumption have been widely noticed in both TEV [Eames et al., 2014; Huang et al., 2014; Wedekind, 1971; Wedekind and Stoecker, 1968; Yasuda et al., 1983] and EEV [Chen et al., 2008; Fallahsohi et al., 2010; Li et al., 2004; Qi et al., 2010b] controlled refrigeration systems. As a vapor-compression refrigeration system, the operational instability was also observed in DX A/C systems [Chen, 2005; Chen et al., 2008]. Furthermore, while the extensive application of VS technique to DX A/C systems has made the continuous control of compressor speed and supply air fan speed more practical, paving the way to simultaneously control indoor air temperature and humidity, VS operation of a DX A/C system may also potentially lead to its operational instability. A previous study [Qi et al., 2010a] showed that when a DX A/C system was VS operated at different inlet air states, the operating DS regulated by a conventional proportional-integral-derivative (PID) controlled EEV would experience fluctuation, leading to the operational instability, or hunting, of the VS DX A/C system. Therefore, for ensuring a safe and efficient operation of an EEV-controlled VS DX A/C system, an investigation on its operational stability should be carried out.

This Chapter presents a critical literature review on various issues related to the operational stability and control of DX A/C systems. An introduction to hunting is presented firstly. Secondly, an extensive review on the possible causes for hunting in refrigeration systems is reported, covering the inherent operational characteristics of an evaporator and the operational characteristics of an EV. This is followed by reviewing the issues related to the operation and control of DX A/C systems, i.e.,

capacity control, indoor humidity control and the inherent operational characteristics of a DX A/C system, the indoor thermal environment control using DX A/C systems and the instability problem encountered in a VS DX A/C system. Finally, the conclusions of the literature review are presented.

## 2.2 Operational stability in vapor-compression refrigeration systems

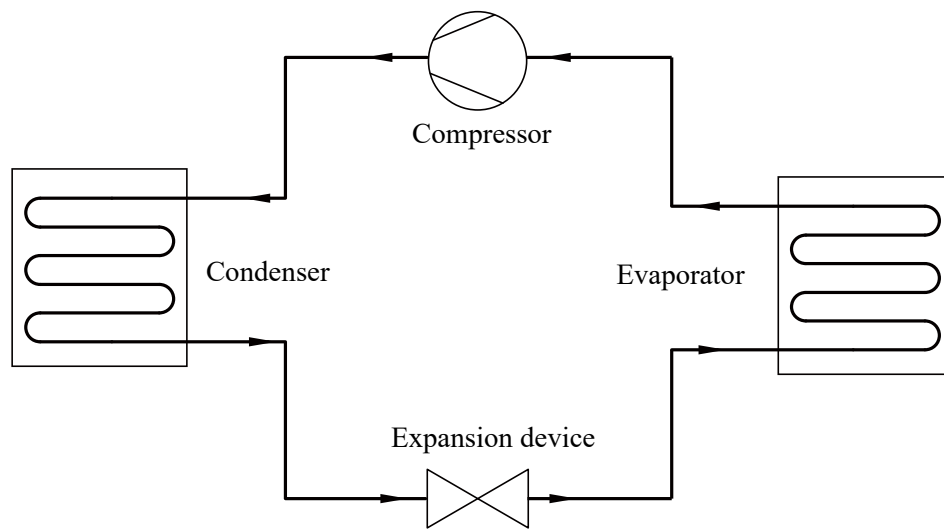


Fig. 2.1 Schematic diagram of a vapor compression refrigeration system

A DX A/C system is operated based on a vapor-compression refrigeration cycle. As schematically shown in Fig. 2.1, there are four key components in a vapor-compression refrigeration cycle: a compressor, an evaporator, a condenser and an expansion device. In a vapor-compression refrigeration system, its evaporator is used directly as a cooling coil to cool the air or water passing through it. There are usually two heat transfer regions in an evaporator, namely, a two-phase region and a superheated region. The heat transfer coefficient between the refrigerant and the evaporator walls in the two-phase region is much higher than that in the superheated region, and thus the heat transfer taking place in the two-phase region is responsible

for almost all of the cooling capacity of the entire evaporator. Therefore, to maximize the effectiveness of an evaporator, its two-phase region should ideally occupy most of the evaporator. However, if the two-phase region gets near to the exit of the evaporator, liquid refrigerant might enter the suction line and damage the compressor. Therefore, the refrigerant mass flow entering an evaporator should be well controlled, so as to ensure safe and reliable operation of the compressor while providing the maximum amount of cooling capacity.

In vapor-compression refrigeration systems, TEVs and EEVs are extensively used for regulating the refrigerant mass flow rate entering an evaporator by changing their valves' opening in response to the DS at the evaporator exit. As shown in Fig. 2.2(a), a TEV utilizes a sensing bulb filled with the same refrigerant as that used in the refrigeration system and clamped to the evaporator exit to detect the refrigerant temperature there. The pressure inside this bulb is the refrigerant saturation pressure corresponding to refrigerant temperature at the evaporator exit. Therefore, based on a force balance among the refrigerant pressure at the evaporator exit, the refrigerant pressure inside the sensing bulb, and an adjustable spring force, the TEV's opening can be accordingly regulated to achieve a controlled refrigerant flow rate entering the evaporator for maintain the required DS setting. Furthermore, as schematically shown in Fig. 2.2(b), an EEV utilizes a temperature sensor and a pressure transducer to respectively measure the refrigerant temperature at the evaporator exit and evaporating pressure to evaluate the DS using a pre-programmed microprocessor controller. EEV's opening will then be regulated by a stepper motor in response to a feedback control signal of the evaluated DS for controlling the refrigerant mass flow rate entering the evaporator. Such an expansion valve (EV)-evaporator loop is an important loop in a

vapor-compression refrigeration system, and its operating performance directly influence the key system operating parameters, i.e., refrigerant mass flow rate, operating DS and evaporating temperature, as well as the system operational stability.

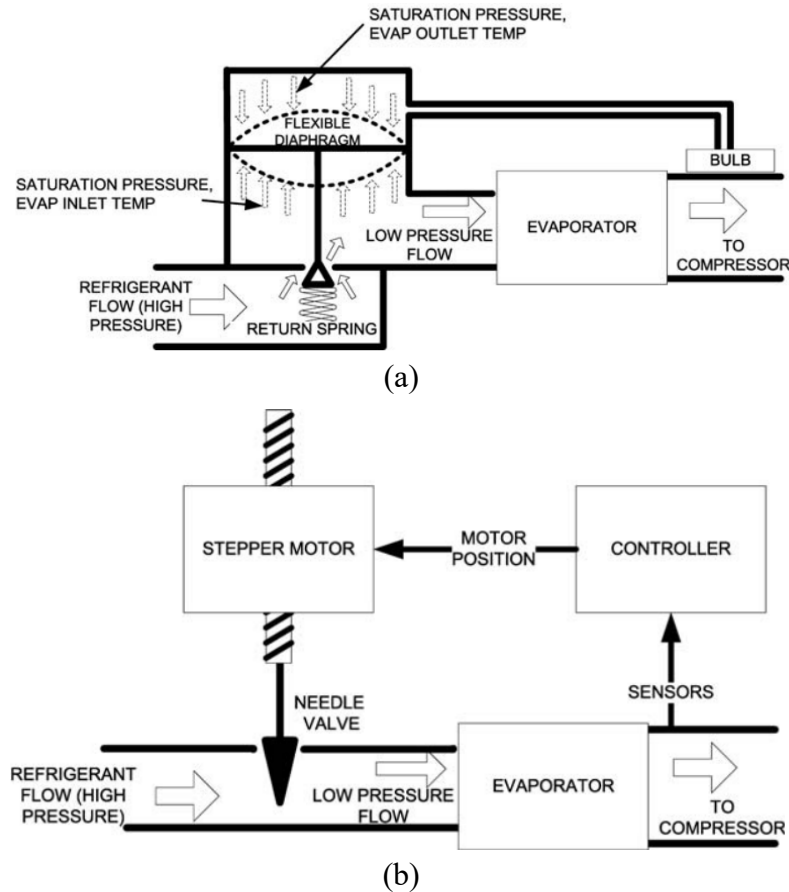


Fig. 2.2 Schematic diagrams of the two typical EVs (a) TEV; (b) EEV

### 2.2.1 Operational instability in vapor-compression refrigeration systems

In a vapor-compression refrigeration system, its EV-evaporator control loop may be underdamped and even unstable after being subject to certain operating disturbances, causing the oscillation of key system operating parameters, such as operating DS, refrigerant mass flow rate and evaporating pressure, leading consequently to an

unstable operation of the refrigeration system. This phenomenon in a refrigeration system has been conventionally known as hunting. Hunting has been widely noticed in the refrigeration systems controlled by either TEVs [Eames et al., 2014; Huang et al., 2007; Huang et al., 2014; Wedekind, 1971; Wedekind and Stoecker, 1968; Yasuda et al., 1983], or EEVs [Chen et al., 2008; Fallahsohi et al., 2010; Li et al., 2004; Qi et al., 2010b]. Fig. 2.3 shows the phenomenon of hunting observed in a TEV controlled refrigeration system. As seen, when hunting occurred, key operating parameters, i.e., (b) evaporating pressure and (d) refrigerant mass flow rate, would fluctuate. For ensuring a safe operation of a vapor-compression refrigeration system, its refrigerant mass flow rate supplied to its evaporator should be well regulated, otherwise liquid refrigerant may enter the suction line and damage the compressor. However, when hunting occurs in a refrigeration system, the fluctuation of the refrigerant flow inside the evaporator may cause the liquid refrigerant to enter the compressor, consequently leading to the failure of the entire refrigeration system [Lenger et al., 1998]. In addition, the oscillation of system operating parameters caused by hunting would cause the frequent opening and closing of an EV, and thus result in a shorter EV's lifespan, negatively affecting the system operational safety [Mithraratne and Wijesundera, 2001; Mithraratne et al., 2000]. Furthermore, the oscillation in the operating DS caused by hunting would also lead to the corresponding fluctuation in compressor suction temperature, resulting in a higher system energy consumption. Therefore, hunting would result in a lower operational safety and a higher energy consumption of the system, and should be avoided as far as possible.

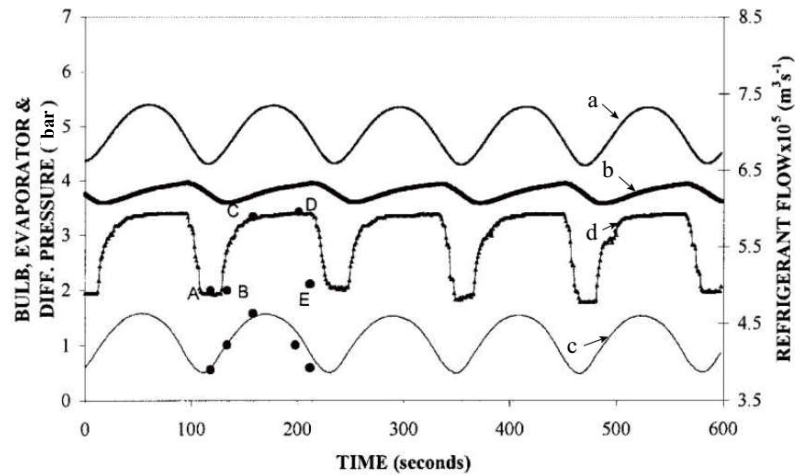


Fig. 2.3 Hunting observed in a TEV controlled refrigeration system. (a) TEV-bulb pressure, (b) evaporating pressure, (c) pressure differential, (d) refrigerant flow rate

[Mithraratne and Wijeyesundera, 2002]

### 2.2.2 Possible causes for hunting in refrigeration systems

Hunting has been studied for decades. There have been two different views on the possible causes for hunting in open literatures. The first concentrated on the inherent operational characteristics of an evaporator, such as the random fluctuation in a refrigerant mixture-vapor transition point and the variation in heat transfer mechanism. The second view however tried to explain the causes of hunting based on the inherent operational characteristics of an EV, as it would take some time for the DS signal to propagate through the EV to adjust the refrigerant mass flow required, which was considered as the fundamental reason for hunting. In this Section, a detailed review on the two views for explaining the possible causes for hunting is presented.

### 2.2.2.1 *Inherent operational characteristics of an evaporator*

Three different phenomena, namely, the random fluctuation in a refrigerant mixture-vapor transition point, variation in heat transfer mechanism and evaporator superheat nonlinearity, have been widely observed and regarded as the inherent operational characteristics of an evaporator, which may be used to explain the hunting in refrigeration systems.

#### *(a) Random oscillation in refrigerant mixture-vapor transient point in an evaporator*

In a vapor-compression refrigeration system, an evaporator where vaporization takes place can normally be divided into two distinct regions, i.e., a two-phase region and a superheated region, as shown in Fig. 2.4. The mixture-vapor transition point refers to the boundary between these the two regions.

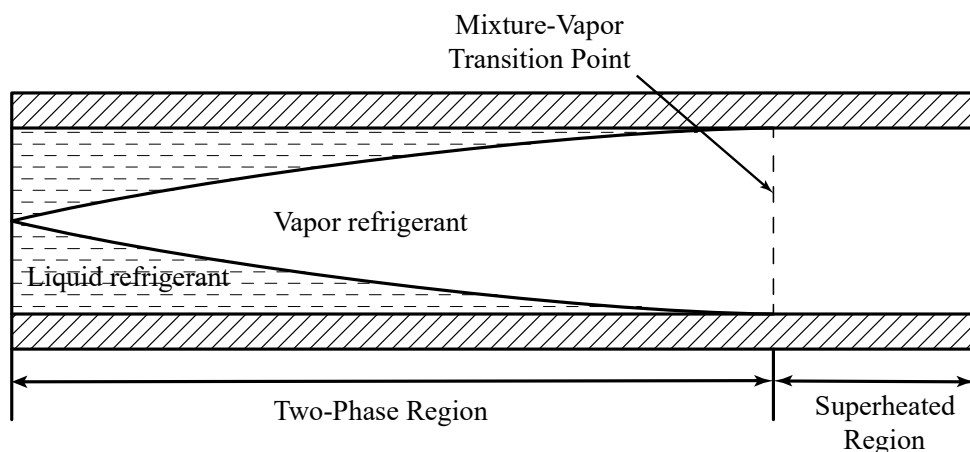


Fig. 2.4 Regions in a horizontal evaporator

Zahn [1964] may be the first one in open literatures who observed the random oscillation of mixture-vapor transition point in an evaporator. He visually inspected



the flow patterns of R-22 when it was vaporized inside a horizontal tube. It was found that the character of the two-phase flow inside the horizontal tube was unsteady with varying rates of fluctuations even through the total refrigerant mass flow rate was held steady. Different pressure, temperature, flow and heat load conditions were set for simulating an actual operation condition of a small cooling coil. Two-phase flow instability in the evaporator was discussed based on his visual observations.

Wedekind [1965] noticed the same phenomenon when investigating transients in fully evaporating refrigerant flow. He used a 30-foot long heated glass tube to record where the refrigerant was last vaporized and how the mixture-vapor transient point moved over time. The results showed that even when a system was operated at steady-state inlet conditions, the length of the two-phase region was continuously fluctuating, with a magnitude of up to 10% of the total flow length. The liquid slugs being formed upstream and propagating down inside the evaporator were used to explain this phenomenon [Wedekind, 1971]. Wedekind [1971] thought the causes for this phenomenon were related to the same mechanisms that caused density-wave instabilities. On a statistical basis, Wedekind and Beck [1974] found that the standard deviation of the mixture-vapor transition point from its mean value was affected by the heat flux and the inlet flow quality. An increase in the heat flux or inlet flow quality would cause a decrease in the standard deviation of the transition point from its mean value.

A modeling study was carried out by Gruhle and Isermann [1985] to study the random oscillation of the mixture-vapor transient point in an evaporator. An evaporator model was established based on a distributed parameter process approximated by several

lumped parameter modules. The dynamic behaviors of the evaporator were examined using this model. According to the modeling study results, it was believed that the random behavior of the transition point was due to the non-linear behavior of the heat transfer coefficient in the location where the quality was near unity. Based on this assumption, even at steady-state inlet conditions, the oscillations of the mixture-vapor transition point in the evaporator at a frequency of 5 Hz could be predicted. However, no detailed discussions on the influences of this random oscillation on the operational stability of the evaporator were presented.

A refrigeration system consisting of a manual EV, an air-cooled condenser, a reciprocating compressor and a water-cooled evaporator was developed by Mithraratne and Wijesundera [2001] to investigate the characteristics of the mixture-vapor transition point oscillations in its evaporator. The random oscillations of the mixture-vapor transition point were recorded using a high-speed camera. It was found that these oscillations were correlated with the fluctuations in the DS at evaporator exit, which may eventually cause the hunting of the system.

Liang et al. [2011] also built up a refrigeration system with a horizontal straight tube evaporator to further study the effects of the random oscillations of the mixture-vapor transition point on two-phase flow instability. Three types of dynamic instabilities including the density-wave instability, pressure drop instability and thermal instability were found under certain operational conditions. Different characteristics of the three types of dynamic instabilities were concluded based on experimental results. It was found that the oscillation caused by the density-wave instability took place at almost

all the mass velocities and had the smallest oscillation periods and the lowest oscillation amplitude in comparison to that caused by the other two types of instability.

In order to illustrate the influences of the random oscillations of mixture-vapor point in an evaporator on the operational stability of a TEV-controlled refrigeration system, Huelle [1967] proposed a so-called minimal-stable-signal (MSS), defined as a critical minimal DS at which a refrigeration system could exhibit unstable operation. It was observed that hunting often occurred when a low DS was set. This was explained by Huelle that, for a given evaporator, the mixture-vapor transition point would move to near evaporator exit and the DS would decrease with an increase in the refrigerant flow rate at the evaporator inlet. The refrigerant supply and EV-evaporator control loop would be stable when the transition point fluctuated within the evaporator. However, when the transition point moved to near the evaporator outlet as the DS was decreased, its fluctuation would cause a corresponding fluctuation in tube wall temperature at evaporator exit, and thus the detected DS, consequently leading to system hunting. Therefore, at a given output cooling capacity, there existed a minimum degree of superheat to ensure a stable system operation. Later, Huelle [1972] introduced a so-called MSS line to demonstrate the operational stability of a TEV-controlled refrigeration system at different cooling loads and operating DS. A typical MSS line is shown in Fig. 2.5. As seen, it was a monotone conic curve starting from the original point on a DS (X-axis) – cooling capacity (Y-axis) chart, and at a specified cooling capacity, there existed a minimal DS to separate a stable operation region from an unstable one. The minimal DS increased as increasing the output cooling capacity of a TEV-controlled refrigeration system. Huelle considered that the MSS line for a specified refrigeration system was determined by the inherent operational

characteristics of its evaporator. Considering the extensive use of VS compressor and EEV nowadays, the MSS line theory was further revised by Chen et al. [2008] when experimentally studying the operational stability of an EEV-controlled refrigeration system having a VS compressor. The experiment results showed that there also existed a MSS in an EEV-controlled refrigeration system. A new modified MSS line, as shown in Fig. 2.6 having a maximum MSS value and a minimal MSS value was proposed to distinguish a stable and an unstable working regions under different output cooling capacities. They also believed the causes for hunting were part of system's inherent characteristics.

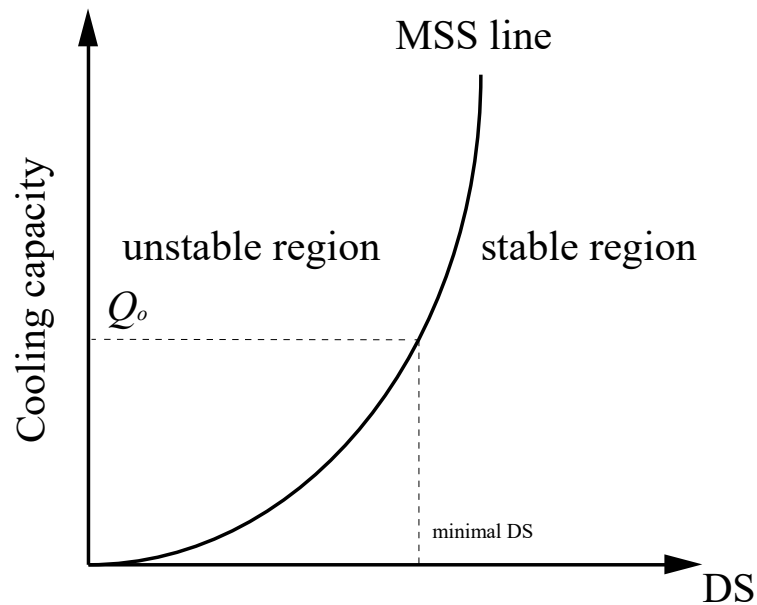


Fig. 2.5 A typical MSS line proposed by Huelle [1972]

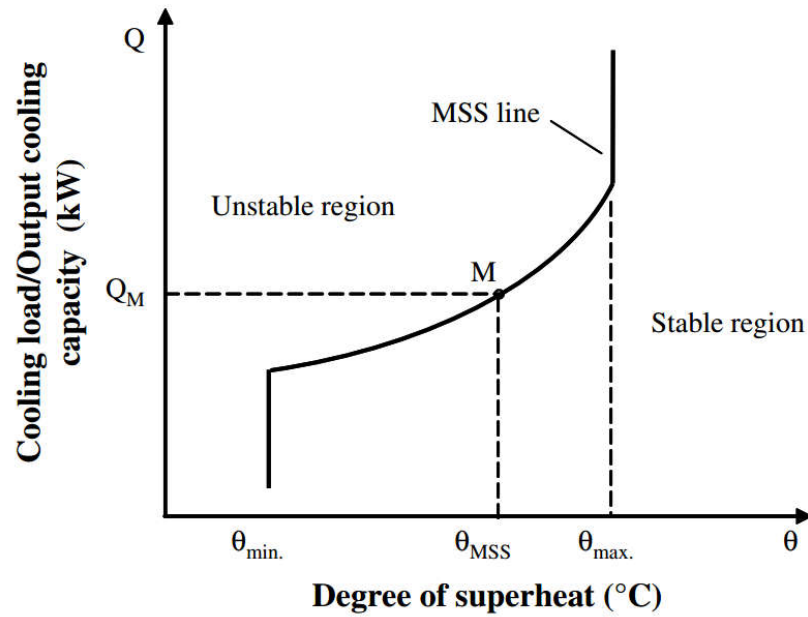


Fig. 2.6 The modified MSS line proposed by Chen et al. [Chen et al., 2008]

*(b) Variation in heat transfer mechanism in an evaporator*

The variation in heat transfer mechanism in an evaporator as the operating DS was decreased at evaporator exit may lead to a sudden decrease in heat transfer coefficient between the refrigerant inside the evaporator and the tube wall, thus causing the flooding of the evaporator, resulting in a sudden decrease in operating DS.

Yasuda et al. [1983] developed a mathematical model for a TEV-controlled refrigeration system to study the transient response of its evaporator. For the sake of simplification, a lumped parameter sub-model was used to describe the refrigerant flow in the two-phase region in the evaporator, but a distributed parameter sub-model that in the superheated region. Transient behaviors of the evaporator following positive and negative step changes in the static superheat settings of the TEV were experimentally examined for validating the model. System hunting could be well

predicted by switching the refrigerant side heat transfer coefficient when the operating DS became lower than 5K, suggesting that a sudden change in heat transfer coefficient in an evaporator may eventually lead to hunting.

A sudden decrease in operating DS was observed by Chen et al. [2002] when studying the minimum stable superheat of an evaporator. It was found for the first time that, although the opening of EV was not changed in experimentation, the operating DS decreased suddenly when it was descended to below a certain value, due to the nonlinear variation of heat transfer coefficient along the evaporator. Nucleation hysteresis [Bergles et al., 1981; Daninowa and Beliski, 1962] was used to explain this phenomenon. When the temperature difference between evaporator tube wall and the refrigerant inside the evaporator can no longer maintain refrigerant nucleate boiling, the nucleate boiling would disappear, leading to a deterioration of heat transfer in the evaporator, and consequently a sudden decrease in the operating DS. Therefore, a large difference in heat transfer coefficient between convection and nucleate boiling would make a DS controller malfunction, leading to potential system hunting.

Shang et al. [2015] also considered that the disappearance of the nucleate boiling causing a decrease in the operating DS at evaporator exit was the main reason for causing the hunting in a refrigeration system. A critical heat flux for nucleate boiling [Steiner and Taborek, 1992] was introduced to a state-space dynamic model to decide when the nucleate boiling would disappear [Shang et al., 2016]. A flow boiling process shown in Fig. 2.7 was introduced to demonstrate the variation in heat transfer mechanism in an evaporator. Generally, conditions for the onset of nucleate boiling were satisfied, nucleate and convective boiling coefficients were superimposed.

However, when heat flux was lower than the critical heat flux for nucleate boiling, the liquid refrigerant was vaporized by convective boiling mechanism at a smaller heat transfer coefficient as shown in Fig. 2.7. Based on this assumption, the dynamic behaviors of the oscillation in system's operating parameters were simulated successfully.

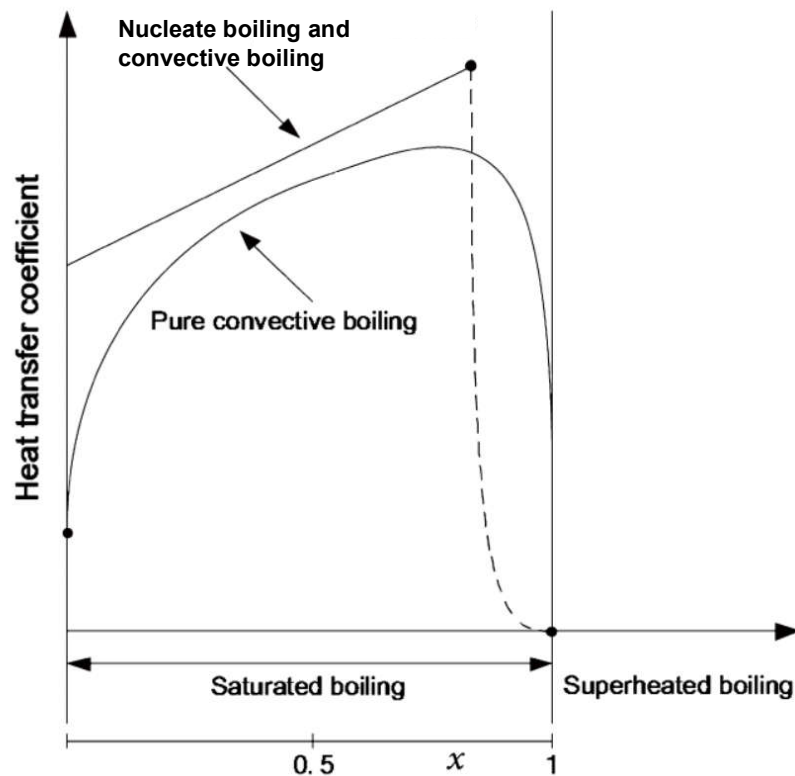


Fig. 2.7 Flow boiling process in an evaporator [Shang et al., 2015]

(c) *Superheat nonlinearity of an evaporator*

The superheat nonlinearity of an evaporator is a further observed phenomenon that can be used for explaining system hunting. When an evaporator is subject to a same disturbance but at different operational conditions, the responses for operating DS at evaporator exit may exhibit nonlinear characteristics, as expressed in terms of different

system gains, transport lags or time constants. Consequently, when the evaporator in a refrigeration system is controlled by a TEV or an EEV, the EV-evaporator control loop may be underdamped or even unstable after experiencing sudden disturbances, thus leading to the instability of the refrigeration system. Therefore, classical control theory and dynamic modeling of an evaporator using transfer function, lumped parameter or distributed parameter models, have been frequently used to study the evaporator superheat nonlinearity and its influences on the operational stability of a refrigeration system.

Stoecker [1966] may be the first investigator in open literatures to study the operational stability of EV-evaporator control loop using classical control theory. A Bode plot method was used to examine the operational stability of an EV-evaporator control loop. The superheat nonlinearity expressed in terms of transport lag and time constants was examined. There were two observations. Firstly, an increase in the transport lag would reduce the system stability. Secondly, the time constant reflecting the thermal capacity of the sensing bulb also impacted the system stability. A time constant of either smaller than 5 seconds or greater than 2 minutes would ensure a stable loop. Broersen and Vanderjagt [1980] used an open-loop transfer function for modeling a TEV-controlled dry evaporator in a refrigeration system. A single-input single-output feedback for regulating refrigerant mass flow rate and the operating DS was used to study its operational stability. Using frequency-domain analysis, the operational stability of the refrigeration system under different operating conditions was examined. It was found that a larger refrigerant mass flow rate supplied to the evaporator would lead to a smaller phase margin, and thus a higher chance to instability. Hence, increasing the operating DS would help decrease chance for



instability, but at the expense of losing output cooling capacity due to reduced refrigerant mass flow rate supplied to the evaporator. A mathematic model for the dynamically distributed parameters of an evaporator and a TEV was derived by Chen and Jiang [1990] to establish the transfer function of a TEV-evaporator control loop. The root locus method was utilized to analyze the operational stability of the control loop. It was found that increasing the evaporating temperature or the heat transfer coefficient in the superheated region would help mitigate system hunting.

Grald and Macarthur [1992] used a lumped parameter approach to model an evaporator. A so-called moving-boundary refrigerant model was proposed to predict the position of the two-phase/vapor interface, or the mixture-vapor transient point. The modeling results showed that the DS would respond faster to a step decrease in the refrigerant flow rate than it would to a step increase due to the nonlinear characteristics of the evaporator. A lumped parameter approach was also adopted by Ibrahim [1998] for modeling a TEV-controlled evaporator to analyze its operational stability under different partial load conditions. The modeling results suggested that there existed a critical time constant for an evaporator, below which the system can be operated in a stable manner. It was found this critical time constant was decreased when decreasing partial load ratio and increased when increasing the contact thermal resistance between the TEV's sensing bulb and the refrigerant pipeline, and the two-phase region heat transfer coefficient. Ibrahim [2001] later used this model to study the dynamic behaviors of a refrigeration system with a TEV-controlled evaporator when it was subject to sudden changes in inlet water temperature and mass flow rate. It was found that the system was more likely to be unstable at a low partial load ratio. Tahat et al. [2001] further incorporated an evaporator's time-constant equation into this model for

describing the time-dependent behaviors of a refrigeration system. It was found that a step decrease in the inlet water temperature would increase the evaporator time constant, which might cause instability. However, all these results were based on simulation, no experimental validation were carried out.

Jia et al. [1995] developed a distributed parameter model for predicting the transient performance of an evaporator. The model was capable of predicting the distributions of the refrigerant velocity, void fraction and temperature, tube wall temperature, air temperature and humidity, in both position and time domains. The dynamic behaviors of the evaporator were then investigated following a step change in the inlet refrigerant mass flow rate. From the modeling results, it was observed that the evaporator thermal response was faster following a step decrease than that following a step increase in refrigerant flow rate, which agreed with the results of Grald and Macarthur's two-zone model [Grald and Macarthur, 1992]. A distributed dynamic model was also established by Mithraratne et al. [2000] to simulate the transient behaviors of a counter-flow water cooling evaporator controlled by a TEV in a vapor compression refrigeration system. The liquid-vapor slip in the two-phase region of the evaporator was accounted for by a void fraction module. The model was experimentally validated. Based on the simulation and experimental results, Mithraratne and Wijesundera [2001] found that the approximate time constants of the evaporator following a step increase in the refrigerant flow and a step decrease in the water flow rate were significantly larger than those following the same changes in the opposite direction due to the nonlinear characteristics of the evaporator.

On the other hand, in practical control applications, the transient response for the operating DS at evaporator exit to a sudden change in refrigerant mass flow rate supplied to the evaporator can be approximately modeled by a first-order plus dead time model [Aprea and Renno, 2001; Beghi and Cecchinato, 2009; Beghi et al., 2011; Maia et al., 2014; Maia et al., 2013; Outtagarts et al., 1997; Yang et al., 2011a; Yang et al., 2011b], which can be expressed as the following transfer function:

$$G_e(s) = K_e \frac{1}{1 + \tau s} e^{-\theta s} \quad (2.1)$$

where  $K_e$  is the evaporator gain, defined as a ratio of the variation of DS from one steady-state to another to that of the refrigerant mass flow rate supplied. The time delay, or transport lag,  $\theta$ , represents the time between the change of input (mass flow rate) and the corresponding change of output (DS).  $\tau$  denotes the time constant of the response for the DS.

However, due to the nonlinear characteristics of an evaporator, such transient responses to the same input may be different, as reflected by different identified parameters in a first-order plus dead time model, when the evaporator was operated at different operational conditions. It was previously shown that the operating DS had a significant impact on these identified parameters [Otten, 2010]. As shown in Fig. 2.8, a larger value of time delay, evaporator gain, and time constant would be resulted in when a refrigeration system was operated at a lower operating DS. Moreover, a number of reported studies showed that the evaporator gain was increased with a decrease in evaporating temperature or an increase in compressor speed [Aprea and Renno, 2001; Maia et al., 2014; Maia et al., 2013; Outtagarts et al., 1997] and the time

constant was increased with a decrease in evaporating temperature [Maia et al., 2014; Maia et al., 2013]. Therefore, it became clear that hunting may occur in a conventional TEV-controlled refrigeration system or PI /PID based EEV-controlled refrigeration system when it was operated at different operational conditions.

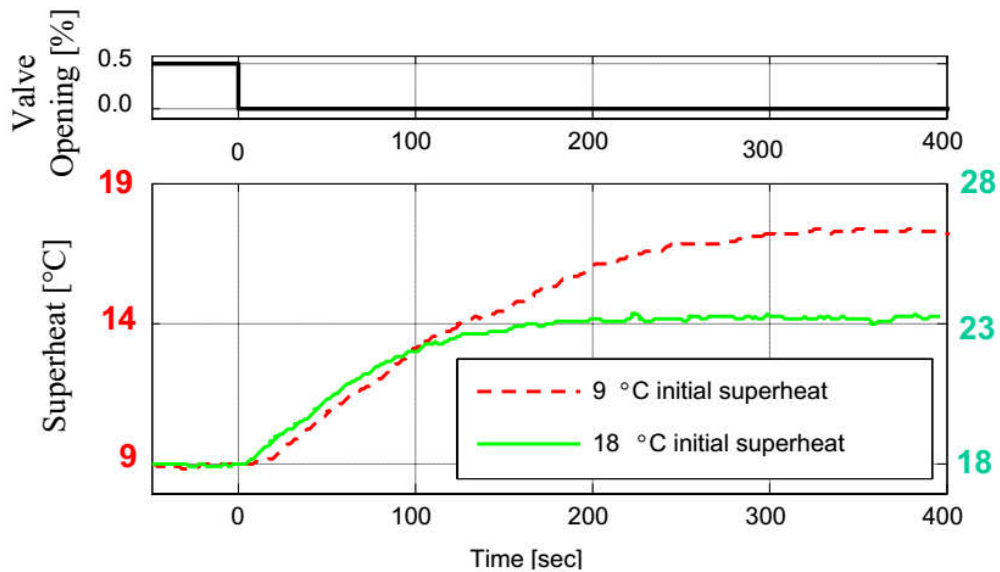


Fig. 2.8 DS responses to a step change in valve's opening at different initial operating DS [Otten, 2010]

#### 2.2.2.2 Operational characteristics of an EV

The second view on the possible causes for hunting in refrigeration systems attempted to establish the causes based on the operational characteristics of an EV.

For those TEV-controlled refrigeration systems, it has been shown that a TEV's configuration and the characteristics of its sensing bulb significantly affected the operational stability. Dhar [1978] developed a model for a window type air conditioner to understand its transients during normal operation. Simulation was conducted for

studying the transient response of its TEV at different valve gains. It was found that the TEV would become unstable at a larger gain and it took a longer time for the valve to reach a stable operating condition at a lower gain. Tassou and Al-Nizari [1993a] investigated the effects of refrigerant flow control on the steady-state and transient performances of refrigeration systems to establish a basis for EV design and control criteria development on the energy efficiency of the system. The results indicated that a high valve gain reduced the on/off cycling losses but resulted in the oscillation of operating DS at steady-state conditions. Low valve gain, on the other hand, increased the cycling losses but improved the operational stability at steady-state conditions. Lenger et al. [1998] developed a mathematic model of a TEV that took into account the pressure forces on the diaphragm as well as the pressure drop across the orifice when predicting the refrigerant mass flow rate. The simulation results showed that, for a TEV, decreasing its orifice area /diaphragm area or increasing its initial spring force would help increase the operational stability of the TEV-controlled refrigeration system. In addition, Mithraratne and Wijesundera also pointed out that increasing static superheat setting would also be beneficial to system operational stability, but the presence of even a small amount of hysteresis in the TEV was able to bring about system hunting [Mithraratne and Wijesundera, 2001, 2002; Mithraratne et al., 2000]. In addition, Eames et al. [2014] concluded that oversizing a TEV would cause system hunting, because it would cause the evaporator controlled to be alternately over and under-fed with liquid refrigerant.

Furthermore, the characteristics of a TEV's sensing bulb would affect the operational stability of a TEV-controlled refrigeration system, as it directly affected the transfer time for the DS signal to propagate through the TEV to adjust the refrigerant mass

flow required, which was considered as the fundamental reason for hunting. For modeling the dynamics of a TEV's sensing bulb, a third order differential equation was proposed by Broersen and Vanderjagt [1980]. The theoretical analysis results indicated that slowing down the bulb transients by increasing the thermal resistance between the bulb and the evaporator wall could be utilized for preventing hunting. De Bruijn et al. [1979] further concluded that either increasing or decreasing the thermal resistance could reduce hunting. This was because either increasing or decreasing the thermal resistance between the bulb and evaporator wall would lead to a larger phase margin of the TEV-evaporator control loop, thus a lower chance to instability [Broersen and Vanderjagt, 1980]. Same conclusions were also suggested in a number of related studies [Chen and Jiang, 1990; Ibrahim, 1998, 2001; Karajgikar et al., 2005; Kulkarni et al., 2003; Kulkarni et al., 2002; Lenger et al., 1998; Mithraratne and Wijesundera, 2001, 2002; Mithraratne et al., 2000; Mulay et al., 2005]. In addition, it was previously shown that the operational stability of a TEV-controlled system was sensitive to the location of the sensing bulb [Kulkarni et al., 2002; Lakhkar et al., 2003] and its incorrect positioning would cause system hunting [Eames et al., 2014; Mulay et al., 2005].

On the aspect of the operational characteristics of an EEV, it was previously shown that the nonlinearities of an EEV would affect the operational stability of the EEV-controlled refrigeration systems [Elliott and Rasmussen, 2010; Elliott et al., 2010; Singhal and Salsbury, 2007]. An inspection of refrigerant mass flow as a function of valve position for a typical EEV revealed a nonlinear relationship, as shown in Fig. 2.9. As seen, a step change of the same magnitude in EEV's opening at a lower valve position would lead to a larger variation in refrigerant mass flow, and thus a larger

variation in the operating DS at the evaporator exit, as shown in Fig. 2.9(b). Consequently, such a nonlinearity would cause inadequate superheat control and even system hunting. This illustrated why a gain scheduling approach was frequently used for superheat control. When adopting the gain scheduling approach to reduce the effect of superheat nonlinearities, the relationship between the refrigerant mass flow rate and valve position for a certain EEV should be obtained. Therefore, based on the known relationship, the control settings could be automatically adjusted for ensuring the control performance as the variation in valve position.

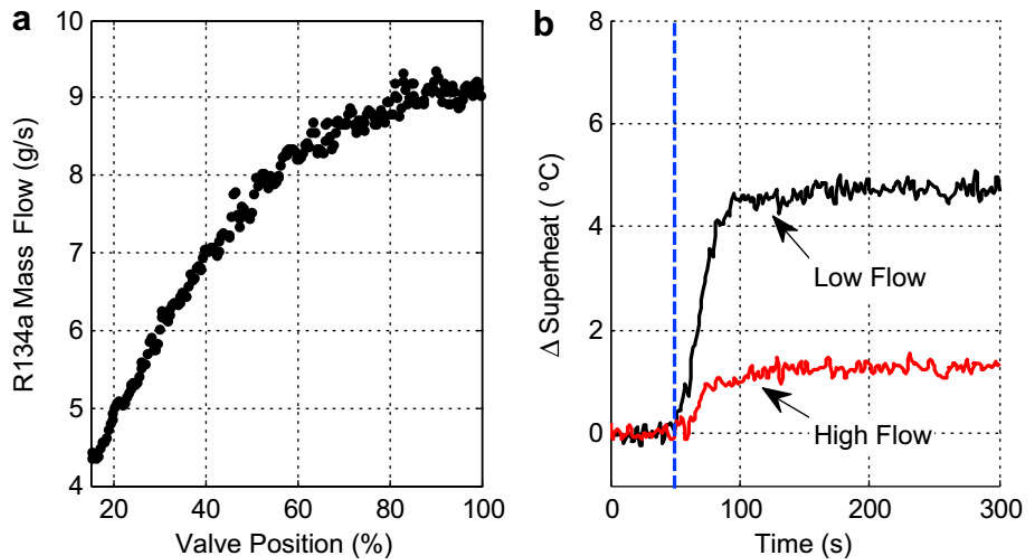


Fig. 2.9 Nonlinearity of an EEV: (a) Mass flow vs. valve position, and (b) Step responses for low and high flows [Elliott et al., 2010]

### 2.2.2.3 Other possible causes for hunting

In addition to these possible causes for hunting as mentioned above, other related studies also suggested that pressure oscillations at compressor suction [Lenger et al., 1998], water flow mal-distribution in a two-circuit double-pipe evaporator [Huang et

al., 2014], frosting on evaporator surfaces in a heat pump [Huang et al., 2007] and the mismatching of certain components in the entire refrigeration system, e.g. oversizing of an EV [Eames et al., 2014; Schoen, 1990] would potentially lead to system instability. Tian et al. also concluded that the two-phase flow at a throttling device inlet or at evaporator outlet was the necessary but not sufficient condition for system hunting following an investigation on the hunting in a TEV-controlled automotive air conditioning system with a variable displacement compressor [Tian et al., 2005a, b; Tian and Li, 2005].

From the detailed review on the possible causes for hunting, it was clear that most reported studies were carried out based on TEV-controlled refrigeration systems, but only limited numbers of studies on investigating the effects of the operational characteristics of an EEV on the operational stability of EEV-controlled refrigeration systems may be identified. A recent review on instability in refrigeration systems also concluded that the research on the operational stability for variable capacity refrigeration systems equipped with EEVs was much less seen than those with TEVs, and thus more efforts should be made [Liang et al., 2010]. As far as the operational characteristics of an EEV is concerned, the dynamics of its temperature sensor should also influence the operational stability of an EEV-controlled refrigeration system, as it directly affects the rate of the DS signal transfer through the EEV to regulate the refrigerant mass flow rate passing through it. However, no previous studies in open literatures on investigating the dynamics of EEV's temperature sensor on the operational stability of an EEV-controlled refrigeration system may be identified.



### **2.3 Operation and Control of DX A/C systems**

A DX A/C system as a special type of vapor-compression refrigeration system is mainly composed of a DX evaporator, a condenser, an EV and a compressor and usually provides basic air conditioning functions including air distribution, fresh air induction, filtration, and cooling/heating of the conditioned air. The evaporator in its refrigeration plant is of DX type and is used directly as a cooling coil to simultaneously cool and dehumidify the air passing through it. A DX A/C system may also include air-distribution ductwork which is conventionally known as central DX A/C system. This distinguishes itself from a residential small-size window-type or split-type air conditioner. Meanwhile, a DX A/C system makes use of its evaporator to handle directly the conditioned air. This again distinguishes itself from a conventional central chilled-water based A/C system where chilled water is used in a cooling coil for cooling and dehumidifying. DX A/C systems vary in size from 1.5 to over 100 tons of cooling capacity, and are dominated by the systems having the cooling capacity below 10 tons. These smaller DX systems accounted for about 50% of the total installed DX cooling capacity in the US [Kenneth 1997 and Jabobs 2002].

DX A/C systems are extensively used in buildings, especially in small-to medium-scale buildings. One of the most important control objectives for an A/C system is to maintain the required air temperature and/or humidity in a conditioned space served by the A/C system. Generally, if A/C systems were operated at constant loads, no control would be needed. However, most A/C systems are designed to meet the demands under the worst conditions, namely, at the highest or lowest outdoor air temperatures. Therefore, for most of time, the A/C systems are operated at part-load

condition. Consequently, all A/C systems need to be appropriately controlled to output different cooling capacities to cope with the varying cooling loads in the conditioned space so as to maintain the indoor air temperature and/or humidity required.

### **2.3.1 Control and operational issues for DX A/C systems**

In this section, two specific issues related to the control of DX A/C systems, i.e., capacity control and indoor air humidity control, as well as the studies on investigating the inherent operational characteristics of a VS DX A/C system, are extensively reviewed.

#### *2.3.1.1 Capacity control*

Thermal loads in building always vary with time. Therefore, in order to continuously adjust its output capacity to match the varying building loads, certain capacity control schemes should be adopted to a DX A/C system. In open literatures, various capacity control schemes have been applied to a DX A/C system to regulate its output cooling capacity, which will be reviewed as follows.

Firstly, the most frequently used capacity control scheme in small sized residential DX A/C systems is intermittent running of compressor, namely, on-off cycling [Ilic et al., 2002; Poort and Bullard, 2006; Tassou and Al-Nizari, 1993b; Vargas and Parise, 1995]. When a compressor of a DX A/C system is on-off cycled, the indoor air temperature in the conditioned space can be controlled within a preset range. However, due to the frequent on-off cycling, it may impose wear and tear on the compressor,

and consequently leading to a lower lifespan of the compressor. Moreover, due to the inherent characteristics of this control scheme, it is also difficult to maintain a steady indoor air temperature as it always fluctuates within the preset range.

Secondly, other capacity control schemes including suction-gas throttling [Tso et al., 2001], hot-gas bypass [Yaqub and Zubair, 1996; Yaqub et al., 1995] and cylinder-unloading [Fallahsohi et al., 2010] were also extensively used in DX A/C systems for regulate their output cooling capacities. For suction gas throttling, the suction gas is throttled before entering a compressor. Due to the throttling effect, a larger specific volume will be resulted in, and thus leading to a corresponding decrease in refrigerant mass flow rate being circulated. Consequently, the cooling capacity can be reduced. With respect to hot-gas bypass control scheme, the refrigerant is bypassed from compressor and injected back into the suction line to decrease the refrigerant mass flow rate being circulated. Through regulating the refrigerant mass flow rate bypassed, the output cooling capacity could be modulated. For the cylinder-unloading control scheme, the cooling capacity is reduced by unloading one or more cylinders so as to decrease the refrigerant mass flow rate being circulated. Yaqub and Zubair [2001] carried out a numerical study on investigating the above three capacity control schemes for HFC-134a refrigeration systems. The study results showed that a higher coefficient of performance (COP) was achieved when using the cylinder-unloading control scheme in comparison to that using the other two control schemes. However, the output cooling capacity only can be reduced by about 25%, 50% or 75% of the total cooling capacity for a 4-cylinder compressor. On the other hand, hot-gas bypass scheme resulted in the lowest COP among these three control schemes, and thus it was not suitable from the thermodynamic point of view. Furthermore, due to the restriction

of a very high compressor discharge temperature, the output cooling capacity could be reduced by up to around 50% when using the hot-gas bypass scheme. In addition, the suction-gas throttling control scheme gave an accurate control over indoor air temperature and humidity and its COP was at between those by the other two schemes. Furthermore, under this control scheme, compressor discharge temperature was the lowest, and it was possible to achieve a wide range of cooling capacity reduction by varying the degree of throttling at compressor inlet.

Finally, capacity control may be achieved by using VS compressors to vary the refrigerant mass flow rate being circulated in DX A/C systems. It was previously shown that with the wide application of VS compressors and EEVs to variable refrigerant volume (VRV) A/C systems, the refrigerant flow rate can be regulated precisely and hence system's cooling capacity, making possible the accurate matching between output cooling capacity and varying thermal load [Aprea et al., 2006; Aprea and Renno, 2004; Domijan and Embriz-Santander, 1993; Qureshi and Tassou, 1996]. It was previously showed that the output cooling capacity from a residential split-type DX A/C system could be varied between 50 and 100% of its total cooling capacity in proportion to the change in indoor air temperature by regulating its compressor speed [Yamamoto et al., 1982]. Currently, the advancement of VS compressor and EEV technologies has made inverter-aided DX A/C systems possible to vary their output cooling capacities between 20% and 100% of their total output cooling capacity. On the other hand, for a conventional DX A/C system controlled by a single speed compressor, its energy performance was degraded dramatically at part load condition [Silver et al., 1990]. However, when a DX A/C system was variable compressor speed controlled, a potential improvement in energy efficiency of a DX A/C system may be

achieved during part load conditions. This was because when using VS compressors for capacity control, the condensing and evaporating pressures/temperatures would respectively decrease and increase as decreasing its compressor speed, leading to a corresponding increase in COP [Scalabrin and Bianco, 1994]. A study on investigating the energy performance of an inverter-driven VS A/C system used in a hot and humid region was carried out by Yang and Lee [1991]. The study results indicated that an annual energy saving of 20% could be achieved when using a VS compressor for capacity control as compared to that using a constant speed compressor. In addition, the pull-down time for a DX A/C system to reach an indoor air temperature setting during start-up can be also reduced as its compressor can be operated initially at the highest speed to output the maximum cooling capacity. Consequently, A/C systems would operate with a higher energy efficiency at part load conditions, due to the reduced frictional losses in, and the reduced pressure ratio imposed on, the compressor, leading to a higher energy saving on a seasonal basis.

#### *2.3.1.2 Indoor humidity control*

In buildings served by A/C systems, it is very important to maintain indoor humidity at an appropriate level as it directly affects the occupants' thermal comfort and indoor air quality [Arens and Baughman, 1996; Baughman and Arens, 1996; Berglund, 1998; Sterling et al., 1985]. It has been recommended that the suitable range for indoor relative humidity should be between 30% and 60%, and the upper limit be set at 60% RH [ASHRAE, 2000]. Various studies have been carried out on investigating the influences of different indoor humidity levels on indoor air quality and human thermal comfort [Armstrong and Liaw, 2002; De Dear et al., 1989; Miro, 2005; Tanabe and

Kimura, 1994]. These reported studies showed that occupants' thermal comfort was directly and indirectly impacted by the indoor air relative humidity levels in different ways. For example, a high level of indoor air relative humidity may result in health problems for occupants due to the growth of contaminated aerosols produced by spray humidification systems [Arens and Baughman, 1996]. On the other hand, a low relative humidity level also impacts occupants' comfort and health since it can lead to the drying of skin and mucous surfaces, promoting the accumulation of electrostatic charges in fabric and others materials in buildings [Berglund, 1998; Green, 1982].

However, in most residential and commercial buildings, humidity control has been found to be inadequate and unsatisfactory. The conventional principal method for indoor humidity control used in large central HVAC systems is to overcool air to remove more moisture and then to reheat it to a suitable supply air temperature. This method is inherently costly and inefficient since a great deal of energy is required to overcool air and then to reheat it. However, with respect to DX A/C systems used in small-to medium-scaled buildings, reheating is uncommon, and thus the issue of indoor humidity control is often encountered in spaces served by DX A/C systems. In a DX A/C system, dehumidification is less straightforward since moisture removal only takes place when the air passing through its cooling coil, which is strongly affected by the condensation occurred. The cooling coil also plays an important role in temperature control. Therefore, this dual role of cooling and dehumidification for the cooling coil makes the controlled variables of temperature and humidity to become coupled. Furthermore, the current trend in designing a DX A/C system is to have a smaller moisture removal capacity, in an attempt to boost its energy-efficiency rating and COP [Kittler, 1996]. One of the frequently used methods to improve the energy

efficiency of a DX A/C system is to increase the heat exchanger surface area. However, while a higher energy efficiency of a DX A/C system could be achieved, a lower latent cooling capacity would also be resulted in as the system is operated at a higher evaporating temperature and a lower condensing temperature. Moreover, when a DX A/C system is operated at part load conditions, indoor humidity control could become worse with on-off cycling its compressor. This was because the system would remove the sensible load with very little run-time to easily satisfy the thermostat set point and cycle off long before moisture removal can be affected [Hourahan, 2004]. Consequently, indoor RH would rise to above the design level [Shirey III and Henderson Jr, 2004].

A number of studies have been carried out on developing control strategies for removing the high indoor air moisture during part-load conditions. A comparative study was carried out by Chua et al. [2007] to investigating the performances of three control strategies for indoor air humidity control using large central chilled water based A/C systems, namely, chilled water flow control, bypass air control and variable air volume control. Simulation results showed that the use of chilled water flow control strategy resulted in the highest indoor humidity throughout the range of outdoor air conditions and the use of bypass air control strategy could provide an acceptable humidity over a wide range of load conditions at most of the time. While a relatively low and acceptable indoor air humidity could be maintained when using variable air volume control strategy, there also existed two distinct disadvantages that influenced occupants' thermal comfort, namely, the problem of stuffiness and stillness of air in a space and the unsatisfactory ventilation rate due to the reduced supply air flow rate during part-load operations.

Other enhanced dehumidification technologies have also been applied to DX A/C systems, including solid desiccant-based technology [Harriman et al., 2001; Harriman et al., 1999; Nagaya et al., 2006], liquid desiccant-based technology [Bouzenada et al., 2016; Dai et al., 2001; Dieckmann et al., 2008; Yuan and Riffat, 2010], heat pipe technology [Elgendy, 1993; Yau, 2007], separate sensible and latent cooling technology [Ling et al., 2010] and dual-path systems that pre-treat ventilation air, etc. A comparative study was carried out by Kosar [2006] to evaluate the performances of a conventional DX A/C system with three enhanced dehumidification components, i.e., a wraparound heat pipe heat exchanger, a desiccant dehumidifier in a wraparound configuration and a post-coil desiccant dehumidifier regenerated by using condenser waste heat. With respect to the first enhanced dehumidification component, the heat pipe wrapped itself around a DX cooling coil. Its evaporator was used as a pre-cooler to precool the incoming air and the condenser as a reheating coil to reheat the exiting air. This process lowered the dew-point temperature of the air leaving the cooling coil and shifted some coil cooling capacity from sensible to latent effect. The study results showed that these integrated systems provided the ability to increase the moisture removal capacity, resulting in a lower SHR levels for DX A/C systems to cope with higher latent load conditions.

Generally, the selection of a humidity control method may depend on the application of HVAC systems, which includes the load characteristics, operating conditions and system constraints. For example, in a lightly populated small office, thermal loads are mainly dominated by envelope heat gains. With a light occupancy, a small ventilation rate is required, and thus using a conventional DX A/C system could meet the cooling



and dehumidification loads in most climates. By contrast, a large lecture hall may have few windows and a very high ventilation demand, resulting in a large dehumidification load relative to sensible cooling load. In such an application, it may make sense to directly condition the ventilation air or use desiccant dehumidification technology.

### *2.3.1.3 Inherent operational characteristics for a VS DX A/C system*

In order to achieve a better thermal comfort in a conditioned space served by A/C systems, it is critically important to maintain both the indoor air temperature and humidity within a suitable range. While DX A/C systems have been widely used in small-to medium-scaled buildings, most DX A/C systems are equipped with single speed compressors and on-off controlled, resulting in a poor indoor humidity control performance. With the introduction of variable-frequency inverters to DX A/C systems, both the compressor and supply fan speeds can be varied, making it possible to simultaneous control indoor air temperature and humidity, as the variation in compressor and supply fan speeds will lead to the corresponding changes in the output sensible and latent cooling capacities of the DX A/C systems [Krakow et al., 1995b].

When studying the characteristics of space cooling load and the ability to cool and dehumidify air for an A/C system, sensible heat ratio (SHR) is an important parameter. There are two different but related SHRs, Equipment SHR (E SHR) and Application SHR (A SHR). The former is defined as the ratio of the output sensible cooling capacity to the total cooling capacity (TCC), the latter the ratio of the space sensible cooling load to the total space cooling load. For an air conditioned space served by a DX A/C system, to maintain the indoor air temperature and humidity, not only the

matching between the TCC and the space cooling load should be required, but also between E SHR of the DX A/C system and A SHR of the conditioned space [Li and Deng, 2007c]. Therefore, in order to achieve simultaneous control over indoor air temperature and humidity using a DX A/C system, the relationships between the output TCC and E SHR at various speed combinations of compressor and supply fan, or the inherent operational characteristics of a VS DX A/C system, have been extensively studied.

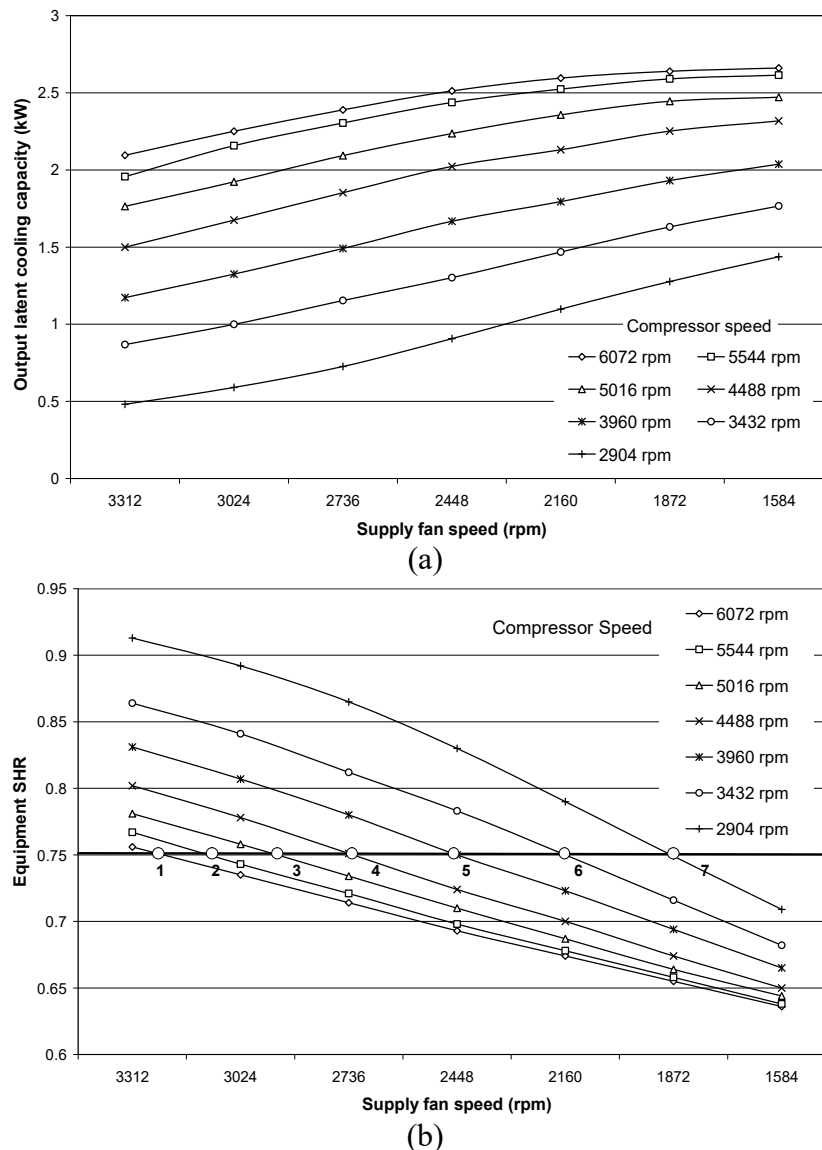


Fig. 2.10 The variations in TCC and E SHR at different combinations of compressor and supply fan speeds [Li and Deng, 2007c]

The operational characteristics of a DX A/C system under VS operation were firstly studied by Li and Deng [2007c]. The experimental results of the variations in TCC and E SHR at different combinations of compressor and supply fan speeds are shown in Fig. 2.10. As seen, the output TCC from the DX A/C system was predominately affected by changing compressor speed, although at a given compressor speed, reducing supply fan speed would also reduce, but less significantly, the output TCC. On the other hand, at higher compressor speed, further increasing compressor speed would not significantly increase the output TCC, as compared to the increases at the lower compressor speeds. In addition, at a given compressor speed, although there were not significant changes in the output TCC with varying supply fan speed, there were significant changes in the ratio between the sensible and latent components of the output TCC, with a lower supply fan speed or smaller air-flow rate leading to a larger latent heat removal, thus a lower E SHR, as shown in Fig. 2.10(b).

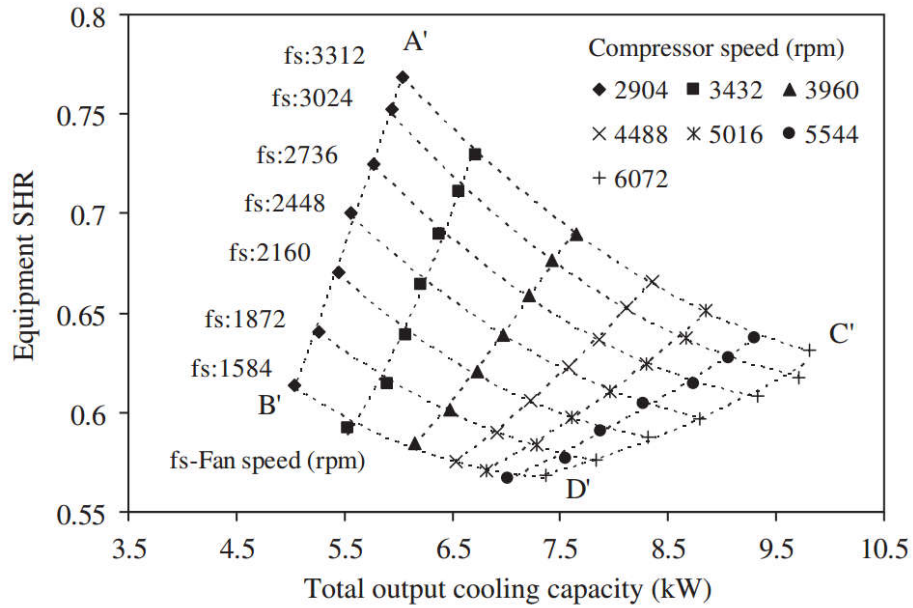


Fig. 2.11 The IC between TCC and E SHR at different speed combinations of compressor and supply fan for a VS DX A/C system [Xu et al., 2010]

The inherent correlations (ICs) between the output TCC and E SHR at different speed combinations of compressor and supply fan were introduced by Xu et al. [2010] when studying the inherent operational characteristics of an experimental VS DX A/C system. The study results clearly revealed that, for a VS DX A/C system, its output TCC and output E SHR under VS operation were strongly coupled but mutually constrained within a trapezoid if these two parameters were presented on the same diagram as shown in Fig. 2.11. As seen, it was impossible for the experimental VS DX A/C system to output those E SHR/TCC combinations represented by those points outside the trapezoids when varying its compressor speed from the lowest of 2904 rpm to the highest of 6072 rpm and its supply fan speed from the lowest of 1584 rpm to the highest 3312 rpm. Li et al. [2015b] further studied the inherent operational characteristics of the same experimental VS DX A/C system but at different inlet air states. The experimental results demonstrated that both inlet air temperature and RH

level would significantly influence the ICs of the VS DX A/C system. At a constant inlet RH, varying inlet air temperature would cause the position shifting of a TCC-E SHR trapezoid, but the trapezoid shapes were maintained. Varying inlet RH level would however result in both position shifting and the changes in trapezoid shapes. Based on the obtained ICs between TCC and E SHR at different inlet air states, an artificial neural network model was trained and tested to predict the compressor and supply fan speeds when the experimental VS DX A/C system was operated at different combinations of sensible and latent cooling loads. Consequently, a novel neural network aided fuzzy logic controller was successfully implemented in the experimental VS DX A/C system for simultaneously controlling indoor air temperature and humidity [Li et al., 2015a].

### **2.3.2 Indoor thermal environment control using DX A/C system**

In an A/C system, the airflow rate is a critical operating parameter as it will directly influence system's output sensible and latent cooling capacities. An experimental study carried out by Chua et al. [2007] concluded that for dehumidification control, airflow rate was of the prime concern. It was previously shown that lowering the airflow rate passing through a cooling coil or lowering cooling coil surface temperature could enhance dehumidification efficiency [Hourahan, 2004; Shaw and Luxton, 1988; Shirey III and Henderson Jr, 2004]. Space humidity level could be reduced by 10% to 15% RH when implementing this strategy. The reduction in energy costs associated with various type of A/C systems used would cover the full range of climates, but was mostly significant in humid and tropical climates [Shaw and Luxton, 1988].

While much available open literature focused solely on reducing airflow rate with multi- or variable-speed supply fans, which itself was an improvement for A/C systems, a limited number of research work were carried out on investigating the feasibility of varying the speeds of both the supply fan and the compressor in a DX A/C system for achieving a better indoor thermal environment control. A control method was proposed Krakow et al. [1995b] to control indoor air temperature by varying compressor speed, and humidity by varying supply fan speed, respectively. The experimental results illustrated that space air temperature and RH level could be maintained within  $\pm 0.3^{\circ}\text{C}$  and  $\pm 2.5\%$  RH of their respective set points. A numerical simulation model incorporating PID control was also developed to further demonstrate the feasibility of this control strategy [Krakow et al., 1995a]. However, in their study, only simple comparisons and analysis were given, no detailed temperature and RH data and the related energy consumption data were given. Moreover, due to the strong cross-coupling between air temperature and humidity control, the control performance was inherently poor. In addition, in the simulation study carried out by Andrade and Billiard [2002], a detailed, physical based A/C simulation model was augmented by adding equations describing space sensible and latent cooling loads experienced by a typical residential building. The simulation results showed that the use of a VS compressor and a VS supply fan can help prevent short on-off cycling and improve indoor humidity control. A potential improvement in system's energy efficiency could be achieved by having different combinations of compressor and fan speeds at the expense of running a DX A/C system longer. However, all the study results were based on simulation and no actual experimental validation was carried out. Also, its

compressor was on-off cycled, without continuous control over the condensing unit in the DX A/C system.

In addition to the traditional PI or PID control strategies [Krakow et al., 1995b], various advanced control strategies aiming at simultaneously controlling indoor air temperature and humidity by varying the speeds of both compressor and supply fan have been designed for, and adopted in DX A/C systems. Li and Deng [2007a] developed a novel direct digital control (DDC)-based capacity controller for a VS DX A/C system to control indoor air temperature and humidity simultaneously. A numerical calculation algorithm using a number of real-time measured system operating parameters was developed to generate the control signals of compressor and supply fan speeds under various operational conditions. [Li and Deng, 2007a, b]. The inadequacy of this control strategy was its unacceptable control sensitivity as it would take time for the controller to obtain the information required if the space cooling loads were changed. Besides, the controller's disturbance rejection ability was also poor because there was no feedback loop to reflect the controlled process. Xu et al. [2008] developed a new control algorithm, the so-called H-L control strategy, for a VS DX A/C system to improve indoor humidity control. When the indoor air dry-bulb temperature setting was not satisfied, the controller enabled both compressor and supply air fan to operate at high speeds, otherwise, at low speeds. The controllability tests showed that an improved indoor humidity level and a higher energy efficiency would be achieved under the H-L control as compared to that under the traditional on-off control. Using the Linear Quadratic Gaussian (LQG) technique, Qi and Deng [2009] developed a Multi-Input Multi-Output (MIMO) control strategy for simultaneously controlling the indoor air temperature and humidity by regulating the speeds of

compressor and supply fan in an experimental DX A/C system. This MIMO controller took into account the coupling effects among multiple operating parameters of the DX A/C system, using a dynamic mathematical model written in a state-space format [Qi and Deng, 2008]. However, the controller can only perform as expected near the operating point where the governing equations in the state-space model were linearized. Li et al. [2012a] developed a dynamic ANN model based controller for the VS DX A/C system. Similar to Qi and Deng's MIMO controller, since the dynamic ANN model was trained at a fixed operating point, the controller cannot function well when the DX system was operated away from the training point. To enable the controller to be functional over a wider operational range, an on-line adaptive ANN based controller was further developed. Using the real-time measured operating parameters, the ANN model could be continuously updated. The adaptive controller therefore can achieve the required control accuracy and sensitivity over a wider operational range, with, however, a much more complicated configuration [Li et al., 2013]. An ANN aimed fuzzy logic controller for simultaneous control of indoor air temperature and humidity using a DX A/C system was developed by Li et al. [2015b], combining the benefits of fuzzy logic controllers and ANN modeling. While this fuzzy logic controller could be functional at the normal operational range of indoor air parameters, the used ANN model was trained based on the inherent operational characteristics of the controlled DX A/C system, making this controller infeasible to be implemented in other DX A/C systems. Li et al. [2015a] further developed a simple Proportional Derivative (PD) law based Fuzzy Logic Controller (PFC) for a DX A/C system. However, the determination of the weights assigned to each linguistic variable in the PFC depended mainly on personal experience regarding the operation of a DX



A/C system. No generalized approach for determining or optimizing the weights assigned to each linguistic variable was proposed.

### **2.3.3 Operational instability of a DX A/C system under VS operation**

An examination on the reported studies related the operation and control of DX A/C systems revealed that the operational instability was ignored when studying the inherent operational characteristics of a VS DX A/C system and developing control strategies for simultaneously controlling indoor air temperature and humidity. No studies in open literatures on investigating the operational stability of an VS DX A/C system under VS operation may be identified. As a matter of fact, it was previously shown that the oscillation of a DX A/C system's key operating parameters would occur when only its compressor was VS controlled to cope with the variations in thermal load [Chen et al., 2005]. Furthermore, the issue of operational stability became much more complicated for a VS DX A/C system when both its compressor and supply fan are VS operated at different inlet air states. For example, a previous study showed that when an experimental DX A/C system was VS operated for simultaneously controlling indoor air temperature and humidity, its operating DS regulated by a conventional PID controller would be unstable if the respective set points of indoor air dry-bulb and wet-bulb temperatures were reduced [Qi et al., 2010a], as shown in Fig. 2.12. As seen in Fig. 2.12 (a) and (d), after the settings of indoor air dry-bulb and wet-bulb temperatures were both reduced by 0.5 °C at  $t = 510$  s, both compressor and supply fan speeds were increased to provide a greater output cooling capacity. While both indoor air dry-bulb and wet-bulb temperatures were finally controlled to their respective set points, the resultant operating DS experienced

significant fluctuation, which lasted for many minutes after the speed changes were introduced, resulting in system hunting as shown in Fig. 2.12 (b). Such a phenomenon would impact the performance of a refrigeration system, leading to a higher energy consumption and lower operational stability. Although a new DS controller was developed for mitigating hunting in the experimental VS DX A/C system [Qi et al., 2010a], the reasons why the variation of compressor and supply fan speeds and change of inlet air states would cause the oscillation of system's operating parameters remained to be known.

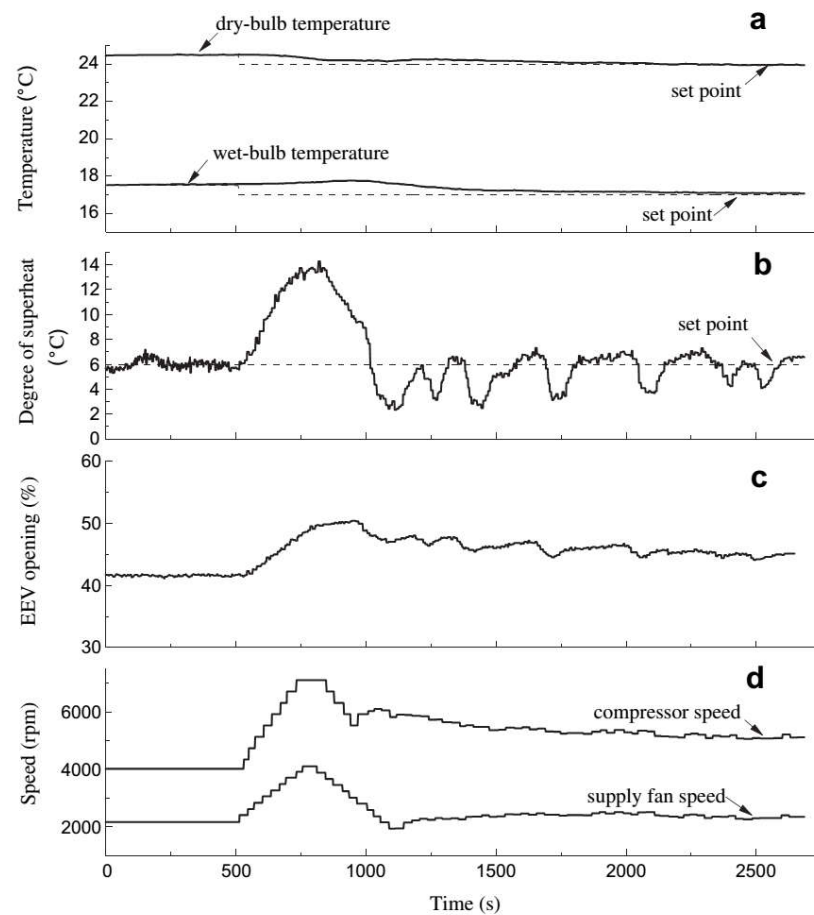


Fig. 2.12 The hunting in a VS DX A/C system when both of compressor and supply fan were VS operated for simultaneously controlling indoor air temperature and humidity [Qi et al., 2010a]

## 2.4 Conclusions

DX A/C has been widely used in small- to medium-scaled buildings. A DX A/C system operates based on vapor-compression refrigeration cycle, and there exists an EV-evaporator control loop to regulate the refrigerant mass flow rate entering its evaporator in response to the operating DS at the evaporator's exit. However, the EV-evaporator control loop in a vapor-compression refrigeration system may be underdamped or even unstable after experiencing certain operating disturbances, resulting in the oscillation of system's key operating parameters, and the instability, or hunting, of the system. Hunting leads to a lower operational safety and higher energy consumption of a refrigeration system, and thus should be avoided as far as possible.

The operational instability, or hunting, in refrigeration systems have been extensively studied for decades. A number of modeling and experimental studies have been carried out for investigating the operational stability in a refrigeration system in order to reveal the possible causes for hunting and to suggest measures for mitigating hunting. There have been two different views on the causes for hunting. The first concentrated on the inherent operational characteristics of an evaporator. Three observed phenomena, namely the random fluctuation in a refrigerant mixture-vapor transition point, the variation in heat transfer mechanism and superheat nonlinearity, are frequently used to explain the causes for hunting. The second view tried however to explain the causes of hunting based on the operational characteristics of an EV, as it would take some time for the DS signal to propagate through the EV to adjust the refrigerant mass flow

required, which was considered as the fundamental reason for hunting. Previous studies indicated that the valve gain and static superheat setting for a TEV, time constant of a TEV's sensing bulb, bulb position and the thermal resistant between sensing bulb and evaporator pipe wall would impact the operational stability of a TEV-controlled refrigeration system. However, among these reported studies on hunting, limited numbers of studies on the operational characteristics of an EEV on the operational stability of an EEV-controlled refrigeration system may be identified.

On the other hand, VS technology has been widely applied to DX A/C systems, and both compressor and supply fan speeds in a DX A/C system can be varied to output different sensible and latent cooling capacities to cope with space sensible and latent thermal loads, paying a way to simultaneously control indoor air temperature and humidity. For the purpose of achieving accurate simultaneous control over indoor air temperature and humidity, previous studies on influences of varying both compressor and supply fan speeds in a VS DX A/C system on the variations of its output sensible and latent cooling capacities have been carried out. The inherent operational characteristics of a VS DX A/C system expressed in terms of the ICs between its output TCC and E SHR have been extensively investigated, but all at a fixed DS setting and without considering operational stability. As a matter of fact, hunting was observed when a DX A/C system was VS operated for simultaneously controlling indoor air temperature and humidity, resulting in a low operational safety and high energy consumption of the system.

Therefore, the literature review reported in this Chapter revealed that further studies on: 1) the influences of the operational characteristics of an EEV on the operational

stability of the EEV-controlled DX A/C system and 2) the inherent operational characteristics of a DX A/C system under VS operation at different inlet air states with its operational stability included so as to help develop advanced controllers for a VS DX A/C system for achieving a balance between operational safety and efficiency should be carried out. These two are the targets of the investigations to be reported in this Thesis.

## **Chapter 3**

### **Proposition**

#### **3.1 Background**

From the literature review presented in Chapter 2, it is evident that the operational instability, or hunting, and its consequence of a lower operational safety and a higher energy consumption have been widely noticed in both TEV [Eames et al., 2014; Huang et al., 2014; Wedekind, 1971; Wedekind and Stoecker, 1968; Yasuda et al., 1983] and EEV [Chen et al., 2008; Fallahsohi et al., 2010; Li et al., 2004; Qi et al., 2010b] controlled refrigeration systems. As a typical vapor-compression refrigeration system, DX A/C systems are widely used in small- to medium-scaled buildings and its operational instability has also been observed [Chen, 2005; Chen et al., 2008; Qi et al., 2010a].

Over the years, a number of studies have been carried out to reveal the possible causes for hunting in refrigeration systems. There have been two different views on the possible causes for hunting in open literatures, namely, the inherent operational characteristics of an evaporator and operational characteristics of an EV. However, there has been no verdict on which view would reflect truly what leads to hunting in a refrigeration system. Furthermore, the detailed review on hunting presented in Chapter 2 indicated that a fewer number of studies on investigating the operational characteristics of an EEV on the operational stability in an EEV-controlled refrigeration system were carried out, and therefore more studies should be carried out. As far as the operational characteristics of an EEV are concerned, the dynamics of its

temperature sensor should also influence operational stability of the EEV-controlled refrigeration system, as it directly affects the DS signal transfer through the EEV to regulate the refrigerant mass flow rate passing through it. However, no studies in the open literatures on investigating the dynamics of an EEV's temperature sensor on the operational stability of the EEV-controlled refrigeration system may be identified.

On the other hand, in view of the extensive applications of VS technology to DX A/C systems, both compressor and supply fan speeds can be varied to output different sensible and latent cooling capacities to cope with different sensible and latent loads in a conditioned space, paving the way to simultaneously control indoor air temperature and humidity. In order to achieve accurate control over indoor air temperature and humidity simultaneously using a VS DX A/C system, its inherent operational characteristics expressed in terms of its output TCC and E SHR at various speed combinations of compressor and supply fan have been extensively studied [Li and Deng, 2007c; Li et al., 2014; Xu et al., 2010] and advanced capacity controllers for simultaneous control over indoor air temperature and humidity developed [Li et al., 2012a; Li et al., 2015a; Li et al., 2015b; Qi and Deng, 2009]. However, it is noted that in these reported studies, the issues of operational stability were ignored, as it was previously shown that hunting would take place in a VS DX A/C system when both its compressor and supply fan were VS controlled for simultaneously controlling indoor air temperature and humidity [Qi et al., 2010a]. No previous studies in the open literatures on investigating the operational stability of a VS DX A/C system when it is VS operated at different inlet air states may be identified.

Therefore, a research project has been proposed, to firstly examine the influences of the operational characteristics of an EEV on the operational stability of an EEV-controlled DX A/C system; and to secondly investigate the operational stability a DX A/C system when it is VS operated at different inlet air states. The outcome of the proposed project would help establish a balance between the operational safety and energy efficiency when developing advanced control strategies for simultaneously controlling indoor air temperature and humidity using a VS DX A/C system.

### **3.2 Project title**

The proposed project reported in this Thesis focused on the following three pieces of work on operational stability in an EEV-controlled VS DX A/C system: (1) to theoretically and experimentally study the influences of the operational characteristics of an EEV, in terms of its control settings and dynamics of its temperature sensor, on the operational stability of the EEV-controlled DX A/C system; (2) to further experimentally study the inherent operational characteristics of the VS DX A/C system expressed in terms of TCC and E SHR considering its operational stability when it was VS operated at different DS settings and inlet air states; (3) to develop a new capacity controller for the VS DX A/C system that is able to not only control indoor air temperature and humidity, but also select an optimized DS setting for balancing the operational safety and efficiency. The proposed research project is therefore entitled “Operational Stability of a Direct Expansion (DX) Air Conditioning (A/C) system under Variable Speed (VS) Operation and its Control Application”



### 3.3 Aims and objectives

Therefore, the proposed research project has the following objectives:

1. To theoretically and experimentally study the influences of the operational characteristics of an EEV in terms of its control settings and dynamics of its temperature sensor on the operational stability of the EEV-controlled DX A/C system, so as to develop appropriate strategies for mitigating hunting.
2. To experimentally investigate the relationship between the inherent operational characteristics and the operational stability for an experimental VS DX A/C system in terms of its inherent correlations (ICs) between its output TCC and E SHR under VS operation with its operational stability included, so as to establish a balance between operational safety and energy efficiency when developing capacity controller for simultaneously controlling indoor air temperature and humidity.
3. To develop a new capacity controller that is able to not only simultaneously control indoor air temperature and humidity using the experimental VS DX A/C system, but also select an optimized DS setting which can be varied in accordance with the known relationship between the inherent operational characteristics and the operational stability for achieving a balance between operational safety and energy efficiency.

### 3.4 Research methodologies

Theoretical and experimental approaches will be firstly employed when studying the influences of the operational characteristics of a conventional PI-controlled EEV in terms of its PI control setting and dynamics of its temperature sensor on the operational stability of the experimental DX A/C system. Transfer functions for each of the components in the PI-controlled EEV-evaporator control loop will be developed. Using the Frequent Response Method and Nyquist stability criterion in the classical control theory, the influences of EEV's PI settings and the time constants of EEV's temperature sensor on the operational stability of the DX A/C system will be examined and further experimentally validated.

Secondly, steady-state experiments will be carried out using the experimental VS DX A/C system to study the relationship between its inherent operational characteristics and operational stability of the experimental VS DX A/C system at different DS settings and inlet air states when it is VS operated. The ICs between its output TCC and E SHR of the experimental VS DX A/C system considering its operational stability (ICs\_os) will be experimentally obtained by identifying the unstable operating regions in a TCC-E SHR diagram.

Finally, based on the obtained ICs\_os, an ANN based mathematical model will be trained and tested to predict the operational stability of the experimental VS DX A/C system when it is VS operated at different DS settings and inlet air states. Using the developed ANN model, a DS setting establishment (DSE) module will be obtained to select an optimized DS setting for the experimental DX A/C system when it is VS

operated at different inlet air states. The DSE module will be incorporated in a previously developed Proportional Derivative (PD) law based Fuzzy Logic Controller (PFC) [Li et al., 2015a] to develop a new capacity controller that is able to not only simultaneously control indoor air temperature and humidity using the experimental VS DX A/C system, but also select an optimized DS setting for properly balancing the operational safety and energy efficiency. Controllability tests for the new capacity controller will be carried out, and its measured control performance will be compared to that of the previous capacity controller [Li et al., 2015a] with a constant DS setting.

## **Chapter 4**

### **Description of the Experimental DX A/C System**

#### **4.1 Introduction**

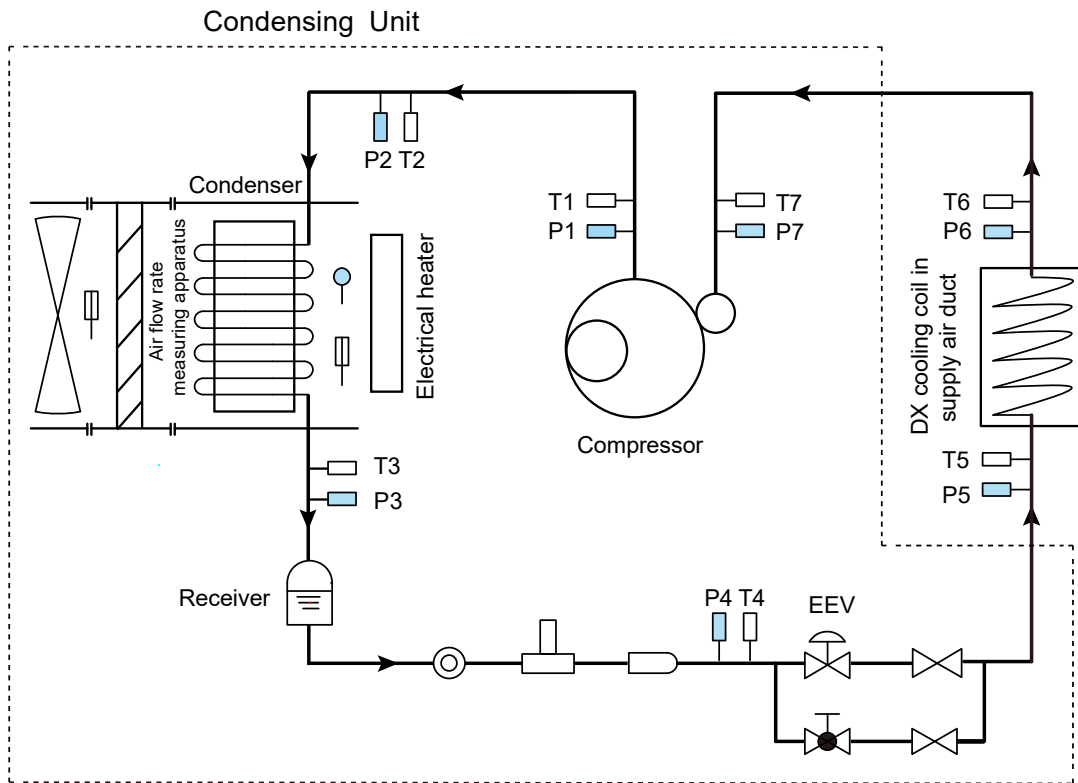
An experimental VS DX A/C system is available in the HVAC Laboratory of Department of Building Services Engineering in The Hong Kong Polytechnic University. The primary purpose of having the experimental system is to facilitate carrying out the research project related to VS DX A/C technology

Advanced technologies such as VS compressor and supply fan, and EEV, as well as computerized data measuring, logging and control, have been used in the experimental DX A/C system.

This Chapter presents firstly detailed descriptions of the experimental VS DX A/C system and its major components. Secondly, a computerized instrumentation and a data acquisition system is detailed. Finally, a computer supervisory program used to operate and control the experimental VS DX A/C system is detailed.

#### **4.2 Descriptions of the experimental system and its major components**

The experimental VS DX A/C system is mainly composed of two parts, i.e., a DX refrigeration plant (refrigerant side) and an air-distribution sub-system (air side). The schematic diagrams of both the DX refrigeration plant and the complete experimental DX A/C system are illustrated in Fig. 4.1 and Fig. 4.2, respectively.





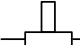


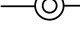


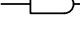

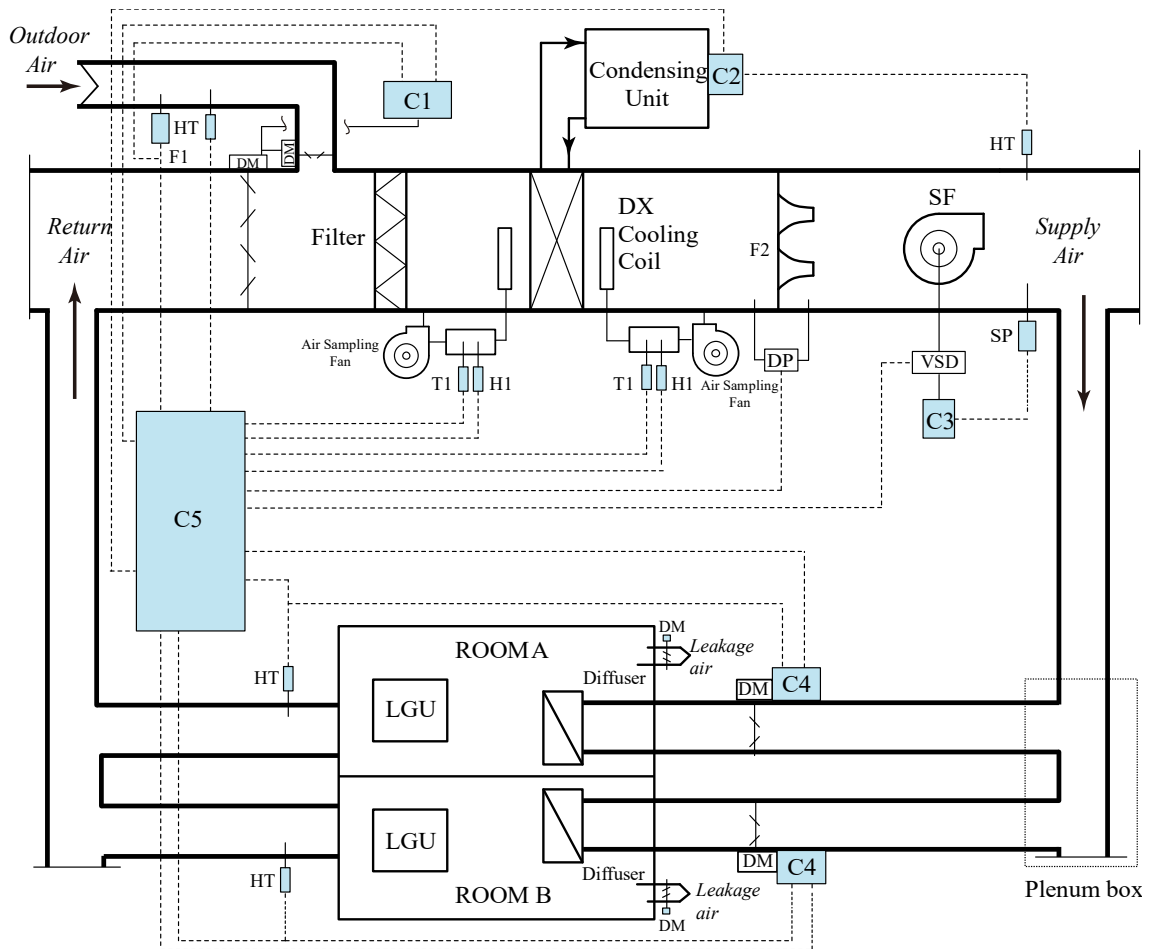
- |   |                                 |   |                        |   |                             |
|---|---------------------------------|---|------------------------|---|-----------------------------|
|  | Refrigerant temperature sensor  |  | EEV                    |  | Refrigerant mass flow meter |
|  | Air temperature sensor          |  | Manual expansion valve |  | Sight glass                 |
|  | Refrigerant pressure transducer |  | Manual valve           |  | Filter                      |
|  | Air humidity sensor             |   |                        |   |                             |

Fig. 4.1 Schematic diagram of the DX refrigeration plant



- |  |   |
|--|---|
| C1 - controller of outdoor/return air damper | H1 - air wet-bulb temperature sensor      |
| C2 - controller of condensing unit           | HT - humidity and temperature transmitter |
| C3 - controller of supply fan                | DM - damper                               |
| C4 - controller of supply air damper         | DP - differential pressure transducer     |
| C5 - data acquisition and control unit       | SF - supply fan                           |
| F1 - air velocity transducer                 | SP - static pressure measuring device     |
| F2 - supply airflow rate measuring apparatus | LGU - load generating unit                |
| T1 - air dry-bulb temperature sensor         | VSD - variable speed drive                |

Fig. 4.2 Schematic diagram of the complete experimental VS DX A/C system

#### 4.2.1 The DX refrigeration plant

As shown in Fig. 4.1, the major components in the DX refrigeration plant include a VS rotary compressor, an EEV, a high-efficiency tube-louver-finned DX evaporator and an air-cooled tube-plate-finned condenser. The evaporator was placed inside the supply air duct to work as a DX air cooling coil. Its details are given in Fig. 4.3, with

its geometric parameters listed in Table 4.1. The design air face velocity for the DX cooling coil was 1.98 m/s. The nominal output cooling capacity from the DX refrigeration plant was 7.5 kW. The compressor was driven by a variable-speed drive (VSD) and its details can be found in Table 4.2. The EEV consisted of a throttling needle valve, a step motor and a pulse generator, which could be manually or program controlled to regulate the refrigerant mass flow rate passing through it in response to the operating DS at evaporator exit. The details of the EEV can be found in Table 4.3. An environmental friendly refrigerant, R410a was used as the working fluid in the DX refrigeration plant, with a total charge of 5.8 kg.

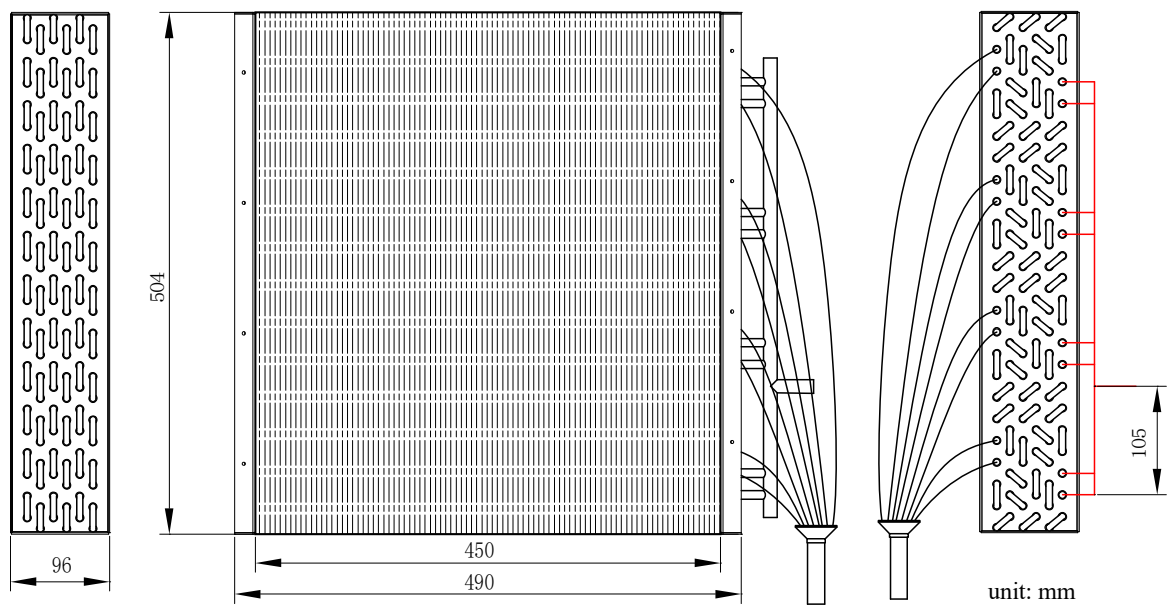


Fig. 4.3 The details of the DX air cooling and dehumidifying coil used in the experimental VS DX A/C system

Table 4.1 Geometric parameters of the DX cooling coil

Configuration	
Transverse tube pitch:	21 mm
Longitude tube pitch:	12.7 mm
Fin pitch:	1.3 mm
Fin thickness	0.115 mm
Outside tube diameter:	7 mm
Inside tube diameter:	6.4 mm
Length of the windward area:	450 mm
Height of the windward area:	504 mm
Number of the windward transverse tube:	24
Number of the tube row:	6
Number of refrigerant loop:	8

In addition, a condenser air duct was used to duct the condenser cooling air carrying the rejected heat from the condenser away to outside the Laboratory. The condenser fan, housed inside the condenser air duct, can also be VS operated. An electrical heater controlled by Solid State Relay was used to adjust the temperature of the cooling air entering the condenser for various experimental purposes. A refrigerant mass flow meter was installed upstream of the EEV to measure the refrigerant mass flow rate being circulated in the DX refrigerant plant. Other necessary accessories and control devices, such as an oil separator, a refrigerant receiver, a sight glass and safety devices, were provided in the refrigeration plant to ensure its normal and safe operation.



Table 4.2 Details of the VS rotary compressor

Model	MITSUBISHI-TNB220FLHMC
Allowable Frequency range:	10-110 Hz
Nominal Power input	2.2 kW $\pm$ 5%
Nominal Capacity:	7.13 kW $\pm$ 5%
Displacement:	22 ml/rev

Table 4.3 Details of the experimental EEV

Model:	SANHUA DPF(TS)1.8
Pulse range	0~500
Nominal capacity:	8.4 kW
Port diameter:	1.8 mm

#### 4.2.2 The air-distribution sub-system

The air-distribution sub-system in the experimental DX A/C system is schematically shown in Fig. 4.2. It included an air-distribution ductwork with return and outdoor air dampers, a VS centrifugal supply fan, and a conditioned space. The frequency of supply fan can be modulated by a VSD (Model: MITSUBISHI FR-E700-2.2K). The details of the supply fan are given in Table 4.4.

The air conditioned space included two rooms with each measuring at 3.2 m (L)×3.7 m (W)×3.3 m (H). Inside the space, there were two sets of sensible heat and moisture load generating units (LGUs), each measuring at 550 mm (L)×700 mm (W)×840 mm

(H). The units were intended to simulate the cooling load in the conditioned space. Its heat and moisture generation rate as regulated by Solid State Relay may be varied manually or automatically with a pre-set pattern through operator's programming. The maximum heat and moisture generation rate were 5.4 kW and 4.5 kW respectively for each set of the LGUs. In addition, leakage outlets with residual-pressure relief dampers were installed in the space so that a positive internal pressure of not more than 20 Pa can be maintained at all time. In the air-distribution subsystem of the experimental DX A/C system, return air from the space mixed with outdoor air in a plenum box upstream of an air filter. The mixed air was filtered and then cooled and dehumidified by the DX cooling coil. Afterwards, the cooled and dehumidified air passed through the supply fan, to be supplied to the space to deal with the cooling load generated from LGUs.

Table 4.4 Details of the VS supply fan

Model:	SHANG HAI NANTAI 4-72
Nominal speed:	2900 rpm
Modulation range:	0~3600 rpm
Nominal flow rate:	1300 m <sup>3</sup> /h

### 4.3 Computerized instrumentation and data acquisition system

The computerized instrumentation for the experimental VS DX A/C system is also shown in both Fig. 4.1 and Fig. 4.2. The A/C system was fully instrumented for measuring all of its operating parameters, which may be classified into three types,

i.e., temperature, pressure and flow rate. Since all measurements were computerized, all sensors and measuring devices were able to output direct current signal of 4-20 mA or 1-5 V, which were transferred to a data acquisition system for logging and recording.

#### **4.3.1 Sensors/measuring devices for temperatures, pressures and flow rates**

Four sets of humidity and temperature transmitters (Model: E+E EE160, marked as HT in Fig. 4.2) were located in the air-distribution sub-system of the experimental VS DX A/C system for directly measuring air RH and temperature with a reported uncertainties of  $\pm 0.5\%$  RH and  $\pm 0.1$  °C. To minimize the influence of uneven distribution of air parameters inside the air duct, standard air-sampling devices as recommended by the ISO Standard 5151 [ISO, 2004] were provided to ensure measuring accuracy. Two sets of air dry-bulb and wet-bulb temperature sensors, denoted by T1 and H1 in Fig. 4.2, were placed in the air-sampling devices for indirectly measuring the RH of the air entering and leaving the DX cooling coil. As shown in Fig. 4.1, there were also seven temperature sensors for measuring refrigerant temperatures in the DX refrigeration plant. To ensure fast response of the sensors for facilitating the study of transient behaviours of the DX refrigeration plant, these temperature sensors were well clamped to the refrigerant pipe wall and thermally insulated. The temperature sensors for air and refrigerant were of platinum resistance type, using four-wire Wheatstone bridge connection and with a pre-calibrated accuracy of  $\pm 0.1$  °C. The specifications of the resistance temperature devices (RTDs) were: JUMO Pt100/0°C-4W, Class A.

Refrigerant pressures in various locations in the DX refrigeration plant were measured using pressure transmitters with an accuracy of  $\pm 0.2\%$  of full scale reading (Model: DRUCK Unik5000).

There were two sets of air flow rate measuring apparatus in the air-distribution system. One set of air flow rate measuring apparatus was used to measure the total supply airflow rate, i.e., the airflow rate passing through the DX cooling coil and the other for measuring the airflow rate passing through the condenser. The two sets of air flow rate measuring apparatus were constructed in accordance with ANSI/ASHRAE Standard 41.2 [ASHRAE, 1987], consisting of nozzles of different sizes, diffusion baffles and a differential pressure transducer with a measuring accuracy of  $\pm 0.1\%$  of full scale reading (Model: YOKOGAWA EJA110A-DLS5A-92NN). The number of nozzles in operation can be altered automatically.

Outdoor airflow rate was measured using a hot-film anemometer with a reported accuracy of  $\pm 0.2\%$  of reading (Model: E+E EE65-VB5). As recommended by its manufacturer, the anemometer was installed 200 mm downstream of the outdoor air inlet to ensure the measuring accuracy for outdoor airflow rate. The power consumption of the VS compressor was measured using a digital power meter with a reported uncertainty of  $\pm 0.16\%$  of reading (Model: QINZHI 8775A1). The refrigerant mass flow rate passing through the EEV was measured by a Coriolis mass flow meter with a reported uncertainty of  $\pm 0.25\%$  of full scale reading (Model: KROHNE MFM1081K-10S). The supply air static pressure was measured using a manometer with a reported accuracy of  $\pm 0.1\%$  of full scale reading (Model: YOKOGAWA EJA110A-DLS5A-92NN).

### **4.3.2 The data acquisition system**

A data acquisition unit (Model: YOKOGAWA MX100) was used in this experimental VS DX A/C system. It provided up to 50 channels for monitoring various types of system operating parameters. The direct current signal from various measuring devices/sensors can be scaled into their real physical values of the measured parameters using a logging & control supervisory program which was developed using LabVIEW programming platform. The minimum data sampling interval was two seconds. It should be noted that the flow rates of both supply air and condenser cooling air were calculated using the air static pressure drops across their respective nozzles. The outdoor airflow rate was evaluated by multiplying the measured air velocity with the sectional area of the outdoor air duct. The output cooling capacity from the DX refrigerant plant was calculated based on the enthalpy-difference of air across the DX cooling coil

### **4.4 LabVIEW logging & control supervisory program**

A computer supervisory program which was capable of performing simultaneously data-logging and parameter-controlling was necessary. It needed to communicate with not only the data acquisition unit, but also conventional standalone digital programmable PID controllers, which are to be detailed in Section 4.5. A commercially available programming package, LabVIEW, provided a powerful programming and graphical platform for data acquisition and analysis, as well as for control application.

A data logging & control supervisory program was developed using LabVIEW, with all measured parameters real-time monitored, curve-data displayed, recorded and processed. The program can also perform the retrieval, query and trend-log graphing of historical data for measured parameters. The program ran on a personal computer.

The LabVIEW-based logging & control supervisory program enabled the computer to act as a central supervisory control unit for different low-level control loops, which will be also discussed in Section 4.5, in the experimental VS DX A/C system. The computer can therefore not only modify the control settings of those standalone microprocessor-based PID controllers, but also deactivate any of these controllers. The LabVIEW-based logging & control supervisory program also provided an independent self-programming module (SPM) by which new control algorithms may be easily implemented through programming. A SPM performed in a similar manner to a central processing unit of a physical digital controller. The variables available from all measured parameters can be input to, and processed according to a specified control algorithm, in a SPM to produce required control outputs. Once a SPM was initiated to replace a given standalone controller, the controller must be deactivated, but worked as a digital-analogy converter to receive the control output from the SPM. An analogue control signal was then produced by the controller to initiate the related actuator for necessary control action.

#### **4.5 Conventional control loops in the experimental VS DX A/C system**

Totally, there were twelve conventional control loops in this experimental VS DX A/C system. These loops either were activated using the LabVIEW-based supervisory program or use PID controllers which were digital programmable type with RS-485 communication port (Model: YOKOGAWA UT35A). Resetting controllers' proportional bands, integral times, derivative times and set points were permitted.

Among the twelve control loops, four were for varying heat and moisture generation rate of the LGUs located inside the conditioned space. Electrical power input to the LGU was regulated using Solid State Relay according to the instructions from their respective control loops to simulate the space cooling load.

The remaining eight conventional PID control loops are as follows: 1) degree of refrigerant superheat by regulating EEV's opening; 2) degree of refrigerant subcooling by regulating the condenser fan speed; 3) condenser inlet air temperature through regulating electrical power; 4) supply air temperature by regulating the compressor speed; 5) supply air static pressure by regulating the supply fan speed; 6) outdoor air flow rate by jointly regulating both outdoor and return air dampers' openings; 7) air temperature in Room A by regulating its VAV terminal damper's opening; 8) air temperature in Room B by regulating its VAV terminal damper's opening. These eight control loops can be activated by using either conventional physical digital PID controllers available in the experimental VS DX A/C system or a SPM specifically for any new control algorithm to be developed.

The control of supply air temperature is used as an example for illustration. When the related conventional PID controller is enabled, the controller measures the supply air temperature and then compares the measured temperature with its set point. The error between the temperature set point and the measured temperature is processed in the controller following a pre-set PID control algorithm and then an analogue control signal of 4~20 mA is produced and sent by the PID controller to the VSD for compressor to regulate its speed. On the other hand, such a conventional PID controller may be replaced by a SPM to be specifically developed based on a new control algorithm for compressor speed control. The SPM may take the advantages of using simultaneously multiple input variables, e.g., supply air temperature and its set point, evaporator and condensing pressures, DS, etc. Control outputs can be created by using the SPM following the new control strategy, and communicated to the physical digital PID controller, which works only as a digital-analog converter. An analog control signal is then generated and sent to the VSD of compressor for its speed control.

#### **4.6 Summary**

An experimental VS DX A/C system was available for carrying out the project reported in this Thesis. The system consisted of two parts: a DX refrigeration plant and an air-distribution sub-system.

The experimental VS DX A/C system was fully instrumented using high quality sensors/measuring devices. Totally forty-two operating parameters in the system can be measured and monitored simultaneously and twelve conventional PID feedback



control loops are provided. Two sets of airflow rate measuring apparatus were constructed in accordance with ANSI/ASHRAE Standard 41.2. Two sets of air dry-bulb and wet-bulb temperature sensors were placed in the air-sampling devices for evaluating the enthalpy of the air entering and leaving the DX cooling coil, and a Corioli mass flow meter was used for measuring the refrigerant flow rate being circulated in the DX refrigerant plant.

An logging & control supervisory program was developed specifically for this experimental VS DX A/C system using LabVIEW programming platform. All parameters can be real-time measured, monitored, curve-data displayed, recorded and processed by the logging & control program. The LabVIEW-based logging & control program provided an independent SPM by which any new control algorithms to be developed may be implemented.

The availability of such an experimental VS DX A/C system is expected to be extremely useful in investigating the inherent operational characteristics and operational stability a DX A/C system under VS operation and developing a capacity controller for simultaneously controlling indoor air temperature and humidity at the same time achieving a balance between operational safety and efficiency. Therefore, the project proposed on the operational stability of a DX A/C system under VS operation and its control applications can be realized based on this experimental rig.

## **Chapter 5**

### **The influences of the operational characteristics of the EEV on the operational stability of the EEV-controlled experimental DX A/C system**

#### **5.1 Introduction**

The review on the possible causes for hunting in refrigeration systems presented in Section 2.2.2 indicated that only limited numbers of studies on investigating the influences of the operational characteristics of an EEV on system operational stability were carried out, and therefore more efforts should be made. In an EEV-controlled refrigeration system, proportional and integral (PI) and proportional, integral and derivative (PID) control algorithms have been extensively used for its EEV to regulate the EEV's opening for controlling refrigerant mass flow rate in response to DS at evaporator exit [Jolly et al., 2000; Li et al., 2009; Li et al., 2008; Qi et al., 2010a]. In practice, a PI controller is adequately capable to provide an acceptable control performance, without the need to consider the problems associated with the derivative actions, namely, the need of properly filtering out the measurement noise [Visioli, 2006]. In addition, in an EEV-controlled refrigeration system, a temperature sensor is used to measure the temperature of refrigerant at evaporator exit, so that the actual operating DS may be evaluated and sent to the EEV for control action. The temperature sensor acts in a similar manner to a TEV's sensing bulb in a TEV-controlled refrigeration system. It was previously shown that in a TEV-controlled system, the TEV's valve gain and the time constant of the TEV's sensing bulb [Mithraratne and Wijesundera, 2001, 2002; Mithraratne et al., 2000] did impact the

system operational stability, because the former directly affected the degree of valve opening and thus the refrigerant mass flow rate, and the latter the time required for the DS signal to propagate through the TEV to adjust the desired refrigerant mass flow rate. This suggested that the operational characteristics of a PI controlled EEV in terms of its PI settings and the time constant of its temperature sensor may also similarly impact on the operational stability of an EEV-controlled refrigeration system. However, no previous investigations on the influences of EEV's PI settings and the time constants of EEV's temperature sensor on the operational stability in an EEV-controlled refrigeration system may be identified.

Therefore, a study on investigating the influences of EEV's PI settings and time constants of EEV's temperature sensor in the PI-controlled EEV-evaporator control loop on the operational stability of the experimental DX A/C system using the classical control theory has been carried out and the study results are reported in this Chapter. Firstly, the descriptions of the PI-controlled EEV-evaporator control loop in the experimental DX A/C system are presented. Secondly, the transfer functions for each of the components in the PI controlled EEV-evaporator control loop are presented. Thirdly, using the transfer functions developed, and following the Frequency Response Method and Nyquist stability criterion in the classical control theory, the influences of EEV's PI settings and the time constant of EEV's temperature sensor on the operational stability of the DX A/C system were analyzed and the results are presented. Finally, the analysis results were experimentally verified using the experimental DX A/C system and the verification results are reported.

## 5.2 The PI controlled EEV-evaporator control loop in the experimental DX A/C system

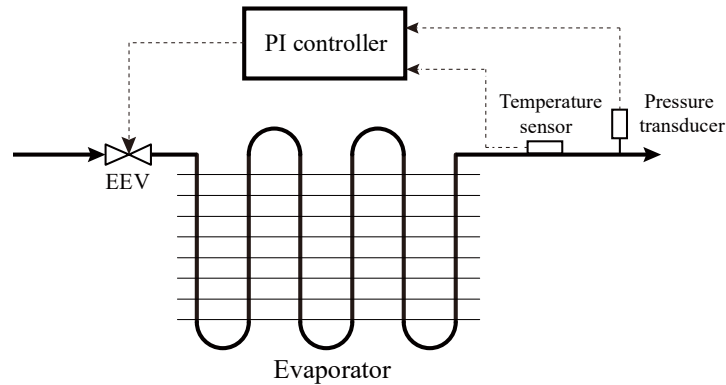
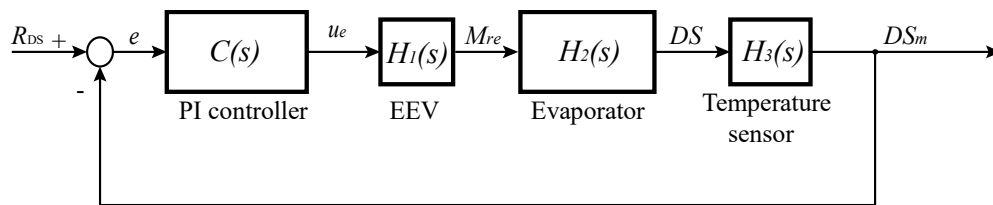


Fig. 5.1 Schematic diagram of the PI controlled EEV-evaporator control loop in the experimental DX A/C system

Using the experimental DX A/C system detailed in Chapter 4, a conventional PI control algorithm to regulate the refrigerant mass flow rate entering the evaporator in response to the DS at the evaporator exit was adopted for the EEV in the study reported in this Chapter. The operating DS hence was used as a representative operating parameter for indicating system stability. Fig. 5.1 shows the schematic diagram of the PI controlled EEV-evaporator control loop which was made of the EEV, evaporator, EEV's temperature sensor and PI controller. As seen, the DS at evaporator exit, as a feedback control signal to the EEV for modulating its opening, can be evaluated by respectively measuring the refrigerant temperature and evaporating pressure using a temperature sensor and a pressure transducer. Considering the heat transfer between the temperature sensor which was usually attached to the outer surface of the refrigerant pipe at evaporator exit, and the vapor refrigerant inside the pipe, it would take some time for EEV's temperature sensor to detect the refrigerant temperature which fluctuates all the time. On the other hand, for a pressure transducer which is

usually in direct contact with refrigerant, the response time of the pressure signal transfer may be negligible because pressure wave travels at speed of sound in tubes. Therefore, the presence of temperature sensor and its installation method in an EEV-controlled refrigeration system for measuring the refrigerant temperature at evaporator exit would cause a delay in the DS signal transfer in the EEV-evaporator control loop. Like in a TEV controlled refrigeration system, such a delay may also affect the operational stability in an EEV-controlled refrigeration system.

### 5.3 Development of a transfer function for the EEV-evaporator control loop



- $C(s)$  - Transfer function for the PI controller
- $H_1(s)$  - Transfer function for the EEV
- $H_2(s)$  - Transfer function for the evaporator
- $H_3(s)$  - Transfer function for the temperature sensor

Fig. 5.2 Block diagram of the PI controlled EEV-evaporator control loop

It is observed that the Transfer Function method has been commonly used to describe the relationships between the input and output of a controlled process, including evaporators used in refrigeration systems [Aprea and Renno, 2001; Broersen and Vanderjagt, 1980; Chen and Jiang, 1990; Stoecker, 1966]. Therefore, Transfer Function method was used in the current study for characterizing the dynamic behaviors of the PI controlled EEV-evaporator control loop.

Fig. 5.2 shows the block diagram of the PI-controlled EEV-evaporator control loop in the experimental DX A/C system. The measured DS at evaporator exit,  $DS_m$ , is directly used as a feedback DS signal to be compared with the reference DS setting,  $R_{DS}$ . Based on the error between  $DS_m$  and  $R_{DS}$ , or  $e$ , the PI controller outputs a corresponding control signal,  $u_e$ , to regulate the EEV's opening. Then, the refrigerant mass flow entering the evaporator,  $M_{re}$ , will be regulated continuously until  $e$  is within its preset range. Consequently, the open-loop transfer function,  $G(s)$ , for characterizing the transient response for  $DS_m$  to a change in EEV's control signal,  $u_e$ , can be expressed as:

$$G(s) = \frac{\Delta DS_m(s)}{\Delta u_e(s)} = H_1(s)H_2(s)H_3(s) \quad (5.1)$$

The closed-loop transfer function for the PI controlled EEV-evaporator control loop,  $G_c(s)$ , can therefore be expressed as:

$$G_c(s) = \frac{C(s)G(s)}{1 + C(s)G(s)} = \frac{C(s)H_1(s)H_2(s)H_3(s)}{1 + C(s)H_1(s)H_2(s)H_3(s)} \quad (5.2)$$

In Eqs. (5.1) and (5.2),  $C(s)$  is the transfer function for EEV's PI controller,  $H_1(s)$  that for the EEV,  $H_2(s)$  that for the evaporator and  $H_3(s)$  that for EEV's temperature sensor. The details of each of these transfer functions are separately presented as follows.

### 5.3.1 Transfer function for each of the four components in the EEV-evaporator control loop

#### 5.3.1.1 EEV's PI controller

For a conventional PI controller, its theoretical output signal,  $u_e$ , can be written as:

$$u_e(t) = K_p e(t) + \frac{K_p}{T_i} \int_0^t e(\tau) d\tau + \phi_0 \quad (5.3)$$

or in its discretized form:

$$u_e(t_k) = K_p e(t_k) + K_i \sum_{i=1}^k e(t_i) \Delta t + \phi_0 \quad (5.4)$$

$$K_i = \frac{K_p}{T_i} \quad (5.5)$$

For a digitally implemented PI controller in a refrigeration system, an incremental algorithm can be written as follows:

$$u_e(t_k) = u_e(t_{k-1}) + K_p (e(t_k) + e(t_{k-1})) + K_i e(t_k) \Delta t \quad (5.6)$$

In Eqs. (5.3) – (5.6),  $\phi_0$  is an offset adjustment parameter for a particular EEV,  $K_p$  the proportional gain,  $K_i$  the integral gain,  $T_i$  the integral time,  $\Delta t$  the sampling time interval ( $\Delta t = t_k - t_{k-1}$ ), and  $e(t_k)$  the error between feedback DS signal and the DS set point.

Applying the Laplace transform to Eq. (5.3), the transfer function for EEV's PI controller,  $C(s)$ , can be expressed as:

$$C(s) = K_p + \frac{K_i}{s} \quad (5.7)$$

### 5.3.1.2 The PI controlled EEV

During experiments, since both the compressor and supply fan speeds were unchanged, the variation range of EEV's opening was not large, and thus a linear valve characteristic can be assumed in the current study. Therefore, the mass flow rate passing through an EEV,  $M_{re}$ , can be considered linearly proportional to its control signal,  $u_e$ . The transfer function for the EEV,  $H_1(s)$ , can hence be written as:

$$H_1(s) = \frac{\Delta M_{re}(s)}{\Delta u_e(s)} = K_v \quad (5.8)$$

where  $K_v$  is the valve gain which is defined as the ratio of the change in refrigerant mass flow rate to the corresponding change in EEV's control signal.

### 5.3.1.3 DX Evaporator

According to the previous studies [Aprea and Renno, 2001], the transient response for the DS at evaporator exit to a sudden change in refrigerant mass flow rate supplied to



the evaporator can be approximated by a second-order plus dead-time process. Thus the transfer function for the evaporator,  $H_2(s)$ , can be expressed as:

$$H_2(s) = \frac{\Delta DS(s)}{\Delta M_{re}(s)} = K_e \frac{\omega_n^2}{s^2 + 2\zeta\omega_n s + \omega_n^2} e^{-\theta s} \quad (5.9)$$

where  $K_e$  is the evaporator gain, indicating the variation of DS from one steady state to another against the variation of the refrigerant mass flow rate supplied.  $\zeta$  is the damping ratio,  $\omega_n$  the natural frequency of the system.

#### 5.3.1.4 EEV's temperature sensor

Fig. 5.3 shows the installation of EEV's temperature sensor attached to the refrigerant pipe at evaporator exit and an equivalent thermal circuit for the heat transfer from refrigerant inside the pipe to the sensor. The heat transfer between the temperature sensor and the refrigerant at evaporator exit yielded:

$$(\rho C_p V)_{se} \frac{dT_{se}(t)}{dt} = \frac{(T_{re}(t) - T_{se}(t))}{R_{re}} + \frac{(T_a(t) - T_{se}(t))}{R_a} \quad (5.10)$$

where  $T_{re}$  is the temperature of vapor refrigerant at evaporator exit,  $T_a$  the ambient temperature,  $T_{se}$  the temperature measured by the sensor.  $R_{re}$  is total thermal resistance between the vapor refrigerant and temperature sensor, and  $R_a$  the convective thermal resistance between the sensor and its surroundings.

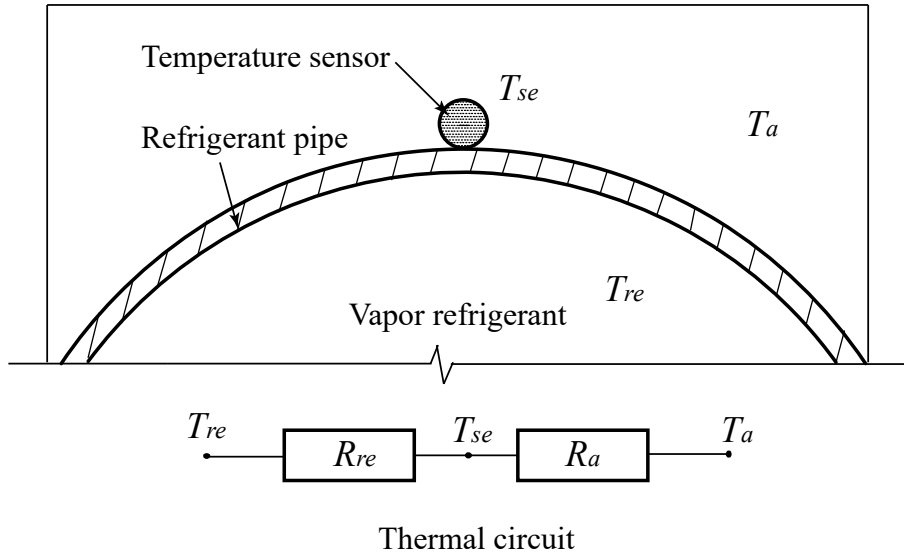


Fig. 5.3 Schematic diagram of the installation of EEV's temperature sensor attached to the refrigerant pipe at evaporator exit and its equivalent thermal circuit

Normally, in a refrigeration system, its EEV's temperature sensor and the refrigerant pipe at evaporator exit are thermally insulated to reduce heat loss. Therefore, the natural convection heat transfer between the sensor and its surroundings can be neglected. Thus, Eq. (5.10) can be simplified to:

$$\frac{dT_{se}(t)}{dt} + \frac{1}{\tau_{se}} T_{se}(t) = \frac{1}{\tau_{se}} T_{re}(t) \quad (5.11)$$

$$\tau_{se} = R_{re} (\rho C_p V)_{se} \quad (5.12)$$

where  $\tau_{se}$  is the time constant of the temperature sensor, which is affected by the thermal resistance between the sensor and vapor refrigerant inside the pipe, as well as the heat capacity of the temperature sensor itself.

Using the Laplace Transform, Eq. (5.11) can be transformed to:

$$\frac{\Delta T_{se}(s)}{\Delta T_{re}(s)} = \frac{1}{\tau_{se}s + 1} \quad (5.13)$$

Therefore, the transfer function for EEV's temperature sensor can be expressed as:

$$H_3(s) = \frac{\Delta DS_m(s)}{\Delta DS(s)} = \frac{\Delta T_{se}(s)}{\Delta T_{re}(s)} = \frac{1}{\tau_{se}s + 1} \quad (5.14)$$

$$\Delta DS_m(s) = \frac{1}{\tau_{se}s + 1} \Delta DS(s) \quad (5.15)$$

Eq. (5.15) suggests that due to the dynamics of EEV's temperature sensor, the transient response for  $DS_m$ , as a feedback control signal to regulate EEV's opening, is slowed down following a change in the actual DS of refrigerant at evaporator exit.

### 5.3.2 Identification of transfer function parameters

Using the transfer functions for each of the components in the PI controlled EEV-evaporator control loop, the open-loop transfer function,  $G(s)$ , can be expressed as:

$$G(s) = \frac{\Delta DS_m(s)}{\Delta u_e(s)} = H_1(s)H_2(s)H_3(s) = \frac{K_v K_e \omega_n^2}{(s^2 + 2\zeta\omega_n s + \omega_n^2)(1 + \tau_{se}s)} e^{-\theta s} \quad (5.16)$$

The parameters in Eq. (5.16), were identified experimentally using the experimental DX A/C system.

Table 5.1 Specifications of EEV's temperature sensor used in the experimental DX

A/C system

Sensor diameter (mm)	Sensor length (mm)	Heat capacity of the sensor, $(\rho C_p V)_{se}$ (J K <sup>-1</sup> )
4	30	1.42

Firstly, it was noted that in the experimental DX A/C system, for the purpose of reducing the influence of EEV's temperature sensor on the rate of DS signal transfer as far as possible, the temperature sensor used in experiments hence had a quick response characteristic and was attached well to the refrigerant pipe at evaporator exit. For the EEV's temperature sensor in the experimental DX A/C system, its specifications are shown in Table 5.1. Assuming a unit contact resistance of  $0.4 \times 10^{-4} \sim 1 \times 10^{-4} \text{ m}^2 \text{ K W}^{-1}$  [Lienhard, 2013] under normal sensor installation and using Eq. (5.12), the time constant of the EEV's temperature sensor could be assessed at about  $0.95 \sim 2.3 \text{ s}$ . Therefore, using an average time constant of 1.6s for the EEV's temperature sensor, Eq. (5.16) can be written as:

$$G(s) = \frac{\Delta DS_m(s)}{\Delta u_e(s)} = H_1(s)H_2(s)H_3(s) = \frac{K_v K_e \omega_n^2}{(s^2 + 2\zeta \omega_n s + \omega_n^2)(1 + 1.6s)} e^{-\theta s} \quad (5.17)$$

When carrying out experiments, compressor and supply fan speeds were fixed at 4680 rpm and 2880 rpm, respectively, and the inlet air state to the DX A/C system was maintained at 25 °C and 50% RH by modulating the LGUs in the conditioned space. The total cooling load under this operating condition was about 7.4 kW with 4.9 kW sensible load and 2.5 kW latent load. The EEV's opening was varied between 35% and 45% of its full opening with an increment of 2%. By tracking the dynamic

responses for the  $DS_m$  to a step change in EEV's control signal, the transfer function,  $G(s)$ , through using the MATLAB system identification toolbox, can be approximated to:

$$G(s) = \frac{-1.6}{(207s^2 + 29.5s + 1)(1.6s + 1)} e^{-31s} \quad (5.18)$$

Eq. (5.18) was further simplified by using Padé Approximation [Golub and Van Loan, 2012] to:

$$G(s) \approx \frac{1.6s - 0.1032}{(270s^3 + 42.85s^2 + 2.903s + 0.06452)(1.6s + 1)} \quad (5.19)$$

For validating Eq. (5.19), a further experiment was carried out when the EEV's opening was firstly changed from 39.5% to 42.5% at 640s, and then from 42.5% to 40.5% at 1814s. Fig. 5.4 shows comparison between the experimental and the predicted responses using Eq. (5.19). As seen, the predicted transient responses for  $DS_m$  agreed very well with the experimental responses.

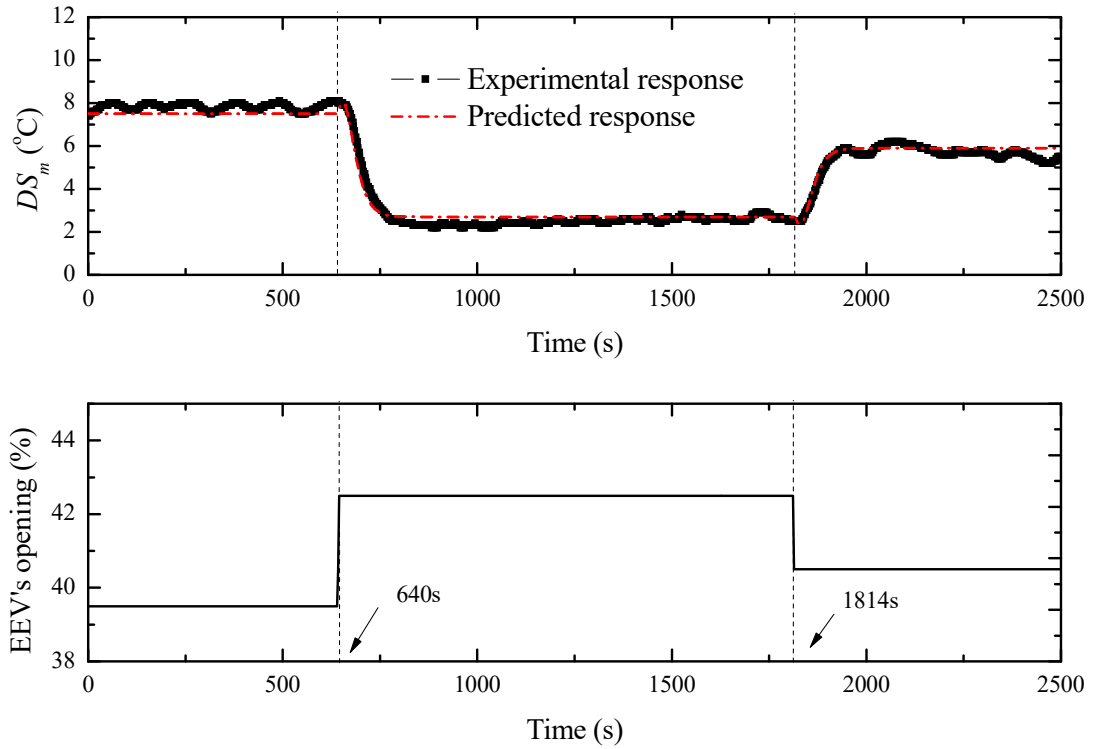


Fig. 5.4 The comparison between the predicted and experimental responses for the  $DS_m$

Therefore, the open-loop transfer function,  $L(s)$ , for the PI controlled EEV-evaporator control loop in the experimental DX A/C system can be expressed as:

$$L(s) = C(s)G(s) = \left(K_p + \frac{K_i}{s}\right) \left(\frac{1.6s - 0.1032}{270s^3 + 42.85s^2 + 2.903s + 0.6452}\right) \left(\frac{1}{1.6s + 1}\right) \quad (5.20)$$

#### 5.4 Stability analysis for the EEV-evaporator control loop using the Frequency Response Method

As mentioned in Chapter 2, the operational stability of a refrigeration system is directly affected by the operating performance of the EV-evaporator control loop.

Therefore, the analysis of the system operational stability of the experimental DX A/C system was via examining the stability of the EEV-evaporator control loop.

With the availability of the open-loop transfer function,  $L(s)$ , for the PI-controlled EEV-evaporator control loop, the Frequency Response Method in the classical control theory was used to assess the stability of the control loop by computing gain and phase margins, which can be used to determine if the control loop was stable or not.

#### **5.4.1 Nyquist stability criterion**

In using the Frequency Response Method in the classical control theory, Nyquist stability criterion is a graphical technique to determine the stability of a dynamic controlled system and has been widely used for designing and analyzing systems with feedback. The importance of Nyquist stability lies in the fact that it can be used to determine the relative degree of system stability by producing the phase and gain stability margins. With the help of Nyquist stability criterion, the stability of the EEV-evaporator control loop was investigated by analyzing the frequency response of its open-loop transfer function,  $L(s)$ .

##### *5.4.1.1 The influences of EEV's PI settings on the stability of the EEV-evaporator control loop*

The open-loop transfer function,  $L(s)$ , i.e., Eq. (5.20), for the PI-controlled EEV-evaporator control loop can be reproduced by designating  $K_p$  and  $K_i$  as variables, as:

$$L(s) = (K_p s + K_i) \frac{1.6(s - 0.0645)}{s(s + 0.0645)(18s + 1)(11.5s + 1)(1.6s + 1)} \quad (5.21)$$

From Eq. (5.21), the poles for  $L(s)$  were 0, -0.0645, -0.0555, -0.0869 and -0.625, respectively. None of the poles lay on the right hand side of  $s$ -plane. Hence, the stability of the closed EEV-evaporator control loop may be determined by examining whether the contour for the open-loop transfer function  $L(s)$ ,  $\Gamma_L$ , encircled the point (-1, 0) on its Nyquist diagram.

To examine the influences of EEV's PI settings on the stability of the control loop, based on the commonly used PI settings for a PI controlled EEV, two groups of different EEV's PI settings, each containing four study cases as shown in Table 5.2, were set to obtain their corresponding Nyquist diagrams shown in Fig. 5.5. As seen in Fig. 5.5(a) which is for Group I results, at a given integral gain,  $K_i = -0.025$ , when increasing the proportional gain,  $K_p$ ,  $\Gamma_L$  changed to tend to encircle the point (-1, 0). When  $K_p$  was less than -1,  $\Gamma_L$  did not encircle the point (-1, 0). However, when the values of  $K_p$  were greater than -1,  $\Gamma_L$  encircled the point (-1, 0), suggesting the instability of the EEV-evaporator control loop. On the other hand, as seen in Fig. 5.5(b) which is for Group II results, at a fixed proportional gain,  $K_p$ , increasing the integral gain,  $K_i$ , may also lead to instability of the EEV-evaporator control loop. Therefore, the EEV's PI settings could impact on the stability of the EEV-evaporator control loop.



Table 5.2 The stability of the EEV-evaporator control loop at two different groups of EEV's PI settings

Group	Study case	Proportional gain ( $K_p$ )	Integral gain ( $K_i$ )	Gain margin (dB)	Phase margin (°)	Stability
I	I - 1*	-0.5		0.636	4.93	stable
	I - 2*	-1		-1.08	-12.3	unstable
	I - 3	-1.5	-0.025	-3.51	-40.9	unstable
	I - 4	-2		-5.56	-61.6	unstable
II	II - 1		-0.01	5.63	63.9	stable
	II - 2		-0.020	2.44	20.2	stable
	II - 3*	-0.5	-0.025	0.636	4.93	stable
	II - 4*		-0.035	-2.61	-18.7	unstable

\* Study cases further experimentally verified in Section 5.5.1.

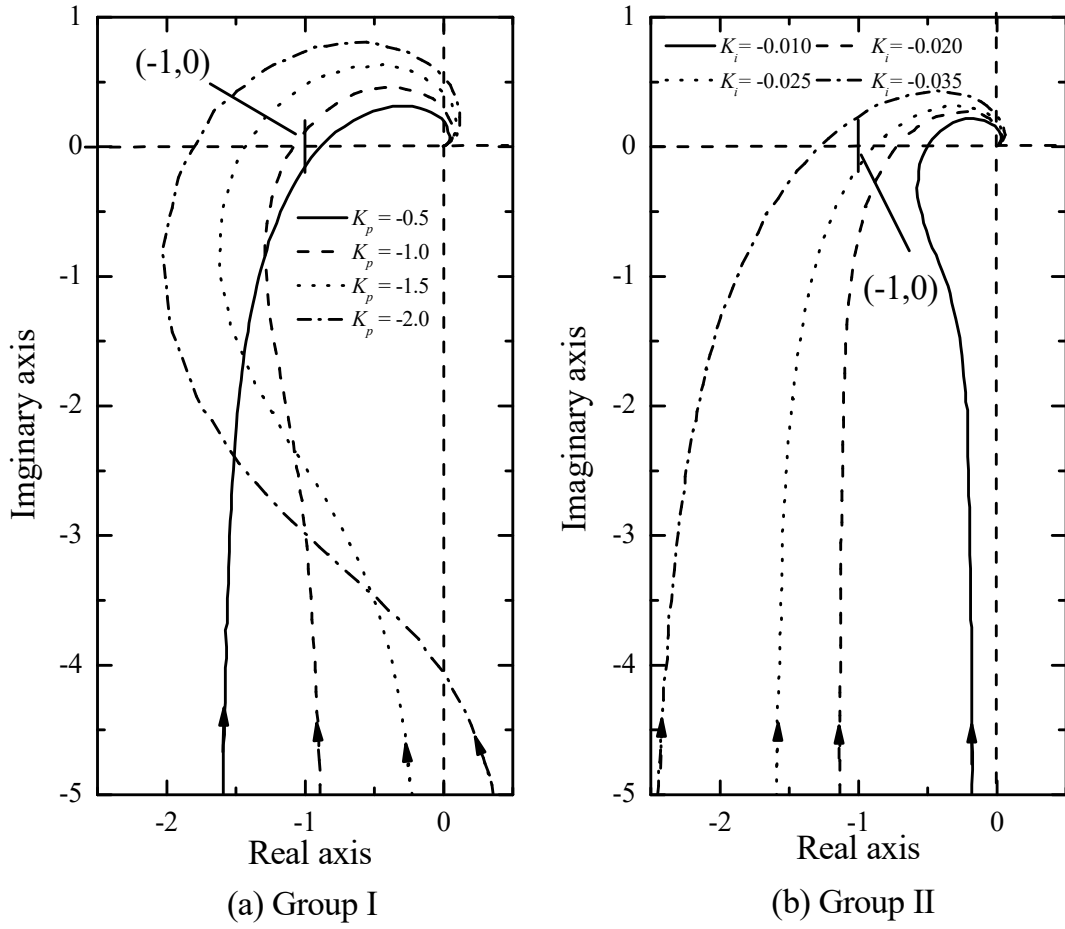


Fig. 5.5 Nyquist diagrams for  $L(s)$  at two different groups of EEV's PI settings

5.4.1.2 *The influences of the time constant of EEV's temperature sensor on the stability of the EEV-evaporator control loop*

For examining the effects of different time constants of EEV's temperature sensor on stability, Eq. (5.20) can also be reproduced by designating  $\tau_{se}$  as a variable, as:

$$L'(s) = (K_p s + K_i) \frac{1.6(s - 0.0645)}{s(s + 0.0645)(18s + 1)(11.5s + 1)(\tau_{se} s + 1)} \quad (5.22)$$

In Eq. (5.22), since none of the poles for  $L'(s)$  lay on the right hand side of the  $s$ -plane, the stability of the closed EEV-evaporator control loop may also be determined by examining whether the contour of  $L'(s)$ ,  $\Gamma_L$ , encircled the point  $(-1, 0)$  on its Nyquist diagram.

In the experimental DX A/C system, the average time constant,  $\tau_{se}$ , of its EEV's temperature sensor was estimated at  $\sim 1.6$ s, as mentioned in Section 5.3.2. However, if the contact between the temperature sensor and refrigerant pipe was insufficient, or EEV's temperature sensor and refrigerant pipe were not adequately insulated thermally, the time constant of the sensor would become relatively large. Therefore, three groups of different time constants,  $\tau_{se}$ , each containing five study cases for EEV's temperature sensor ranging from 0s to 200s at fixed PI settings, shown in Table 5.3, were set to examine their influences on the stability of the EEV-evaporator control loop using Eq. (5.22).

Table 5.3 The stability of the EEV-evaporator control loop at three different groups of time constant of EEV's temperature sensor

Group	Study case	Proportional gain ( $K_p$ )	Integral gain ( $K_i$ )	Time constant, $\tau_{se}$ (s)	Gain margin (dB)	Phase margin ( $^\circ$ )	Stability
	III - 1			0	0.56	7.29	stable
	III - 2			10	-0.44	-6.16	unstable
III	III - 3	-1	-0.015	50	1.65	13.6	stable
	III - 4			100	4.02	20.8	stable
	III - 5			200	7.02	21.2	stable
	IV - 1			0	-3.14	-34.2	unstable
	IV - 2			10	-4.19	-51.5	unstable
IV	IV - 3*	-1.5	-0.025	50	-2.39	-19.3	unstable
	IV - 4*			100	-0.28	-1.5	unstable
	IV - 5*			200	2.33	7.44	stable
	V - 1			0	-5.2	-53.4	unstable
	V - 2			10	-6.13	-72.5	unstable
V	V - 3	-2	-0.025	50	-3.66	-32.4	unstable
	V - 4			100	-0.916	-6.03	unstable
	V - 5			200	2.62	10.9	stable

\* Study cases further experimentally verified in Section 5.5.2.

The Nyquist diagrams for  $L'(s)$  at the three groups of different time constants are shown in Fig. 5.6. From Fig. 5.6(a) which is for Group III results, it can be seen that at fixed  $K_p = -1$  and  $K_i = -0.015$ , when  $\tau_{se} = 0s$ ,  $\Gamma_{L'}$  did not encircle the point  $(-1, 0)$ . However, when  $\tau_{se}$  was at 10s,  $\Gamma_{L'}$  encircled the point  $(-1, 0)$ , so that the EEV-evaporator control loop was unstable. When  $\tau_{se}$  was further increased to over 50s, the

$\Gamma_{L'}$  did not encircle the point  $(-1, 0)$  again, suggesting the stable operation of the control loop. Therefore, for an initially stable EEV-evaporator control loop, slowing down its rate of DS signal transfer by increasing  $\tau_{se}$  may first lead to instability, although further increasing  $\tau_{se}$  can return the loop to be stable again.

Figs. 5.6(b) and 5.6(c) show the Groups IV and V results, where the stability of an initially unstable EEV-evaporator control loop at different values of  $\tau_{se}$  was examined. As seen in Figs. 5.6(b) and 5.6(c), when  $\tau_{se} = 0$ s, the control loop at their PI settings, i.e.,  $K_p = -1.5$ ,  $K_i = -0.025$  and  $K_p = -2$ ,  $K_i = -0.025$ , were unstable initially. When increasing  $\tau_{se}$ ,  $\Gamma_{L'}$  would firstly move away from the point  $(-1, 0)$ , but if further increasing  $\tau_{se}$ , it would move back to be close to the point  $(-1, 0)$ , suggesting that the EEV-evaporator control loop tended to be stable as  $\tau_{se}$  became larger. When  $\tau_{se}$  was at 200s, the contour in Figs. 5.6(b) and 5.6(c),  $\Gamma_{L'}$ , did not encircle the point  $(-1, 0)$ , suggesting the stable operation of the EEV-evaporator control loop. Therefore, it can be observed when the EEV-evaporator control loop was initially unstable, increasing the time constant of the EEV's temperature sensor to a certain value for slowing down the rate of DS signal transfer may help eliminate the instability of the control loop.

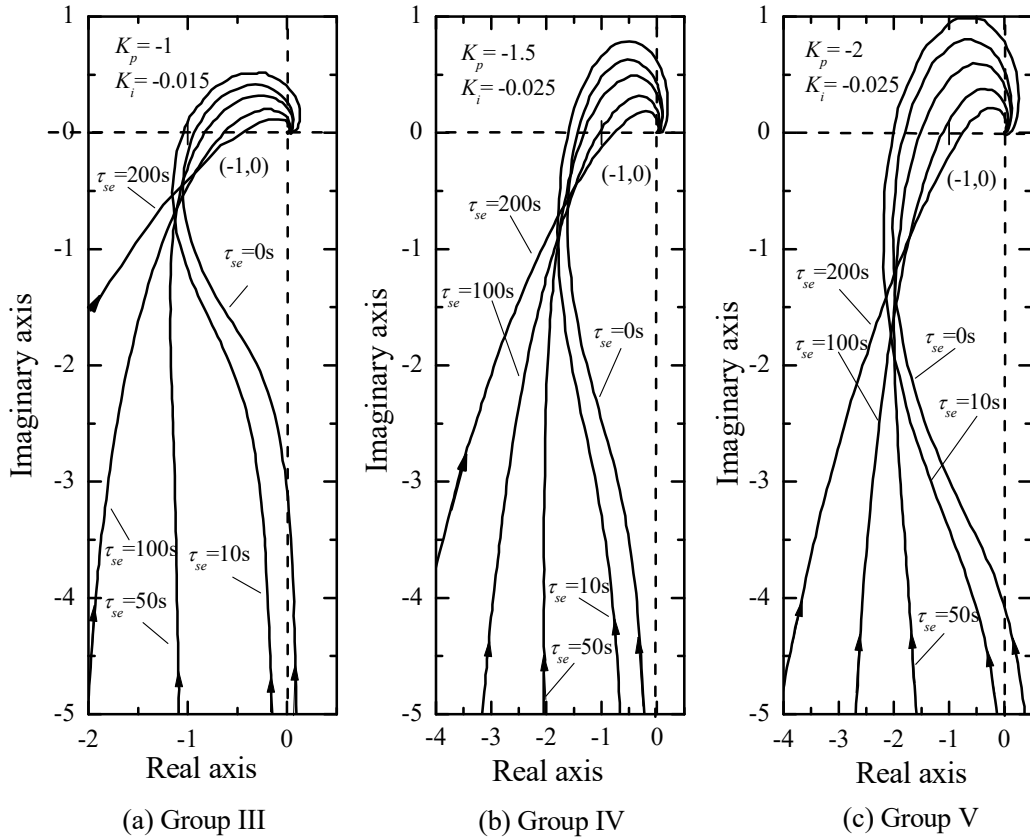


Fig. 5.6 Nyquist diagrams for  $L'(s)$  at three different groups of time constants of EEV's temperature sensor

Therefore, it can be seen that the rate of the DS signal transfer, as reflected by the time constant of EEV's temperature sensor, did impact the operational stability of the EEV-evaporator control loop, thus the DX A/C system. Furthermore, the observations from the analysis were that in general a larger time constant would lead to a stable operation of the DX A/C system.

## 5.5 Experimental validation

In order to validate the theoretical analysis results using the classical control theory presented in Section 5.4, experimental work was carried out for those study cases

marked with an asterisk in Tables 5.2 and 5.3, and experimental results are presented in this Section. The experiments were conducted using the experimental DX A/C system described in Chapter 4. When carrying out the experiments, for simulating the different time constants of EEV's temperature sensor,  $\tau_{se}$ , a first-order transfer function, i.e. Eq. (5.14), was incorporated into the EEV-evaporator control loop in the experimental DX A/C system, as shown in Fig. 5.7

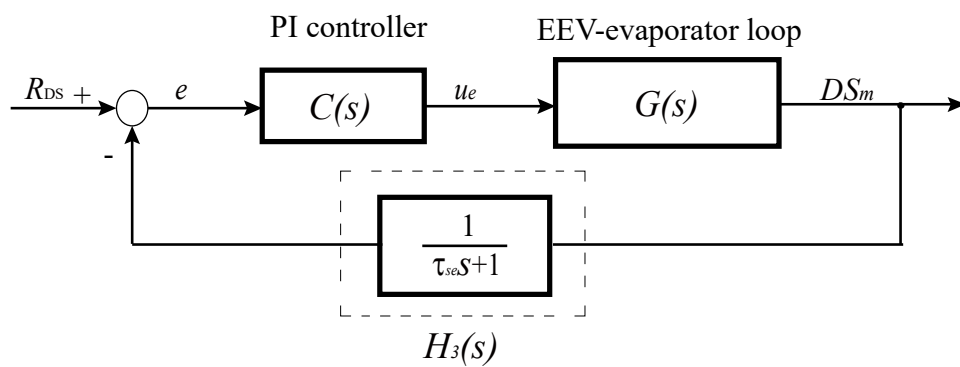


Fig. 5.7 Block diagram of the PI controlled EEV-evaporator control loop after incorporating  $H_3(s)$

During the experiments, the compressor and supply fan speeds were fixed at 4680 rpm and 2880 rpm, respectively. On the other hand, there were an air heater and a water heater in the LGUs. The two heaters were program-controlled to match the sensible and latent loads in the conditioned space, so that the air temperature and relative humidity entering the DX evaporator were maintained at 25 °C and 50%, respectively. The DS setting was fixed at 8 °C.

### 5.5.1 The influences of EEV's PI settings on the stability of the EEV-evaporator control loop

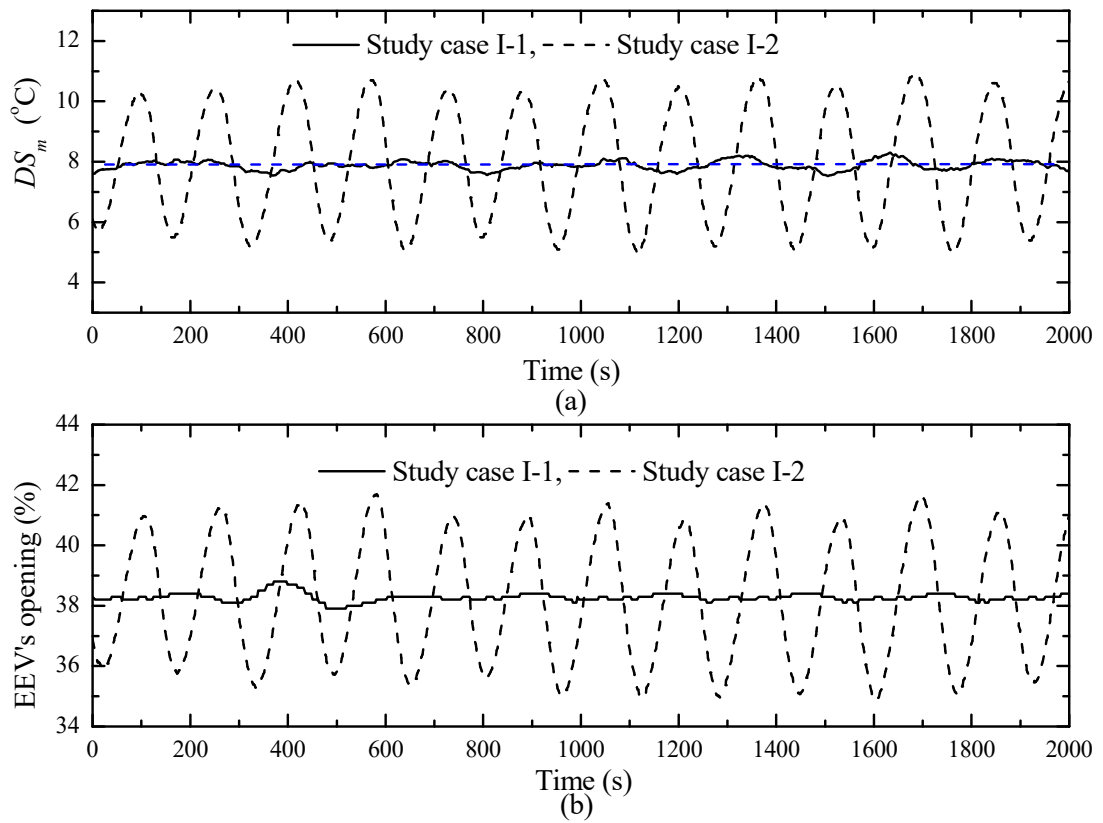


Fig. 5.8 Experimental validation results for the study cases I-1 and I-2



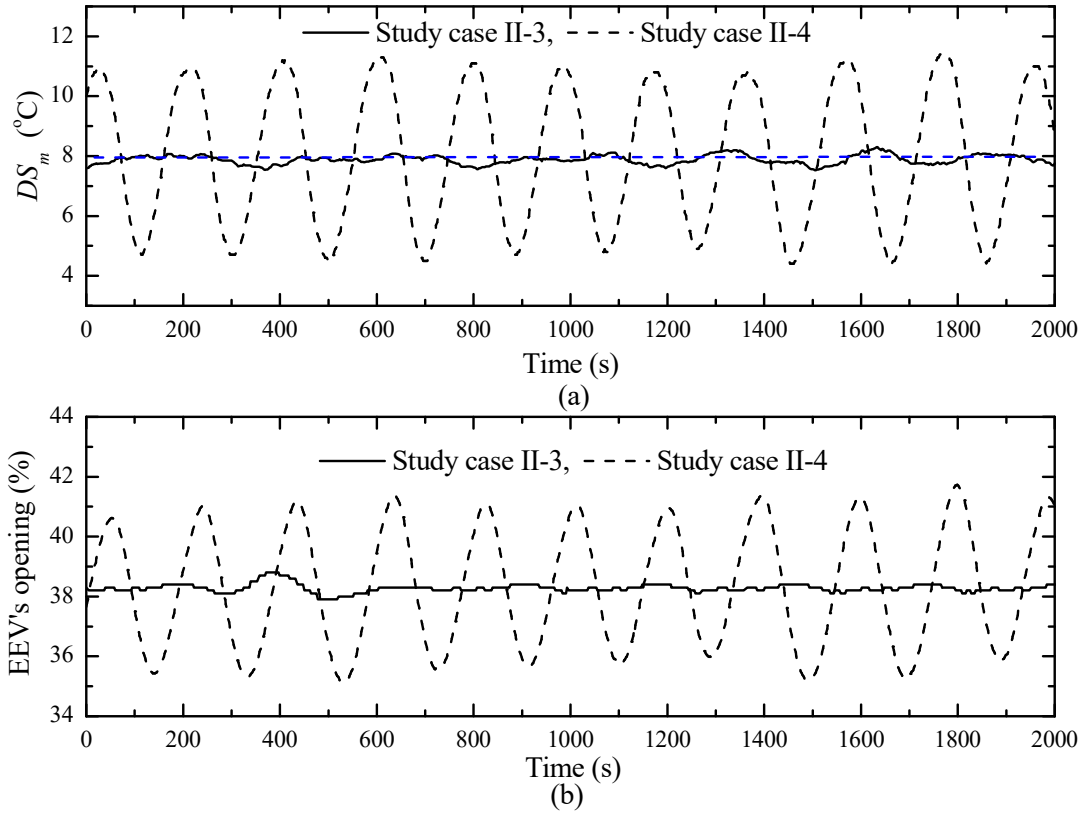


Fig. 5.9 Experimental validation results for the study cases II-3 and II-4

Figs. 5.8 and 5.9 show the experimental results of the  $DS_m$ , an indirectly controlled parameter, and EEV's opening, a directly controlled parameter, for the study cases I-1, I-2 and II-3, II-4, respectively, where different EEV's PI settings on the stability of the EEV-evaporator control loop were examined. As seen, the experimental results for both parameters verified the stability analysis results using the classical control theory presented in Section 5.4.1.1, that the EEV-evaporator control loop was stable for the study cases I-1 and II-3, but not stable for the study cases I-2 and II-4.

### 5.5.2 The influences of the time constants of EEV's temperature sensor on the stability of the EEV-evaporator control loop

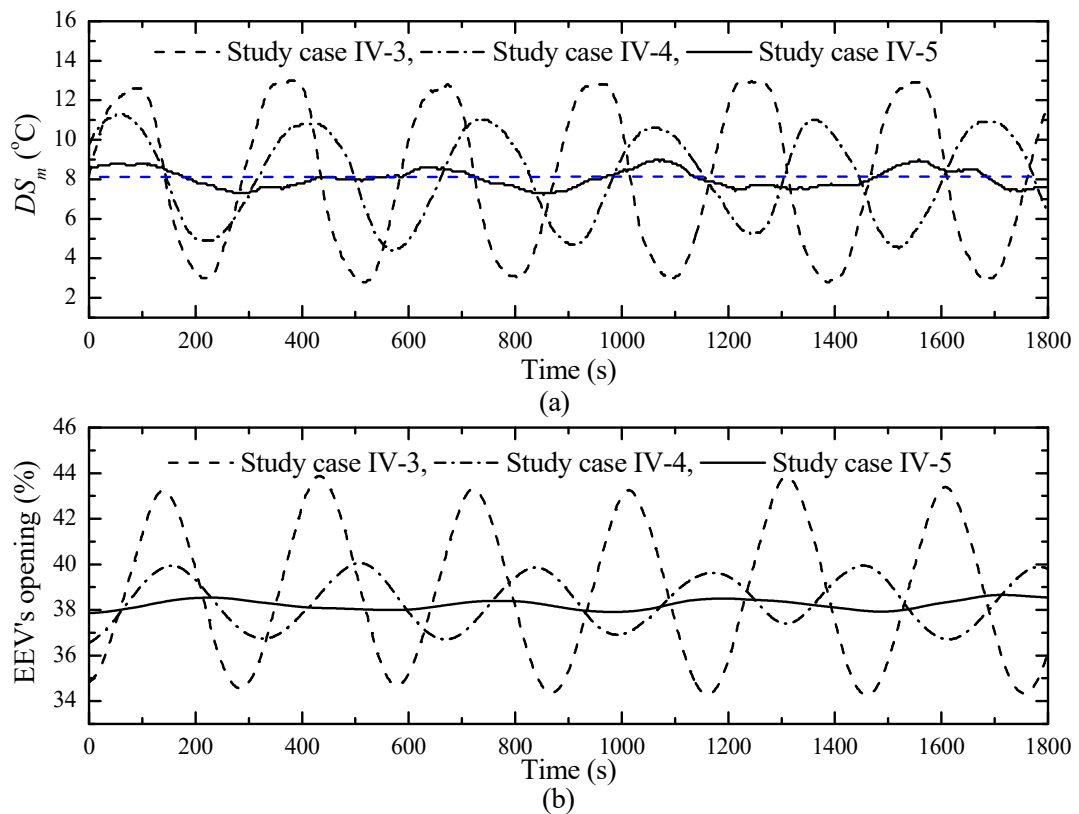


Fig. 5.10 Experimental validation results for the study cases IV-3, IV-4 and IV-5

Fig. 5.10 shows the experimental results of  $DS_m$  and EEV's opening for study cases IV-3, IV-4 and IV-5, respectively, where the influences of different time constants on the stability of the EEV-evaporator control loop were examined. As seen from the Figures, the experimental results for both indirectly and directly controlled parameters verified the stability analysis results using the classical control theory presented in Section 5.4.1.2, that the EEV-evaporator control loop was not stable for the study cases IV-3 and IV-4, but stable for the study case IV-5.

In addition, it is noted the experimental and analysis results reported in this Chapter were based on only one set of the operating condition for the experimental DX A/C system. The different operating conditions only influenced the identified parameters of the transfer function of the evaporator, and the transient response for the DS at evaporator exit to a sudden change in refrigerant mass flow rate supplied to the evaporator can always be approximated by a second-order plus dead-time process. Therefore, the general variation trends observed and the related analysis should remain valid, although the absolute numerical value may be different at different operating conditions .

## **5.6 Discussions**

As mentioned earlier in Chapter 2, there have been two views on the causes for the hunting in a refrigeration system: the inherent characteristics of an evaporator and the operational characteristics of an EV. In a TEV-controlled refrigeration system, it was previously shown that both of the TEV's control characteristics, such as its static superheat setting and valve gain [Lenger et al., 1998; Mithraratne and Wijesundera, 2001, 2002; Mithraratne et al., 2000; Tassou and Al-Nizari, 1993a] and the characteristics of TEV's sensing bulb, including the time constant of TEV's sensing bulb, the thermal resistance between the sensing bulb and refrigerant pipe and the bulb location [Broersen and Vanderjagt, 1980; Chen and Jiang, 1990; Ibrahim, 1998, 2001; Lenger et al., 1998; Mithraratne and Wijesundera, 2001, 2002; Mithraratne et al., 2000; Mulay et al., 2005; Stoecker, 1966; Tassou and Al-Nizari, 1993a], did influence the stability of refrigeration systems. On the other hand, since there were no previous studies on the influences of EEV's PI settings and time constant of the EEV's

temperature sensor on the stability of an EEV controlled refrigeration system, the study results presented in this Chapter filled the gap and further confirmed that the characteristics of an EEV can also influence the stability of an EEV controlled refrigeration system in the following two aspects:

- The control characteristics of a PI-controlled EEV impacted the stability of the EEV-evaporator control loop, thus the refrigeration system. Generally, a larger proportional gain or integral gain would lead to a higher chance for the EEV-controlled refrigeration system to become unstable.
- The theoretical analysis using the classical control theory and the experimental results shown in Sections 5.4.1.2 and 5.5.2, respectively, for the influences of the dynamic characteristics of EEV's temperature sensor on the operational stability of the EEV-evaporator control loop, are the first of its kind reported in open literature. The results demonstrated that a larger time constant of EEV's temperature sensor can also lead to a higher chance for the EEV-evaporator loop to become stable, at however the expense of reducing the sensitivity of superheat control for the EEV during normal operation.

The analysis and experimental results reported clearly suggested that a larger change, as reflected by the controller's P and I settings, and a faster change, as reflected by the rate of DS signal transfer, or the time constant of EEV's temperature sensor, of the refrigerant mass flow supplied to an evaporator, would very likely lead to an instability operation of the EEV-evaporator control loop, thus the DX A/C system. These results also suggested that, similar to the influences of the dynamic characteristics of sensing bulb transients on the operational stability of a TEV-controlled refrigeration system as

mentioned in Chapter 2, slowing down the rate of DS signal transfer by increasing the time constant of EEV's temperature sensor would be beneficial to the operational stability of an EEV-controlled refrigeration system. These results further confirmed that the operating characteristics of an EV in a refrigeration system could impact its operational stability. On the other hand, as a constant valve gain was used in the current study, a further study on investigating the influences of varying EEV's valve gain on the operational stability of the EEV-evaporator control loop should be carried out.

Furthermore, the experimental results also suggested an effective approach to mitigate instability problem encountered in an EEV controlled refrigeration system by incorporating a first-order transfer function in its EEV-evaporator control loop to slow down the rate of DS signal transfer.

## **5.7 Conclusion**

A study on the influences of the operational characteristics of a PI controlled EEV on the operational stability of a DX A/C system has been carried out and study results are reported in this chapter. Using the classical control theory, the influences of EEV's PI settings and time constants of EEV's temperature sensor on the system operational stability were analyzed and further experimentally verified using the experimental DX A/C system.

The theoretical analysis and experimental results showed that EEV's PI settings and the time constant of EEV's temperature sensor which affected the rate of DS signal

transfer, did impact the operational stability of the EEV-evaporator control loop, thus the DX A/C system. A larger proportional gain or integral gain of the EEV's PI controller, and faster DS signal transfer due to a smaller time constant of EEV's temperature sensor would very likely lead to system instability. The study results further confirmed that the operating characteristics of an EV impacted a refrigeration system operational stability and suggested an effective approach to mitigate instability problem encountered in an EEV controlled refrigeration system by incorporating a first-order transfer function in its EEV-evaporator control loop to slow down the rate of DS signal transfer.

## **Chapter 6**

### **Inherent operational characteristics and operational stability of the experimental VS DX A/C system**

#### **6.1 Introduction**

The study reported in Chapter 5 indicated that the operational characteristics of the EEV did impact the operational stability of the experimental EEV-controlled DX A/C system. On the other hand, while the extensive application of VS technique to DX A/C systems has made the continuous control of compressor speed and supply air fan speed more practical, paving the way to simultaneously control indoor air temperature and humidity, VS operation of a DX A/C system may also potentially lead to its operational instability [Qi et al., 2010a]. As a matter of fact, in a VS DX A/C system, the operational characteristics of its DX evaporator including VS operation and different inlet air states would result in different surface wetness of its DX evaporator, significantly affecting the air side heat transfer, and hence, the overall heat transfer characteristics in the DX evaporator, leading to a potential change in the operating DS at evaporator exit. Consequently, the operational stability of a VS DX A/C system may also be affected due to its VS operation and different inlet air states.

However, as presented earlier in Section 2.3.3, for a VS DX A/C system, while its inherent operational characteristics expressed in terms of the inherent correlations (ICs) between its output total cooling capacity (TCC) and equipment sensible heat ratio (E SHR) at different combinations of compressor and supply fan speeds and inlet air states have been extensively studied [Li et al., 2014; Xu et al., 2010], the issues of

operational stability were not taken into consideration. No studies on investigating the influences of varying both compressor speed and supply fan speed at different inlet air states on operational stability may be identified. Therefore, a follow-up study on the inherent operational characteristics of a VS DX A/C system considering its operational stability at i) different combinations of compressor and supply fan speeds, ii) different DS settings and iii) different inlet air states, has been carried out and the study results are reported in this Chapter. This Chapter is organized as follows. Firstly, the experimental conditions, procedures and data interpretation are detailed. Secondly, the experimental results of the inherent operational characteristics of the experimental VS DX A/C system expressed in terms of the ICs between its output TCC and E SHR considering its operational stability are presented. This is followed by reporting the related analysis on the obtained experimental results. Finally, conclusions of this Chapter are given.

## **6.2 Experimental conditions, procedures and data interpretation**

All the experiments were carried out in the experimental VS DX A/C system detailed in Chapter 4. The uncertainties for the sensors/ instruments and the calculated operating parameters used in the current study are given in Table 6.1.



Table 6.1. Measurement/calculation uncertainty of system operating parameters

Operating parameter	Uncertainty	Unit
Air dry-bulb temperature	±0.1 (platinum RTD)	°C
Air wet-bulb temperature	±0.1 (platinum RTD)	°C
Air static pressure difference	±0.1% (differential pressure transducer)	--
Refrigerant temperature	±0.1 (platinum RTD)	°C
Refrigerant pressure	±0.2% (pressure transducer)	--
DS	±0.18 (calculated)	°C
Air flow rate	±1.2% (calculated)	m <sup>3</sup> /h
TCC	1.85% ~ 3.89% (calculated)	kW
E SHR	1.64% ~ 4.02% (calculated)	--

In order to study the inherent operational characteristics of the experimental VS DX A/C system considering the operational stability at different speed combinations, different inlet air states and DS settings, five experimental inlet air states with three different DS settings as shown in Table 6.2, were used. These five inlet air states covered typical indoor air settings for comfort air conditioning. At each of the five inlet air states, typical DS settings used in a refrigeration system at 4 °C, 6 °C and 8 °C were adopted, respectively.

Table 6.2. The experimental cases of inlet air states and DS settings

Group	Case	$T_{db}$ (°C)	$T_{wb}$ (°C)	RH (%)	DS setting (°C)
RH constant	T-23	23.0	16.2	50	4, 6, 8
	T-25	25.0	17.9	50	4, 6, 8
	T-27	27.0	19.5	50	4, 6, 8
T constant	RH-40	25.0	16.2	40	4, 6, 8
	RH-50*	25.0	17.9	50	4, 6, 8
	RH-60	25.0	19.6	60	4, 6, 8

\* Same setting as that in Case T-25

At each of the five inlet air states, the experimental VS DX A/C system was operated at a specified DS setting under different speed combinations as shown in Table 6.3. At a given experimental case listed in Table 6.2, for example, 25 °C/ 50% RH (Case T-25) at 6 °C DS setting, there were five different speeds for the compressor and six for the supply air fan, respectively, resulting in a total of 30 speed combinations.

Table 6.3. The experimental compressor and supply fan speeds

Compressor							
% of max speed		40	50	60	70	80	
Supply:	freq. (Hz)	54	60	66	72	78	
Supply fan							
% of max speed		50	60	70	80	90	100
Supply:	freq. (Hz)	30	36	42	48	54	60
	Air flow rate (m <sup>3</sup> /h)	580	705	832	960	1080	1200

Compressor maximum speed: 90 Hz  
 Supply fan maximum speed: 60 Hz

During all experiments, the cooling airflow rate for the condenser was maintained constant at 4100 m<sup>3</sup>/h, with a fixed condenser cooling air inlet temperature at 35 °C.

The EEV was PI controlled for regulating its opening in response to the DS at evaporator exit. Fixed PI parameters, -0.5 for the proportional gain and 40s for the integral time, were adopted for the PI controller in all experiments. A prescribed range of fluctuation of  $\pm 0.5$  °C in DS was set to assess whether the operation of the VS DX A/C system was stable or not.

The experimental procedures were as follows. At a specific combination of compressor and supply fan speeds listed in Table 6.3, the LGUs and EEV were respectively controlled, so that the required experimental inlet air state and DS setting shown in Table 6.2 were achieved. When the variations for both air dry-bulb and wet-bulb temperatures, namely  $T_{db}$  and  $T_{wb}$ , were less than  $\pm 0.1$  °C, a steady state operation for the experimental VS DX A/C system arrived. Then the operating parameters were recorded continuously for 15 min at an interval of 1 min and the averaged measured data used for evaluating the output TCC and E SHR of the experimental VS DX A/C system. On the other hand, at a given inlet air state and DS setting, the speed combinations of compressor and supply fan at which the operation of the VS DX A/C system was unstable were marked as the unstable operating speed combinations where the variation of the operating DS was outside the prescribed range of  $\pm 0.5$  °C of its setting at a steady-state operation. Given that the difference between two experimental fan or compressor speeds listed in Table 6.3 was 10% of their respective maximum speeds, in order to accurately identify an unstable operating region in a TCC-SHR trapezoid, additional experiments were carried out between an identified unstable operating speed combination and an identified stable one. This was done by changing either the compressor or the fan speed, or both, at an interval of 2% of its maximum speed, respectively, from the identified stable operating speed combination. Then at a

specific operating point of speed combination, if the operating DS was outside the prescribed range of  $\pm 0.5$  °C, this specific operating point of speed combination was regarded as a critical unstable operating point of speed combination. In order to be able to draw an unstable region in the TCC-SHR trapezoid, at least three critical operating points of speed combination were identified.

The output sensible cooling capacity of the experimental DX A/C system was evaluated by

$$Q_s = M_a C_{pa} (T_{dbi} - T_{dbo}) \quad (6.1)$$

The total output cooling capacity of the DX A/C system was then evaluated by

$$\text{TCC} = M_a (h_{ai} - h_{ao}) \quad (6.2)$$

Therefore, E SHR was obtained by

$$\text{E SHR} = \frac{Q_s}{\text{TCC}} = \frac{C_{pa} (T_{dbi} - T_{dbo})}{(h_{ai} - h_{ao})} \quad (6.3)$$

### 6.3 Experimental results

By carrying out the experiments in all the experimental cases as specified in Tables 6.2 and 6.3, so that not only the output TCC and E SHR of the experimental VS DX A/C system may be obtained, but also its operational stability at different speed

combinations and DS settings evaluated. Totally fifteen sets of experimental results at five inlet air states, corresponding to the five experimental cases in Table 6.2, with three different DS settings in each case, were obtained.

As a further development to the ICs between TCC and E SHR previously obtained [Li et al., 2014; Xu et al., 2010], the experimental results of TCC and E SHR for all the experimental cases in the current study were also  $X$  (TCC) –  $Y$  (E SHR) plotted, but with an unstable region also marked on each of the trapezoids, which was so obtained with the availability of at least three critical operating points of speed combination, as mentioned in Section 6.2.

The organization of the experimental results presented in this Section is as follows. Section 6.3.1 presents the experimental results for the experimental Case T-25, at 8 °C DS setting, as an example of the 15 cases of the experimental results. In Sections 6.3.2 and 6.3.3, the influences of the different DS settings and inlet air states on the inherent operational characteristics of the experimental VS DX A/C system considering the operational stability are discussed.

### 6.3.1 Experimental results of Case T-25 at 8 °C DS setting

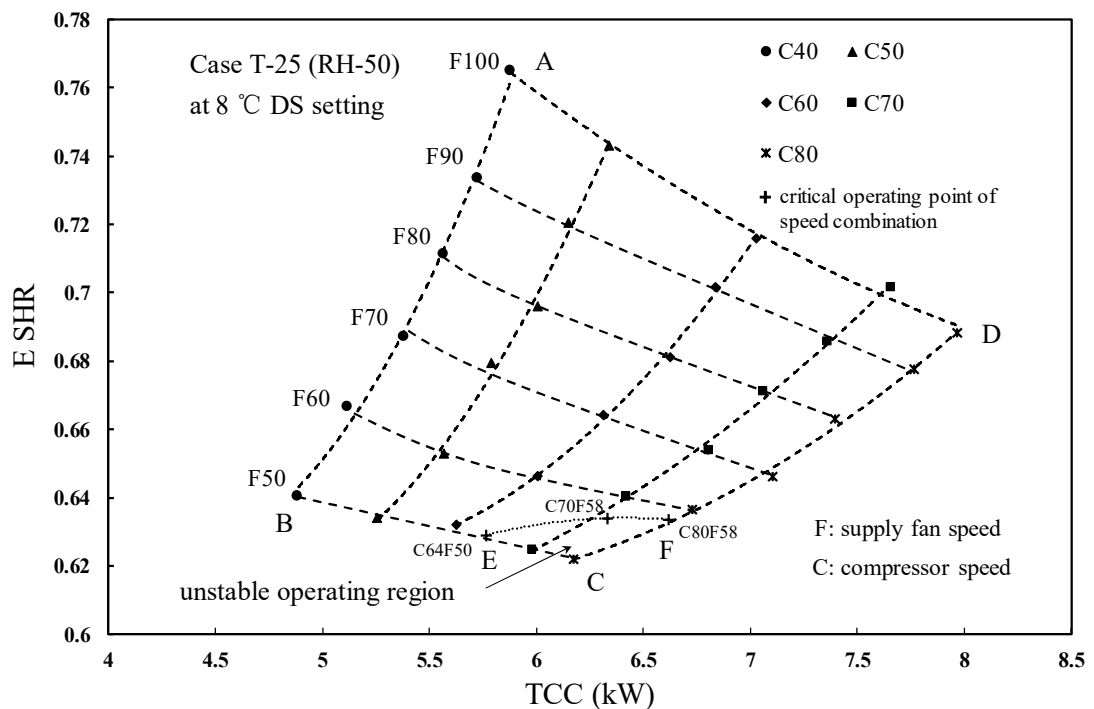


Fig. 6.1. The IC<sub>os</sub> of the experimental VS DX A/C system for Case T-25 at 8 °C DS setting

Fig. 6.1 shows the experimental results, or the IC between TCC and E SHR considering operational stability (IC<sub>os</sub>), for Case T-25 at 8 °C DS setting. Three critical operating points of speed combinations, namely, C64F50 (i.e., 64% compressor speed and 50% fan speed), C70F58 and C80F58, were identified, so that an unstable operating region was depicted in the trapezoid, as shown in Fig. 6.1. As seen, the unstable operating region, E-C-F, was located at the bottom of the trapezoid where the experimental DX A/C system was operated at a higher compressor speed but a lower supply fan speed. With the consideration of the operational safety and energy efficiency, a VS DX A/C system should not be allowed to operate within an unstable operating region.

Figs 6.2 and 6.3 show the measured variations in the operating DS after the change in compressor and supply fan speeds, respectively, in the experimental Case T-25 at 8 °C DS setting, where the influences of VS operation of the VS DX A/C system on its operational stability are demonstrated. As seen in Fig. 6.2, at 1760s, when the compressor speed was increased from 50% to 80% of its maximum speed at a constant fan speed of 50% of its maximum speed (F50), i.e., at point C in Fig. 6.1, the operating DS started to fluctuate at  $\sim \pm 2.5$  °C around 8 °C at steady state, suggesting that increasing only the compressor speed could lead to operational instability. Furthermore, Fig. 6.3 shows the measured variations in the operating DS when the fan speed was subject to a number of step changes at a constant compressor speed of 80% of its maximum speed (C80). As seen, when the supply fan speed was reduced twice, from 80% to 70% at 364s and from 70% to 60% at 2330s, respectively, a stable operating DS was maintained after some fluctuations immediately after speed changes. However, when the fan speed was further reduced to 50% at 3880s, i.e., also at point C, the operating DS significantly fluctuated at  $\sim \pm 2$  °C around the DS setting of 8 °C. Lastly, when the fan speed was raised from 50% to 70% at 5734s, the operating DS returned to be stable again after significant fluctuations shortly after the speed change. Therefore, it became very clear that the VS operation of a VS DX A/C system can significantly impact its operational stability.

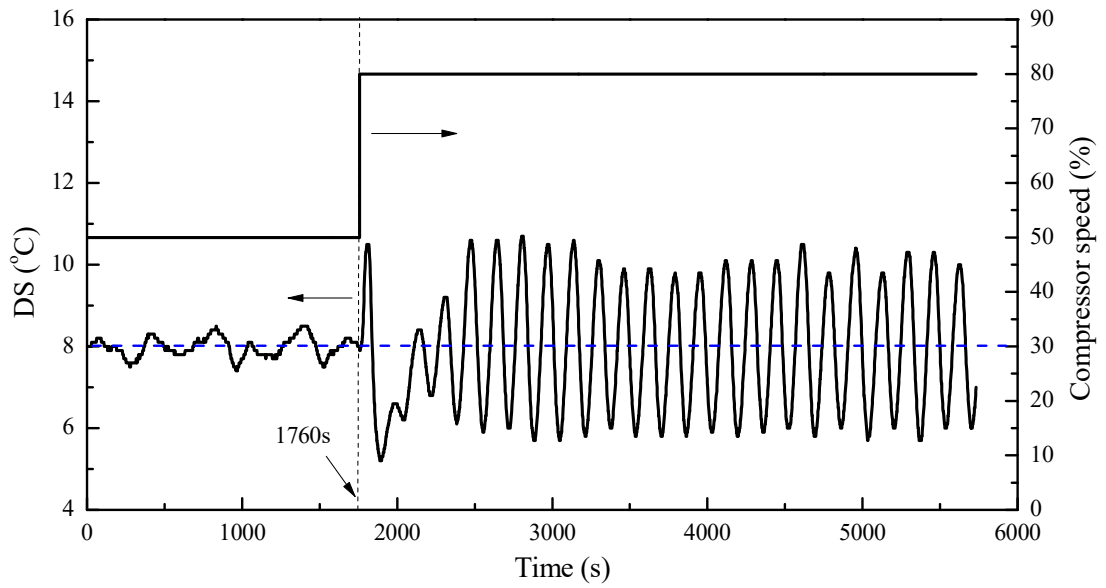


Fig. 6.2. The measured variations in the operating DS after increasing only the compressor speed in Case T-25 and 8 °C DS setting

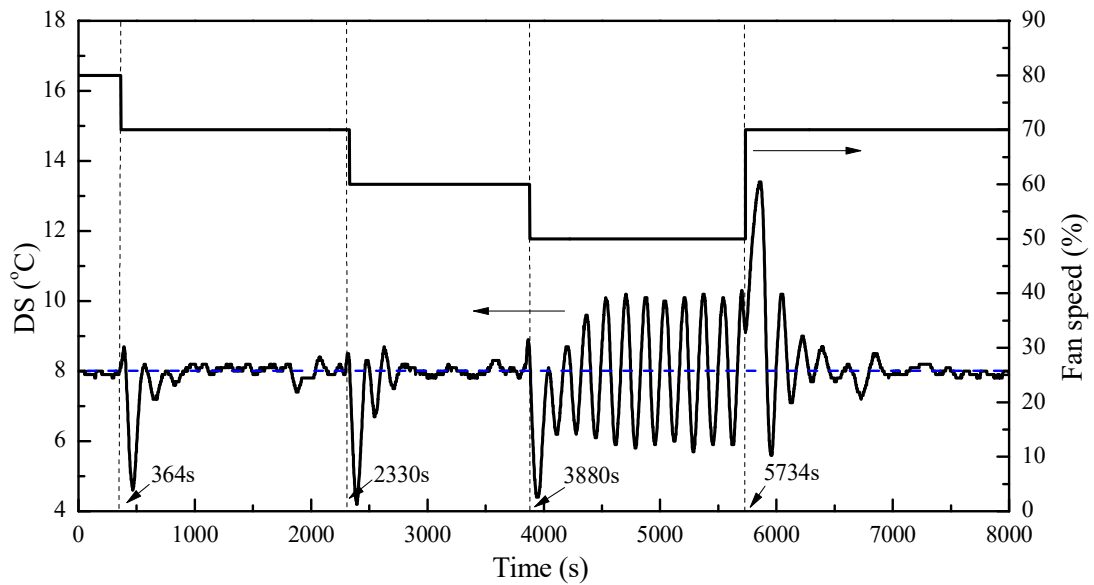


Fig. 6.3. The measured variation in the operating DS after changing only the fan speed in Case T-25 and 8 °C DS setting



### 6.3.2 The ICs<sub>os</sub> of the experimental VS DX A/C system at different DS settings

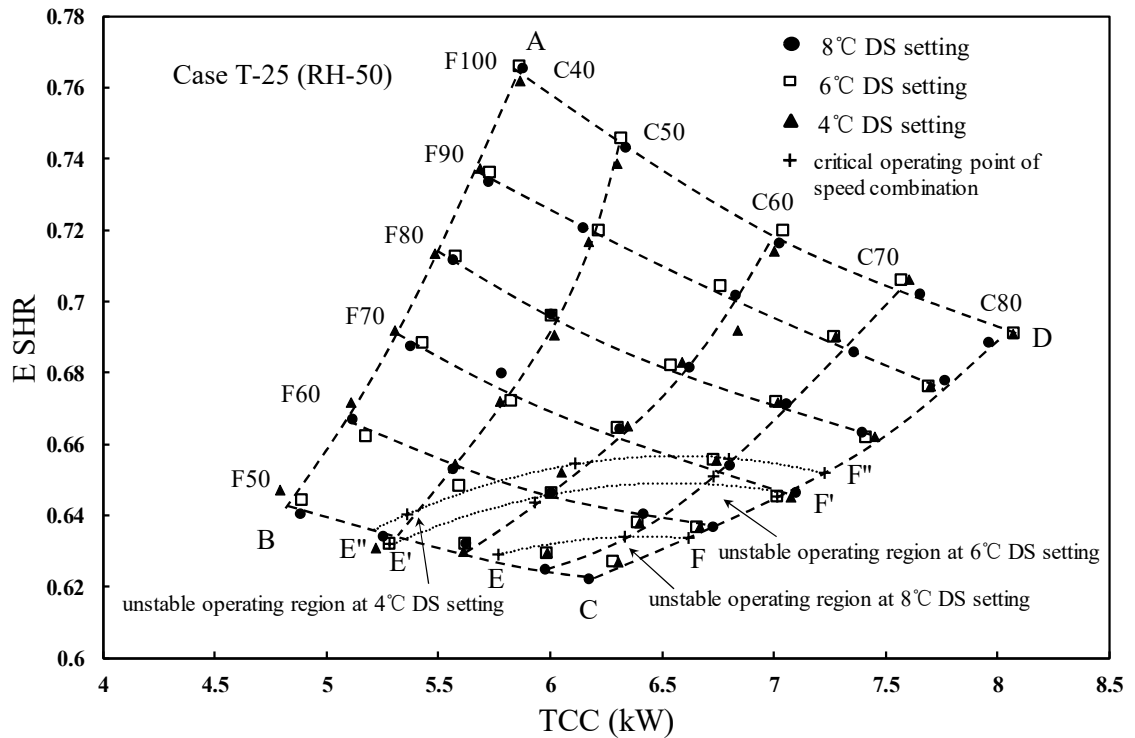


Fig. 6.4. The ICs<sub>os</sub> of the experimental VS DX A/C system for Case T-25 at three different DS settings

Fig. 6.4 shows the experimental results for Case T-25 at different DS settings. As seen, at a given speed combination, different DS settings would not significantly influence the values of TCC and E SHR. This may be due to the fact that at steady state operation of a DX A/C system, the superheated region occupied only small percentage of evaporator's volume, and the heat transfer coefficient in the superheated region was much smaller than that in the two-phase region, hence the heat transfer in the superheated region did not remarkably influence the values of TCC and E SHR at different DS settings. Consequently, the inherent characteristic between TCC and E SHR at various speed combinations under different DS settings almost overlapped and may therefore be simply represented by a trapezoid A-B-C-D, as shown in Fig. 6.4.

On the other hand, three unstable regions in the trapezoid A-B-C-D corresponding to the three DS settings, namely, 4 °C, 6 °C and 8 °C, were also identified and plotted in Fig. 6.4, following the experimental procedure in Section 6.2. As seen, all the three unstable operating regions were located at the lower part of the trapezoid where the DX A/C system was operated at a higher compressor speed and a lower supply fan speed. However, as seen, the size of the unstable operating region at 4 °C DS setting was the largest, and that at 6 °C DS setting the second largest, with that at 8 °C DS setting being the smallest. This suggested that at a lower DS setting there were more unstable operating points of speed combinations.

Fig. 6.5 shows the measured variations in the operating DS following a change in DS setting at an operating point of speed combination of C80F60 (Compressor 80%, Fan 60%), in the experimental Case T-25, where the influences of different DS settings on the operational stability of the VS DX A/C system are demonstrated. As seen, the operating DS was stable at 8 °C DS setting at first. When the DS setting was reduced to 6 °C at 218s, the operating DS started to oscillate and its fluctuation range was about  $\pm 1$  °C around 6 °C. However, the operating DS returned to be stable again after the DS setting was reset to 8 °C at 2040s. Therefore, it became clear that the different DS settings could significantly impact the operational stability of the experimental VS DX A/C system. A lower DS setting would more likely lead to system instability.

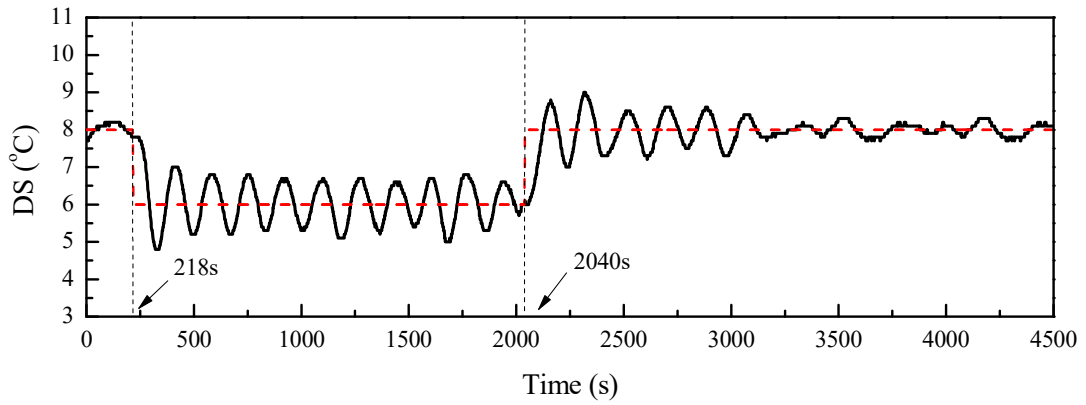


Fig. 6.5. The measured variations in the operating DS following a change in the DS setting at an operating point of C80F60 in Case T-25

### 6.3.3 The IC<sub>os</sub> of the experimental VS DX A/C system at different inlet air states

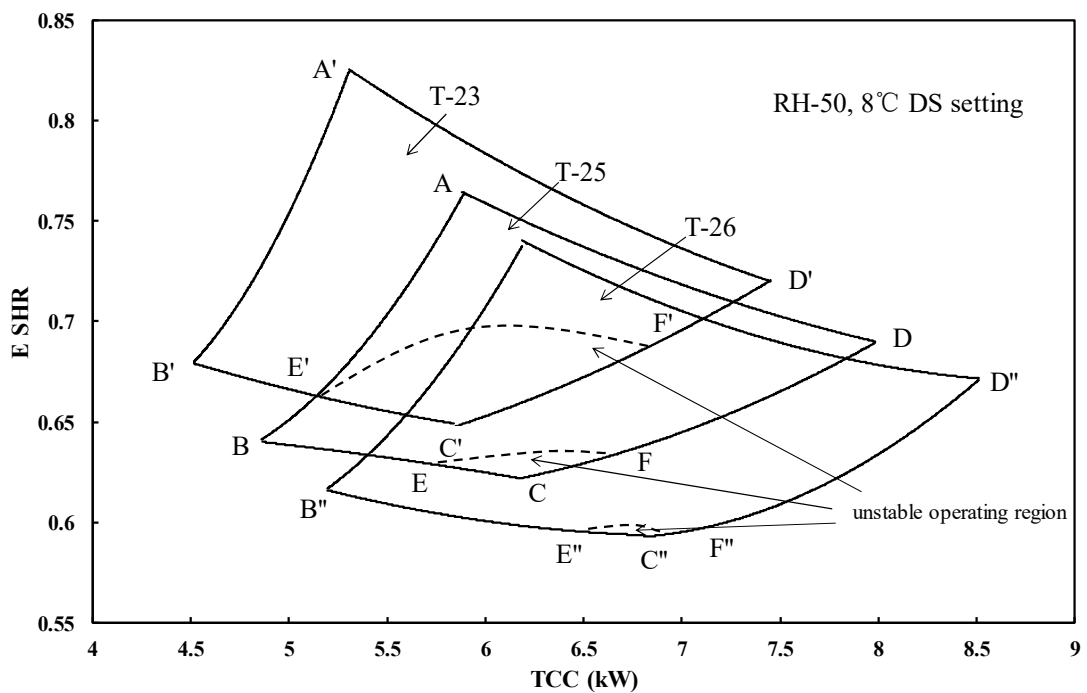


Fig. 6.6. The IC<sub>s\_os</sub> of the experimental VS DX A/C system for the constant RH group at 8 °C DS setting

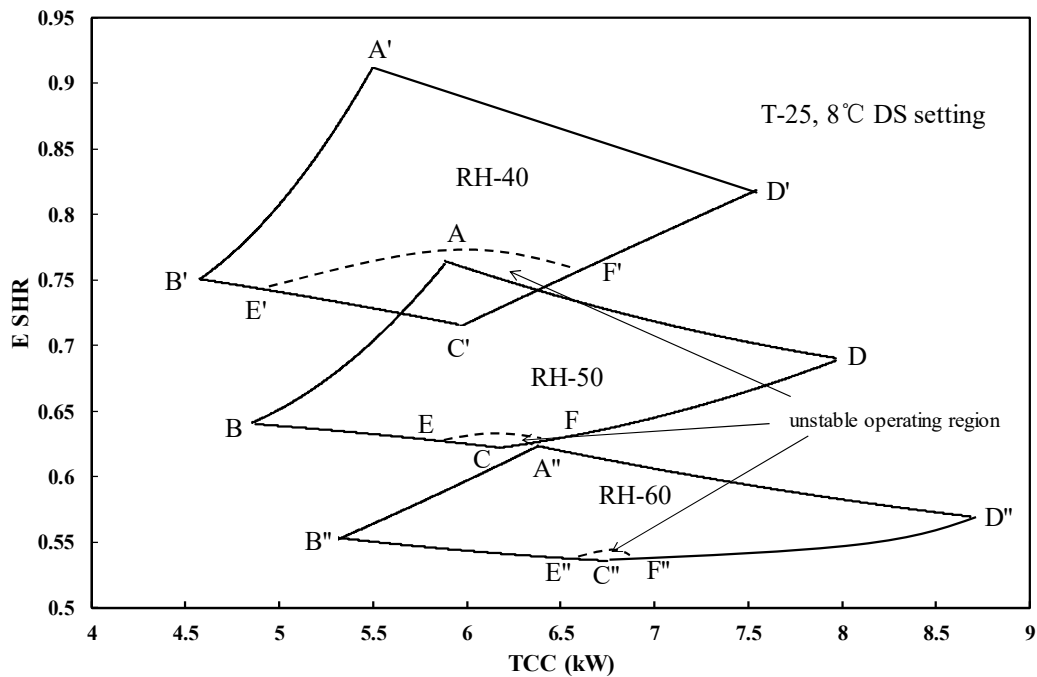


Fig. 6.7. The ICs<sub>os</sub> of the experimental VS DX A/C system for the constant temperature group at 8 °C DS setting

Figs 6.6 and 6.7 show the experimental results for the constant RH group (Case T-23, T-25 and T-27) and the constant temperature group (Case RH-40, RH-50 and RH-60) respectively, but all at 8 °C DS setting.

The unstable regions for both groups were identified and are plotted using the dash line in the trapezoids shown in Figs 6.6 and 6.7, respectively. As seen, while all the unstable operating regions at different inlet air states were also located at the lower part of their trapezoids, their sizes were significantly affected by the inlet air states. A lower inlet air temperature or RH would lead to a larger unstable operating region. In addition, a similar phenomenon was also observed when the DX A/C system was operated at the other two DS settings, namely, 4 °C and 6 °C. Therefore, it can be concluded that the operational stability of the experimental VS DX A/C system would

also be affected by its inlet air states, and a lower inlet air temperature or RH would be more easily to give rise to operational instability.

#### **6.4 Discussions**

In Sections 6.3.1-6.3.3, the ICs<sub>os</sub> of the experimental VS DX A/C system at different combinations of compressor speed and supply fan speed, different DS settings and different inlet air states are presented. As seen, similar to the results in those previously reported studies [Li et al., 2014; Xu et al., 2010], the output TCC and E SHR under different combinations of compressor speed and supply fan speed were correlated to each other but mutually constrained within a trapezoid A-B-C-D, although a different experimental VS DX A/C system was used in the current study. Furthermore, the experimental results of the inherent operational characteristics in terms of TCC-E SHR relationship under different inlet air states as shown in Figs. 6.6 and 6.7 were also similar to those previously presented [Li et al., 2014]. The experimental results on the influences different speed combinations of compressor and supply fan and different inlet air states on the inherent operational characteristics in terms of TCC-E SHR trapezoid were previously analysed [Li et al., 2014]. Therefore, in this Section, an analysis on the obtained experimental results demonstrating the influences of different DS settings, different speed combinations of compressor and supply fan and different inlet air states on the operational stability of the experimental VS DX A/C system is given.

#### 6.4.1 The influences of different DS settings on the operation stability of the experimental VS DX A/C system

The experimental results of the ICs<sub>os</sub> at different DS settings presented in Section 6.3.2 have demonstrated that there would be more unstable operating points of speed combinations, and thus a larger unstable operating region at a smaller DS setting in a TCC-E SHR trapezoid. This may well be explained by the conventional MSS theory [Huelle, 1972; Huelle, 1967] mentioned in Chapter 2 that, at a lower DS, the mixture-vapor transition point inside an evaporator would move to be close to evaporator exit, causing the system to be more prone to unstable operation. As seen from the MSS line shown in Fig. 6.8, at a fixed cooling capacity, reducing the DS from point A to B, would cause the system to move into an unstable operating region. Therefore, at a fixed speed combination of compressor and supply fan corresponding to a fixed combination of sensible and latent cooling capacities, decreasing the DS setting for the VS DX A/C system would lead to a higher chance of unstable operation.

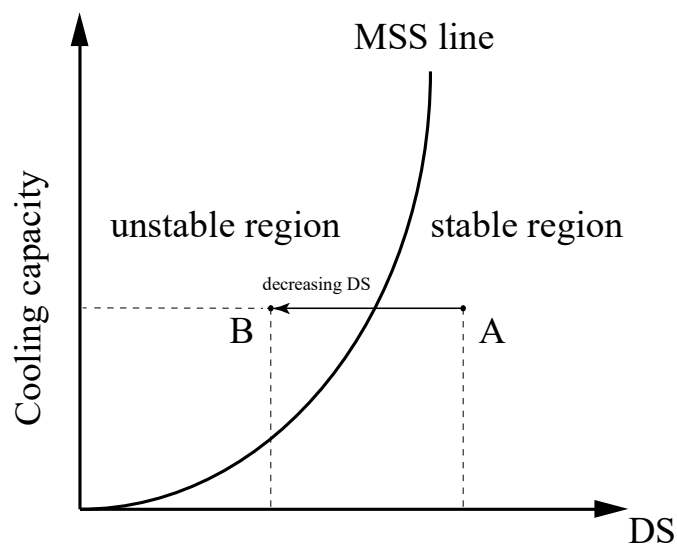


Fig. 6.8 MSS line proposed by Huelle [1972]

#### 6.4.2 The influences of different speed combinations and inlet air states on the operational stability of the experimental VS DX A/C system

The experimental results presented in Section 6.3 have demonstrated the influences of varying either compressor or fan speed, and varying inlet air temperature or RH on the operational stability of the experimental VS DX A/C system. Different speed combinations and inlet air states that led to different values of TCC and E SHR would affect the operational stability. Therefore, the conventional MSS line theory, which only considered the influences of cooling capacity on the operational stability for single speed compressors, may not be proper to explain these experimental results. On the other hand, the superheat nonlinearity of an evaporator under different evaporating temperatures was observed during experimentation, and was thus used to explain the influences of different speed combinations and inlet air states on the operational stability of the experimental VS DX A/C system.

Normally, the response of the operating DS to a step change in the refrigerant mass flow rate entering an evaporator can be characterized by a first-order plus dead time process [Aprea and Renno, 2001; Beghi et al., 2011; Maia et al., 2014], and thus the transfer function for the evaporator,  $G_e(s)$ , can be expressed as

$$G_e(s) = K_e \frac{1}{1 + \tau s} e^{-\theta s} \quad (6.4)$$

where  $K_e$  is the evaporator gain, defined as a ratio of the variation of DS from one steady state to another,  $\Delta DS$ , to that of the refrigerant mass flow rate supplied,  $\Delta M_{re}$ , i.e.,

$$K_e = \frac{\Delta DS}{\Delta M_{re}} \quad (6.5)$$

It was previously shown that, as the inherent operating characteristics of an evaporator, the responses of operating DS to a change in refrigerant mass flow rate were nonlinear and the evaporator gain was increased with a decrease in evaporating temperature [Maia et al., 2014; Maia et al., 2013; Outtagarts et al., 1997]. Therefore, the change in the operating DS at evaporator exit was larger when the system was operated at a lower evaporating temperature after a change in the refrigerant mass flow rate entering the evaporator, leading to a higher chance for the DX A/C system to be unstably operated.

For the experimental VS DX A/C system, its evaporator gains at different evaporating temperatures were experimentally obtained and are shown in Fig. 6.9. As seen, the evaporator gain became larger at a lower evaporating temperature. Hence, the corresponding change in the operating DS at evaporator exit to a change in the refrigerant mass flow rate entering the evaporator was larger when the experimental VS DX A/C system was operated at a lower evaporating temperature. Consequently, it would have a higher chance for the DX A/C system to be unstably operated at a lower evaporating temperature.



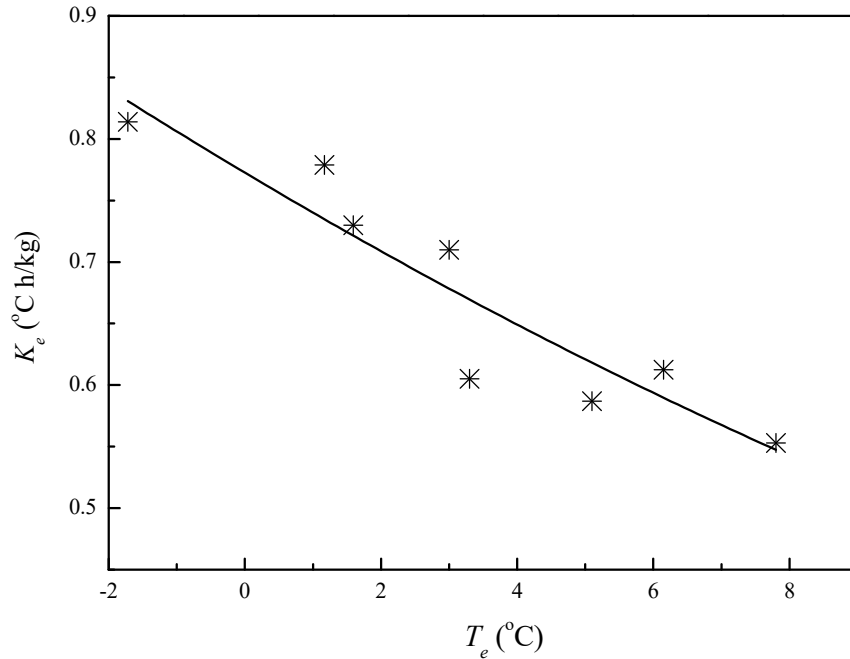


Fig. 6.9. The evaporator gains at different evaporating temperatures for the experimental VS DX A/C system

The experimental results for the ICs<sub>os</sub> suggested that the unstable operating regions were located at the lower part of their respective trapezoids where the DX A/C system was actually operated at a higher compressor speed and a lower supply fan speed. These may be explained by the above superheat nonlinearity of its evaporator at different evaporating temperatures. At a fixed supply fan speed, or a fixed air flow rate passing through the evaporator, an increase in compressor speed would increase the refrigerant mass flow rate entering the evaporator, resulting in a decrease in evaporating temperature. On the other hand, given a fixed compressor speed, lowering supply fan speed would decrease the air flow rate passing through the evaporator, and thus the cooling capacity provided could not be fully taken away by the air passing through it, resulting also in a lower evaporating temperature. Consequently, the evaporator gain was larger at either a higher compressor speed or a lower supply fan speed, leading to the experimental VS DX A/C system being more prone to be unstable.

Furthermore, the experimental results of the ICs<sub>os</sub> presented in Section 6.3.3 also suggested that the unstable operating region in its trapezoid was larger at a lower inlet air temperature or a lower air RH. These may also be explained by the superheat nonlinearity of its evaporator at different evaporating temperatures. At a specific speed combination of compressor and supply fan, a decrease in inlet air temperature or RH would lead to less heat transfer between the refrigerant inside the evaporator and the air passing through it, leading to a lower evaporating temperature. Consequently, the evaporator gain was larger at either a lower inlet air temperature or a lower inlet air RH, leading to a higher chance for the experimental VS DX A/C system to be unstable.

## **6.5 Conclusions**

In this Chapter, a study on the inherent operational characteristics considering the operational stability of the experimental VS DX A/C system detailed in Chapter 4 is reported. The ICs<sub>os</sub> of the experimental VS DX A/C system at different combinations of compressor speed and supply fan speed, DS settings and inlet air states were obtained and are reported. Based on the experimental results, an analysis on the operational stability of the experimental VS DX A/C system is also given.

The study results demonstrated that while different DS settings would not significantly influence output TCC and E SHR, and thus the shape of a TCC-E SHR trapezoid, they did impact the operational stability of the experimental VS DX A/C system. A lower DS setting would result in a larger unstable operating region in a TCC-E SHR trapezoid. In addition, the operational characteristics of the DX evaporator including

VS operation and inlet air states also significantly impacted the operational stability. A higher compressor speed or a lower supply fan speed, and a lower inlet air temperature or RH would result in a higher possibility for the experimental VS DX A/C system to be unstably operated, which could be explained by superheat nonlinearity of an evaporator.

The study results obtained and reported in this Chapter were used as a basis for further developing an existing capacity controller for the experimental VS DX A/C system considering its operational stability, which is reported in Chapter 7.

## **Chapter 7**

### **Development of a new capacity controller for the experimental DX A/C system under VS operation for operational safety and efficiency**

#### **7.1 Introduction**

The study reported in Chapter 6 on investigating the inherent operational characteristics and operational stability of the experimental VS DX A/C system suggested that a higher compressor speed or a lower supply fan speed, and a lower inlet air temperature or RH would result in a greater possibility for the DX A/C system to be unstably operated. A larger operating DS should be set when the DX A/C system is likely to be unstably operated and vice versa, so that hunting may be mitigated and a balance between operational efficiency and operational safety achieved. Therefore, the issues of the operational stability when a DX A/C system is VS controlled for simultaneously controlling indoor air temperature and humidity may be addressed by varying its DS setting in accordance with the changes in compressor/ fan speeds and inlet air states based on the obtained ICs<sub>os</sub> presented in Chapter 6.

Consequently, a previously developed capacity controller [Li et al., 2015a] for the experimental VS DX A/C system for simultaneously controlling indoor air temperature and humidity at a constant DS setting, was further developed by adding a control module which can search for and establish an optimized DS setting for the experimental DX A/C system under VS operation. A new capacity controller that is able to not only simultaneously control indoor air temperature and humidity, but also

select an optimized DS setting to properly balance the operational efficiency and safety, has been developed and the results are presented in this Chapter.

The organization of this Chapter is as follows. Firstly, an overview of the new capacity controller is presented. This is followed by reporting the development of a DS setting establishment (DSE) module. Finally, the results of controllability tests and their related discussions are presented.

## 7.2 Overview of the new capacity controller

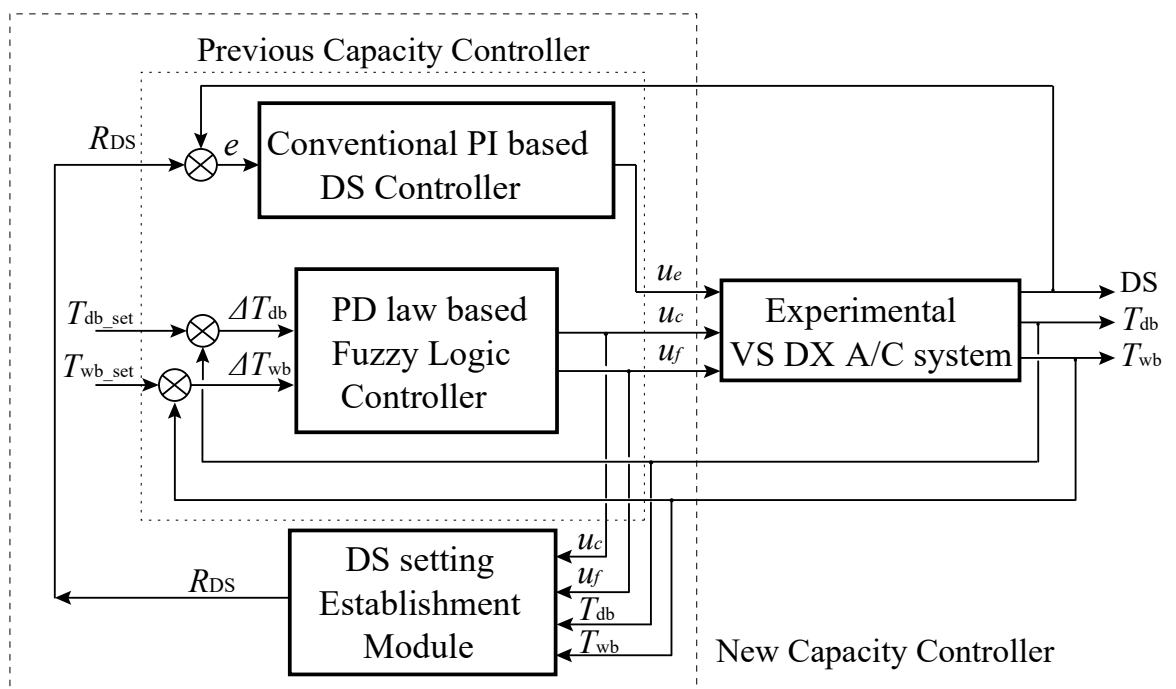


Fig. 7.1 A schematic diagram of the new capacity controller for the experimental VS DX A/C system

The new capacity controller for the experimental VS DX A/C system is schematically shown in Fig. 7.1. As seen, this new capacity controller was developed by adding a DS setting establishment (DSE) module to the previous capacity controller [Li et al.,

2015a]. The new capacity controller was therefore made of three parts. Two of the three parts, a conventional PI based DS controller and a proportional-derivative (PD) law based fuzzy logic controller (PFC) were existing, and the third part, the DSE module, was the additional module developed.

The PFC was previously developed by Li et al. [2015a] for simultaneously controlling indoor air temperature and humidity through varying compressor and supply fan speeds using the experimental VS DX A/C system. It was previously shown that, compared to the other previously developed controllers [Li et al., 2012a; Li et al., 2013; Li and Deng, 2007a, b; Qi and Deng, 2008, 2009], the PFC could achieve the required control accuracy and sensitivity over a wider operational range [Li et al., 2015a]. By applying fuzzy logic principles, a complicated physical model for the experimental VS DX A/C system was not required, thus making the PFC simpler and easier to implement than those physical model based controllers [Li and Deng, 2007a, b; Qi and Deng, 2008, 2009]. Therefore, in the new capacity controller, the same PFC was adopted for the simultaneous control over indoor air dry-bulb temperature,  $T_{db}$  and wet-bulb temperature,  $T_{wb}$ , by continuously outputting the control signals of compressor speed,  $u_c$ , and supply fan speed,  $u_f$ . On the other hand, unlike in the previous capacity controller with a constant DS setting [Li et al., 2015a], in the new capacity controller, the DS setting,  $R_{DS}$ , was established by the DSE module, and could thus be varied in accordance with the changes in compressor/ fan speeds and inlet air states. When the experimental VS DX A/C system was VS controlled by the PFC for simultaneously controlling indoor air temperature and humidity, the information of the above four key operating parameters, i.e.,  $u_c$ ,  $u_f$ ,  $T_{db}$ , and  $T_{wb}$ , was also provided to the DSE module. Based on the known relationship between the inherent operational

characteristics and operational stability of the experimental VS DX A/C system, the DSE module would then output an optimized DS setting,  $R_{DS}$ , to the conventional PI based DS controller. Based on the error between the actual operating DS and the optimized DS setting, or  $e$ , the conventional PI based DS controller would output a corresponding control signal,  $u_e$ , to regulate the EEV's opening until  $e$  was within its preset range.

### **7.3 Development of the DS setting establishment (DSE) module**

As mentioned, in the new capacity controller, the DSE module was used to establish an optimized DS setting,  $R_{DS}$ , which was based on the known relationship between its inherent operational characteristics and operational stability of the experimental VS DX A/C system. The study results reported in Chapter 6 suggested that, for ensuring a stable operation of the experimental DX A/C system, a larger DS setting should be set when the chance of its unstable operation was high; otherwise, a smaller DS setting should be set for getting the highest possible heat transfer effectiveness of the evaporator. Consequently, if DS setting could be varied as guided by the obtained ICs\_os, hunting of the VS DX A/C system may be mitigated and a balance between its operational efficiency and safety achieved when it was VS operated for simultaneously controlling indoor air temperature and humidity.

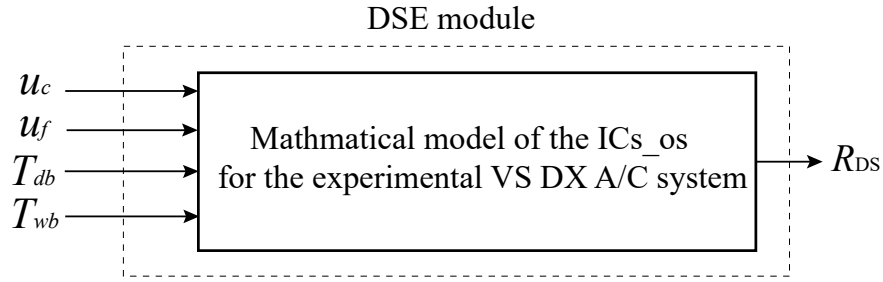


Fig. 7.2 The configuration of the DSE module

Fig. 7.2 shows the detailed configuration of the DSE module for establishing an optimized DS setting,  $R_{DS}$ . As seen, its core was a mathematical model that represented the ICs\_os for the experimental VS DX A/C system, so that at a given set of  $u_c$ ,  $u_f$ ,  $T_{db}$  and  $T_{wb}$ , an optimized DS setting,  $R_{DS}$ , may be established and output to the PI based DS controller. Therefore, the key to the development of the DSE module was to develop the mathematical model of the ICs\_os. When modeling, while a number of modeling techniques were available, ANN based modeling approach was used. This was because, the ANN technique has been increasingly used in modeling the steady-state performances of thermal systems including heat exchangers [Islamoglu et al., 2005; Kim et al., 2010; Xie et al., 2007], heat pump systems [Bechtler et al., 2001; Esen and Inalli, 2009] and refrigeration systems [Ertunc and Hosoz, 2006; Sozen et al., 2003]. Furthermore, it has been shown that the inherent operational characteristics of a VS DX A/C system could be well recognized and captured by using ANN models [Li et al., 2012b; Li et al., 2015b].

### 7.3.1.1 Development of an ANN based mathematical model of the ICs\_os

When developing the ANN based model of the ICs\_os, an index,  $S$ , for indicating the operational stability of the experimental VS DX A/C system was introduced. A value



of 1 was assigned to  $S$  when the system was stable, and 0 otherwise. Therefore, using  $u_c$ ,  $u_f$ ,  $T_{db}$ ,  $T_{wb}$  and  $R_{DS}$  as inputs and  $S$  as an output, a five-in one-out ANN based model of the ICs\_os to assist establishing an optimized DS setting for the experimental VS DX A/C system was established.

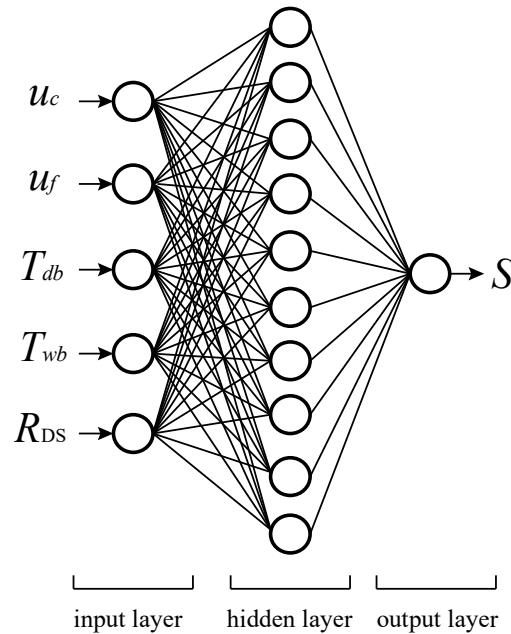


Fig. 7.3 Structure of the selected 5-10-1 network for the ANN based model of the ICs\_os

A multilayer ANN architecture was used which was generally made of three parts: an input layer, a hidden layer or layers and an output layer, each being occupied by a few neurons. All neurons in each hidden layer were connected to all neurons in the previous and following layers through synaptic with weight. By trial and error, a 5-10-1 network was selected for the ANN based model, as it was able to provide the highest prediction accuracy when training the ANN model. Fig. 7.3 shows the structure of the selected ANN with ten neurons in one hidden layer along with five input neurons and one output neuron. The training algorithm used was the feedforward

back-propagation (BP) algorithm. During training, each time adjusting the weights and biases with one set of training data was called a run. A cycle of training consisted of an adequate number of runs for obtaining weights and biases successively from all training data. The calculations were then repeated over many cycles. Two indices, namely correlation coefficient,  $R$ , and root mean square error (RMSE), were used to evaluate the performance of a trained ANN model.

The correlation coefficient between a target output set,  $t$ , and a predicted output set,  $p$ , is defined as [Looney, 1997]:

$$R_c(t, p) = \frac{\text{Cov}(t, p)}{\sqrt{\text{Cov}(t, t)\text{Cov}(p, p)}} \quad (7.1)$$

where  $\text{Cov}(t, p)$  is the covariance between the target output set and the predicted output set. A correlation coefficient indicates the linear relationship between the target output set and the predicted output set. The accuracy of the prediction increases with the closeness of  $R_c$  to unity [Ertunc and Hosoz, 2006; Hosoz and Ertunc, 2006].

The root mean square error represents the standard deviation of the differences between the target output set and predicted output set, which is evaluated by:

$$\text{RMSE} = \sqrt{\frac{1}{N} \sum_{i=1}^N (t_i - p_i)^2} \quad (7.2)$$

where  $N$  is the total number of data sets used in training or testing.

Using the available experimental data for the ICs\_os for the experimental VS DX A/C system, the ANN based model of the ICs\_os was trained and further tested. There were totally 450 experimental data sets which were randomly divided into two parts, namely 382 data sets (~85% of the total data sets) for training and 68 data sets (~15% of the total data sets) for testing. For the ANN model to be developed, its  $R_c$  and RMSE for all the outputs at the last cycle were 0.994 and 0.0063, respectively, showing a high prediction accuracy. On the other hand, the testing results of the trained ANN model showed that  $R_c$  and RMSE between the predicted and tested data were equal to 0.959 and 0.128, respectively, suggesting a relatively poorer performance as compared to the training results. This was because the predicted output of the trained ANN,  $S_p$ , ranged from 0 to 1, but the target output,  $S_t$ , was either 0 or 1. Therefore, for consistency, the predicted output for the trained ANN,  $S_p$ , was taken as 1 when its value was greater than 0.9, or 0 otherwise. Consequently, 67 out of the 68 sets of testing data were predicted with 98.5% accuracy when using the trained ANN based model of the ICs\_os to predict the operational stability of the system, which was adequate for the DSE module to establish an optimized DS setting.

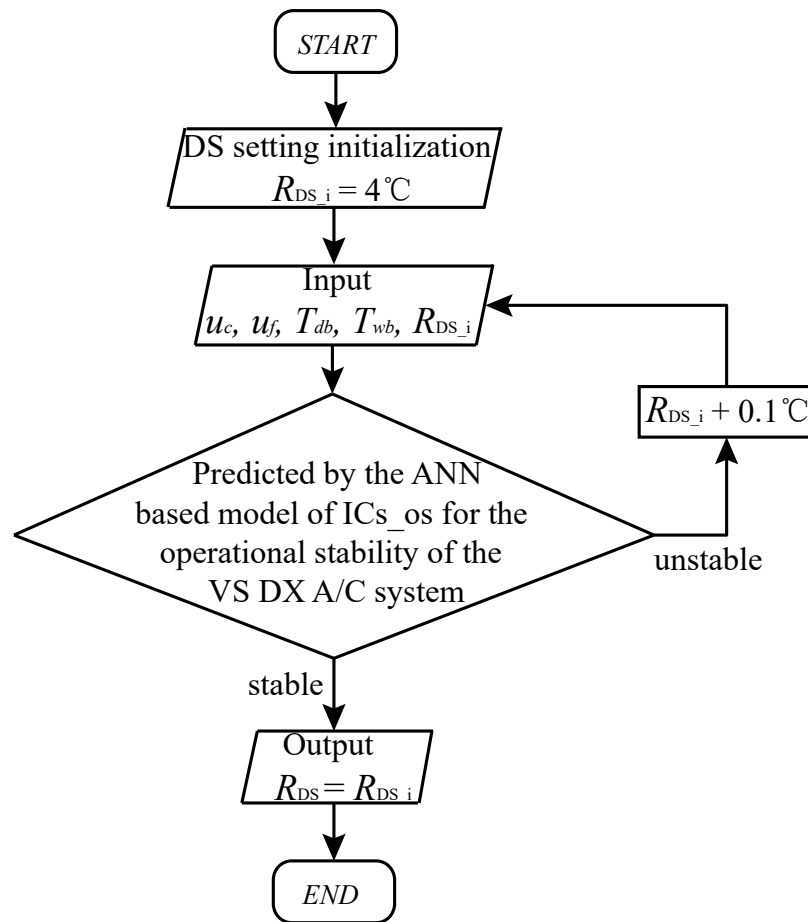


Fig. 7.4 Flowchart of the DSE module for establishing an optimized DS setting

Fig. 7.4 is a flowchart showing the operation of the DSE module. As seen, at the start, an initial DS setting,  $R_{DS\_i}$ , of 4 °C was assigned to  $R_{DS}$ . With the measured inputs of  $u_c$ ,  $u_f$ ,  $T_{db}$  and  $T_{wb}$ , as well as  $R_{DS\_i}$ , the ANN based model of ICs\_os was used to predict the operational stability of the VS DX A/C system. If a stable operation was predicted, the  $R_{DS\_i}$  was taken as the output DS setting, i.e.,  $R_{DS}$ . Otherwise, an increment of 0.1 °C was assigned to  $R_{DS\_i}$  and the whole prediction process was not stopped, until a  $R_{DS}$  that could ensure a stable operation for the VS DX A/C system was identified and output to the PI based DS controller. As indicated by the prediction process, this identified  $R_{DS}$  would be a minimal DS that can on one hand ensure a stable, and on the other an efficient operation of the VS DX A/C system.

## 7.4 Controllability tests

### 7.4.1 Experimental conditions

To experimentally demonstrate the performances of the new capacity controller, using the measured performances of the previous capacity controller [Li et al., 2015a] with a constant DS setting of 6 °C as the basic for comparison, two sets of controllability test were carried out and the test results are reported in this Section.

The first set (Test I) was for testing the controllability of the experimental VS DX A/C system using the previous capacity controller and the new one when the set points of indoor air dry-bulb and wet-bulb temperatures were reduced, and the second set (Test II) for that when their respective set points were increased.

All the controllability tests were carried out using the experimental VS DX A/C system detailed in Chapter 4. Table 7.1 lists the uncertainties for the sensors/instruments and the calculated system operating parameters used in the current study. In addition, since the selection of the optimized DS setting,  $R_{DS}$ , was determined by the DSE module based on the ICs\_os of the experimental VS DX A/C system, therefore, the same set of PI control settings, namely -0.5 for the proportional gain and 40s for the integral time, were also adopted for the PI based DS controller in all the tests. During experimentation, the DS setting for the previous capacity controller was fixed at 6 °C. The condenser cooling air flow rate remained unchanged at 4100 m<sup>3</sup>/h with a fixed condenser cooling air inlet temperature of 35 °C. A prescribed range of

fluctuation of  $\pm 0.5$  °C in DS was set to assess whether the operation of the VS DX A/C system was stable or not.

Table 7.1. Measurement/calculation uncertainty of system operating parameters

Operating parameter	Uncertainty	Unit
Air dry-bulb temperature	$\pm 0.1$ (platinum RTD)	°C
Air wet-bulb temperature	$\pm 0.1$ (platinum RTD)	°C
Refrigerant temperature	$\pm 0.1$ (platinum RTD)	°C
Refrigerant pressure	$\pm 0.2\%$ (pressure transducer)	bar
Refrigerant mass flow rate	$\pm 0.25\%$ (Coriolis mass flow meter)	kg/h
DS	$\pm 0.18$ (calculated)	°C
COP	$\pm 1.01\%$ (calculated)	--

## 7.4.2 Experimental results

### 7.4.2.1 Test I results

In this test, both  $T_{db}$  and  $T_{wb}$  stayed steadily at 26 °C and 19 °C at the beginning of the test, when the compressor speed and supply fan speed were maintained at 60% and 80% of their maximum speeds, respectively. Then their respective set points were changed to 25 °C and 18 °C at 1000s, respectively. The test results are shown in Figs. 7.5-7.8.

Figs. 7.5 and 7.6 show the measured variations in the operating parameters under the previous and the new capacity controllers, respectively. As seen in Figs. 7.5 (a) and

7.6 (a), the two controlled parameters of  $T_{db}$  and  $T_{wb}$  under both controllers could reach their new respective set points at about 4500s and were maintained at the new setting for the rest of the test. However, as shown in Fig. 7.5 (b), while the measured DS under the previous capacity controller was stable at 6 °C at first, it started to oscillate and finally became unstable with a fluctuation range of  $\sim \pm 2$  °C after  $T_{db}$  and  $T_{wb}$  reached their respective set points, resulting in frequent opening and closing of the EEV. On the other hand, as shown in Fig. 7.6 (b), the measured DS under the new capacity controller was stable at 4 °C at the beginning of the test. After changing the air temperature set points at 1000s, a stable DS was also maintained at 4 °C, although experiencing some fluctuations during transition. When  $T_{db}$  and  $T_{wb}$  reached and were maintained at their respective set points, the measured DS was increased and finally settled at 7 °C.

Fig. 7.7 shows the detailed comparison of the measured DS under both controllers. It clearly indicated that the new controller can appropriately adjust the DS setting from 4 °C to 7 °C to avoid the unstable system operation, when the experimental VS DX A/C system was operated at a lower indoor air temperature, a higher compressor speed and a lower supply fan speed than those at the beginning of the test, requiring a larger DS setting to ensure its stable operation. However, this was not possible with the previous capacity controller, as a constant DS was incorporated.

Fig. 7.8 shows the comparison of the measured operational efficiency in terms of coefficient of performance (COP) under both controllers. The average COP of the experimental VS DX A/C system after it reached the new steady state was about 2.91 under the control of the previous capacity controller and 2.95 under the control of the

new capacity controller, respectively. This represented an improvement of 1.2% in COP.

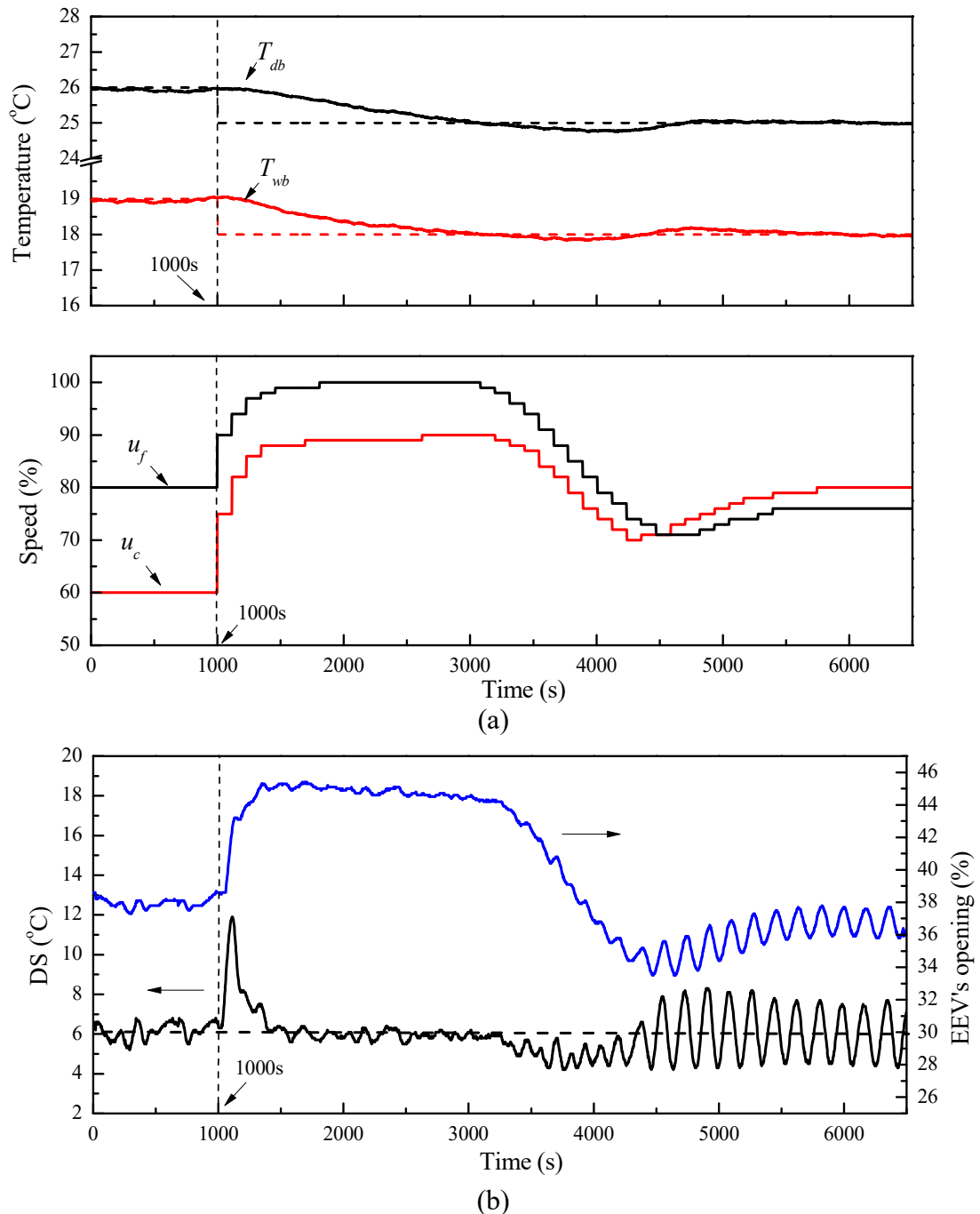
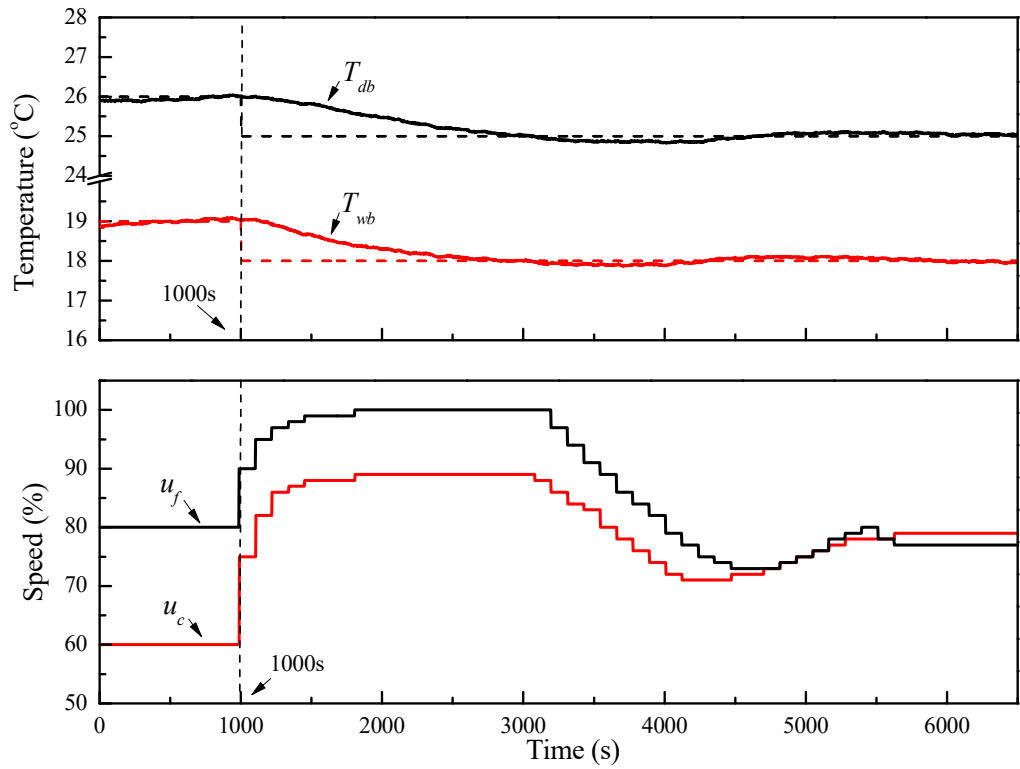
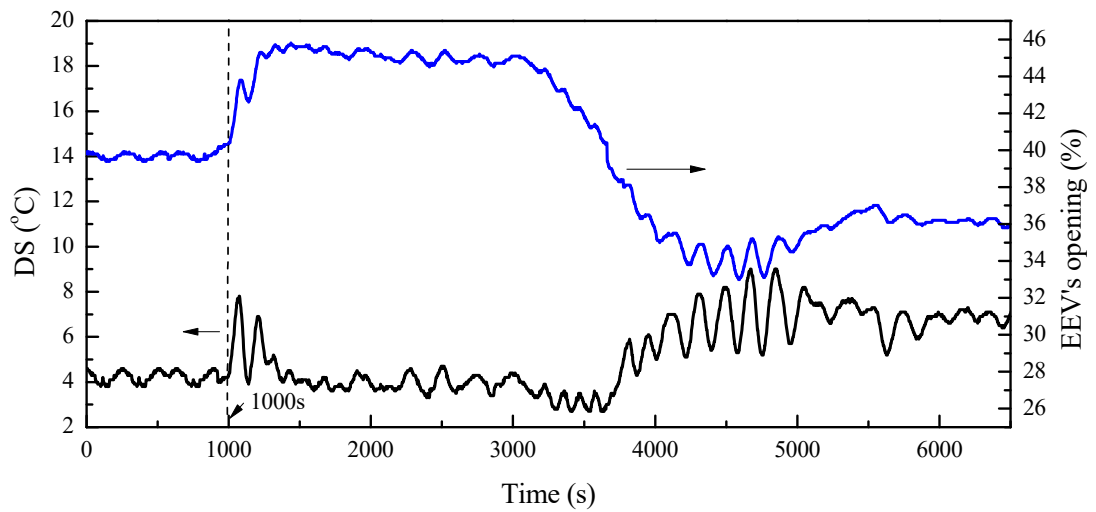


Fig. 7.5 Measured variations in the operating parameters in the Test I under the previous capacity controller (a) Temperatures and speeds variations; (b) DS and EEV's opening variations





(a)



(b)

Fig. 7.6 Measured variations in the operating parameters in the Test I under the new capacity controller (a) Temperatures and speeds variations; (b) DS and EEV's opening variations

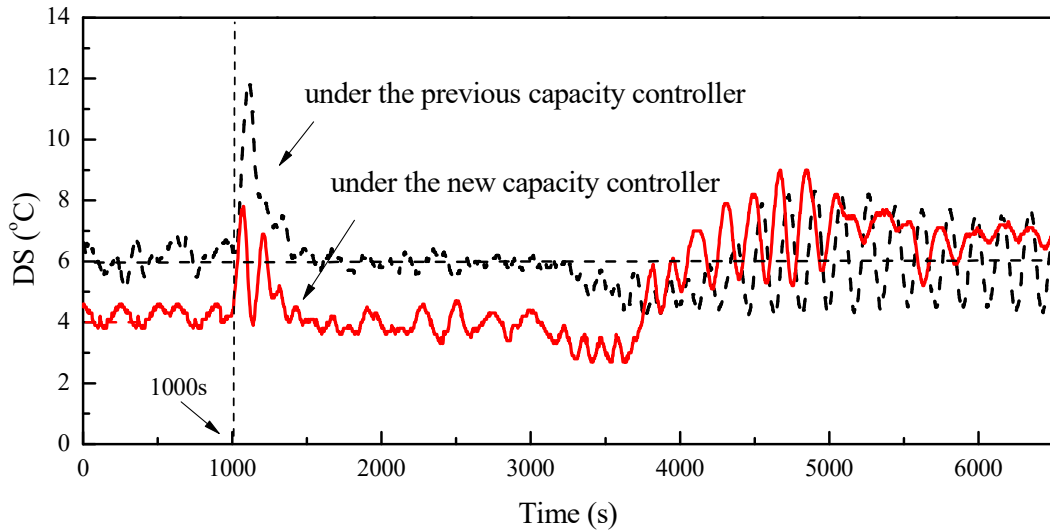


Fig. 7.7 Comparison of the measured DS under both controllers in Test I

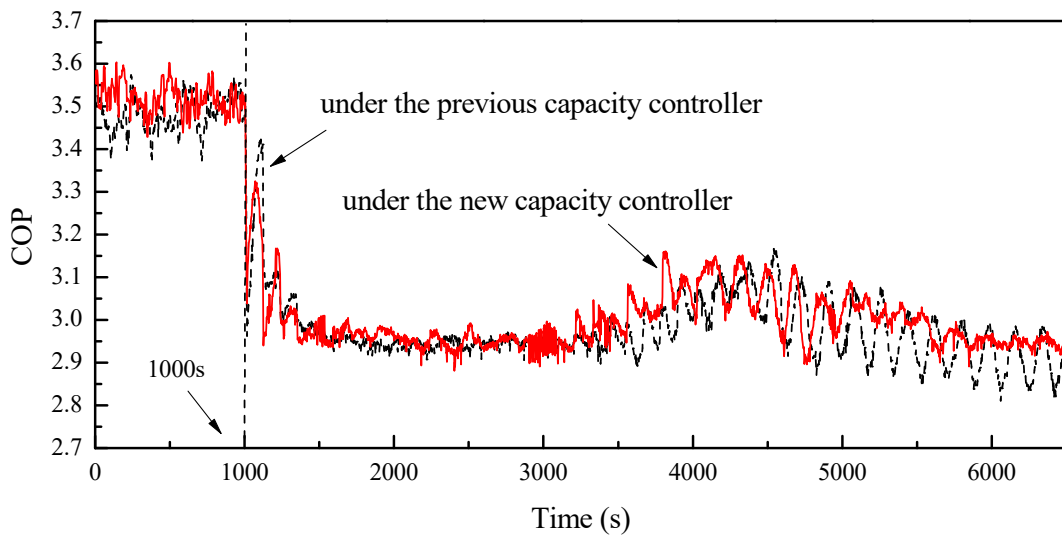


Fig. 7.8 Comparison of the COP under both controllers in Test I

#### 7.4.2.2 Test II results

In this test, both  $T_{db}$  and  $T_{wb}$  stayed steadily at 25 °C and 17.5 °C at the beginning of the test, respectively, when both the compressor and supply fan speeds were maintained at 80% of their maximum speeds. At 1000s the set points for  $T_{db}$  and  $T_{wb}$

were increased to 26 °C and 18.5 °C, respectively. The test results are shown in Figs. 7.9-7.12.

Figs. 7.9 (a) and 7.10 (a) show the measured variations in air temperatures and speeds under both controllers. As seen, the control over  $T_{db}$  and  $T_{wb}$  to their respective set points was achieved at about 3500s under both controllers. On the other hand, Figs. 7.9 (b) and 7.10 (b) show the measured variations in the measured DS and EEV's opening under both controllers, and Fig. 7.11 shows the detailed comparison of the measured DS under both controllers. As seen, the measured DS under both controllers was stable at 6 °C at the beginning of the test. After increasing air temperature set points, the measured DS under the previous capacity controller could become stable again after experiencing certain fluctuations during transient period and was maintained at its setting of 6 °C for the rest of the test. However, the measured DS under the new capacity controller remained virtually stable at its minimal setting of 4 °C, after  $T_{db}$  and  $T_{wb}$  reached their new settings at about 3500s. This demonstrated that, as shown in Figs. 7.9 (a) and 7.10 (a), after the experimental VS DX A/C system reached a new steady state, it was operated at a higher indoor air temperature, a lower compressor speed and a higher supply fan speed, than those at the beginning of the test, and thus a smaller stable DS could be adopted.

Fig. 7.12 shows the comparison of the measured COP under both controllers. As seen, while the COP values under both controllers were almost the same at the beginning of the test, the COP value under the new capacity controller was always higher than that under the previous capacity controller when the operating DS was maintained at 4 °C. Consequently, after the A/C system reached the new steady state at about 3500s, the

COP was improved by 1.2%  $\sim$  5.6% in comparison with those under the previous capacity controller, demonstrating a better operational efficiency.

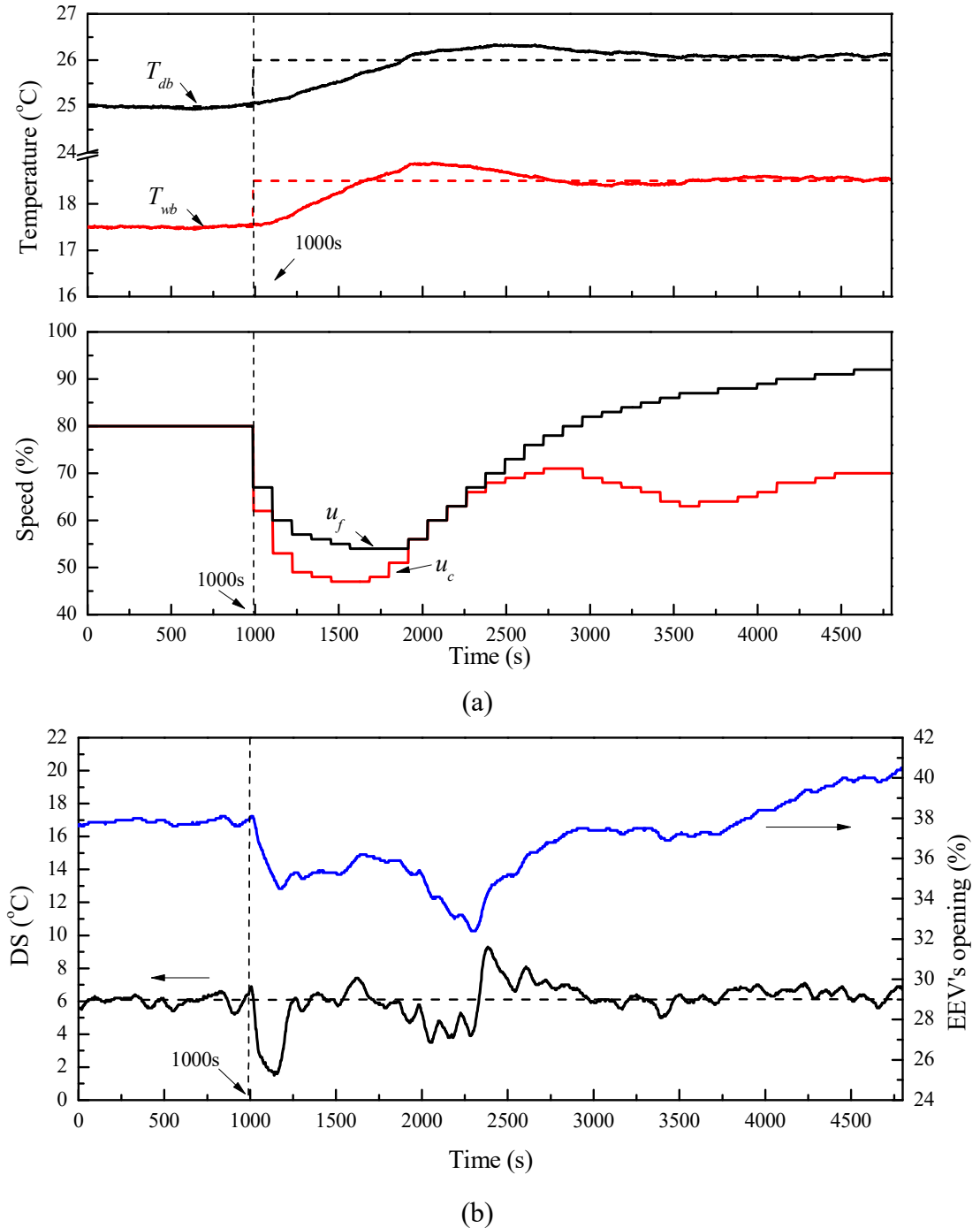


Fig. 7.9 Measured variations in the operating parameters in Test II under the previous capacity controller (a) Temperatures and speeds variations; (b) DS and EEV's opening variations

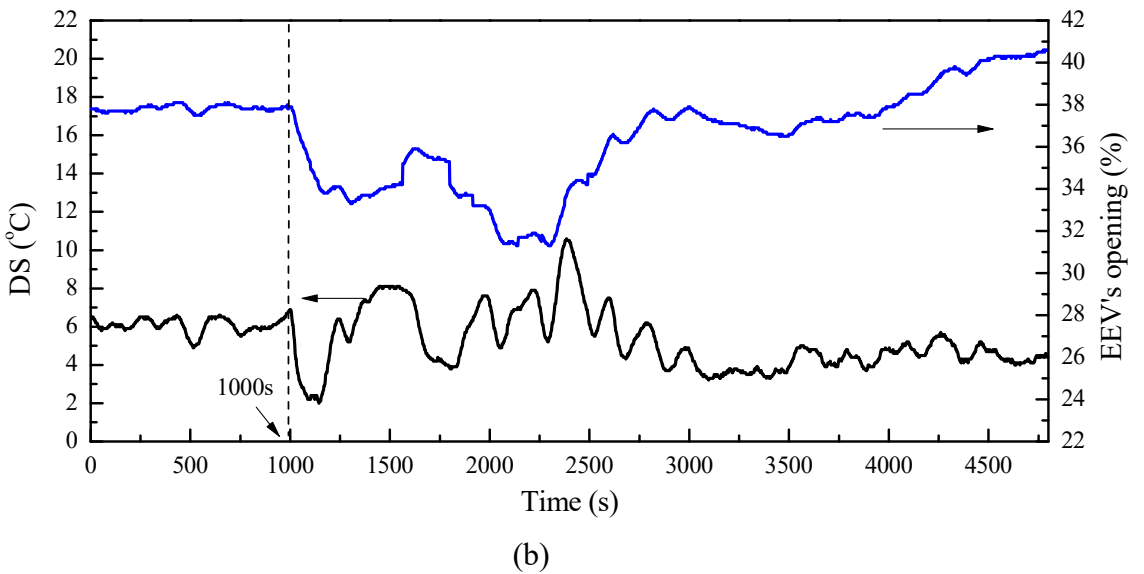
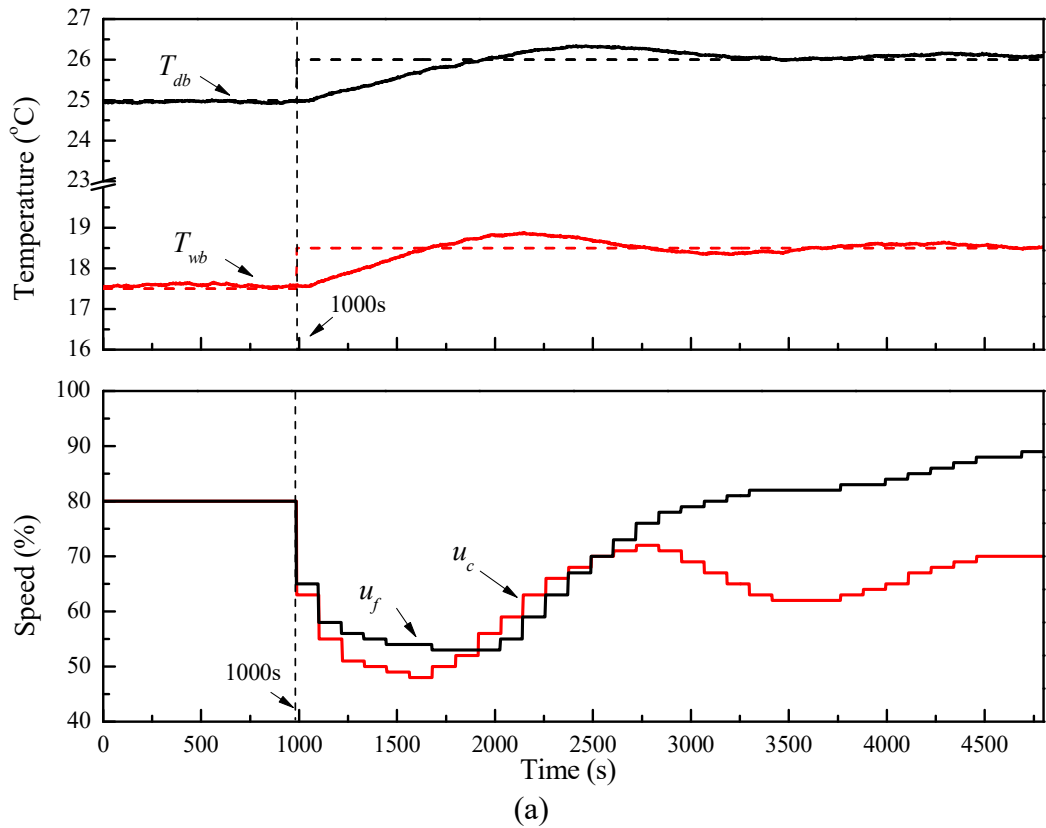


Fig. 7.10 Measured variations in the operating parameters in Test II under the new capacity controller. (a) Temperatures and speeds variations; (b) DS and EEV's opening variations

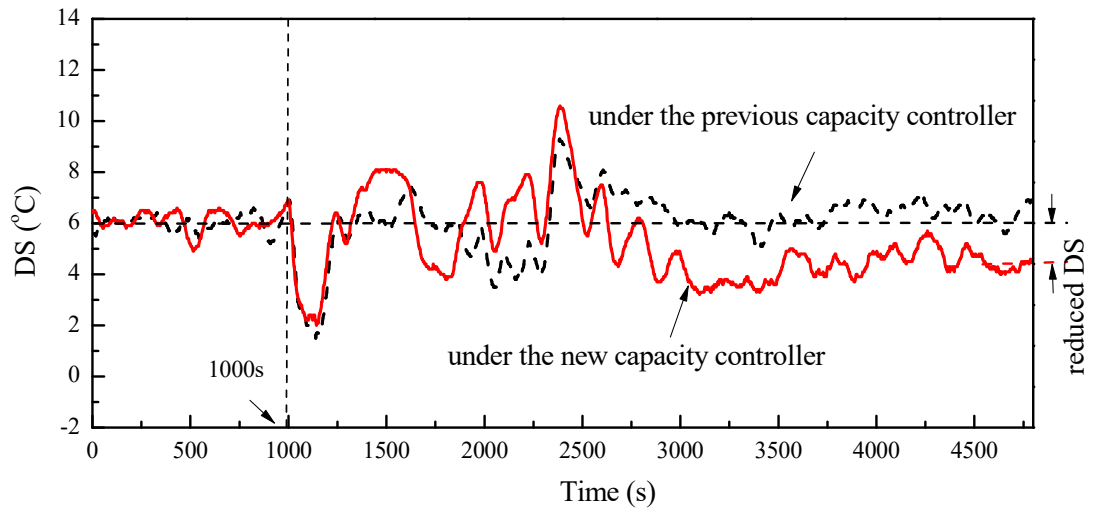


Fig. 7.11 Comparison of the measured DS under both controllers in Test II

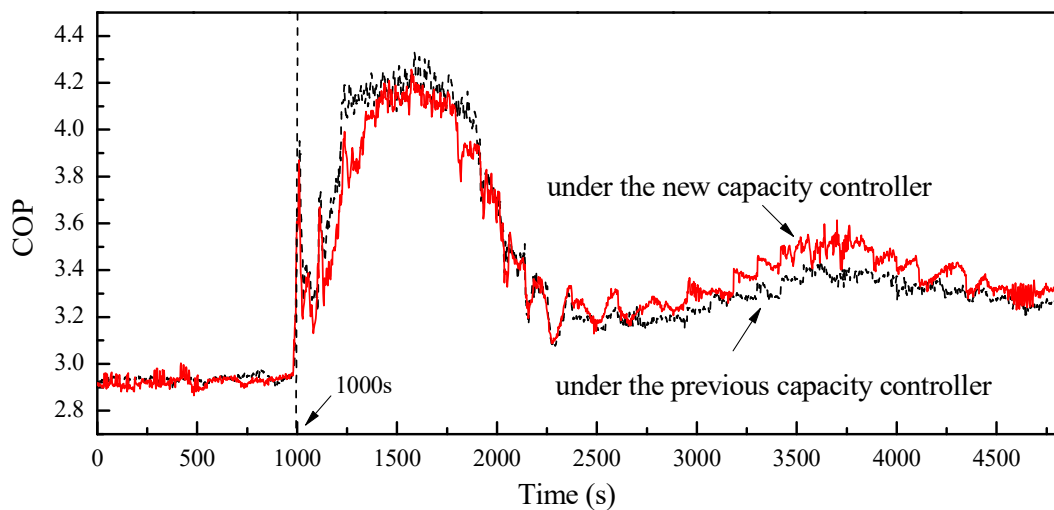


Fig. 7.12 Comparison of the COP under both controllers in Test II

## 7.5 Discussions

From the experimental results, it can be seen that using the new capacity controller, because of using the varied DS setting, two improvements for the experimental VS DX A/C system can be achieved when VS operated for simultaneously controlling indoor air temperature and humidity. Firstly, when a larger DS setting was selected by

the new capacity controller, although the improvement in operational efficiency was limited as the improvement in COP was only 1.2% with  $\pm 1.01\%$  calculation uncertainty, the hunting of the experimental VS DX A/C system can be mitigated. Hunting, as reflected by the oscillation of system operating parameters, would result in a shorter lifespan of EEV due to its frequent opening and closing, and might eventually lead to the failure of a compressor [Mithraratne and Wijesundera, 2001; Mithraratne et al., 2000], and therefore should be avoided as far as possible. Secondly, when a smaller DS setting was selected by the new capacity controller, a slight improvement in COP of the experimental VS DX A/C system can be achieved due to the more effective use of the evaporator. Consequently, by using the new capacity controller for simultaneously controlling indoor air temperature and humidity, possible hunting of the experimental DX A/C system may be mitigated, and the improvements of both the operational safety and efficiency also achieved. Furthermore, the development of the new capacity controller also demonstrated the application of the ICs<sub>os</sub> of solving practical control problems.

## **7.6 Conclusions**

Based on the known relationship between the inherent operational characteristics and operational stability of the experimental VS DX A/C system reported in Chapter 6, a new capacity controller has been developed. A DSE module was added to a previous capacity controller to achieve the balance between the operational safety and efficiency of the experimental VS DX A/C system, when simultaneously controlling indoor air temperature and humidity. The core of DSE module was an ANN based model representing the known relationship between the inherent operational

characteristics and operational stability of the experimental VS DX A/C system. Using the DSE model, an optimized DS setting for the experimental VS DX A/C system may be identified when it was VS operated for simultaneously controlling indoor air temperature and humidity.

Controllability tests for the new capacity controller were carried out using an experimental VS DX A/C system. The test results suggested that not only the simultaneous control over indoor air temperature and humidity was achieved, but also the hunting of the experimental VS DX A/C system was mitigated and a slight improvement in COP achieved when the system was controlled by the new capacity controller, suggesting a better control performance in terms of not only control accuracy, but also operational safety and efficiency of the DX A/C system.



## **Chapter 8**

### **Conclusions and Future Work**

#### **8.1 Conclusions**

A programmed research project on investigating the operational stability of the experimental EEV-controlled VS DX A/C system and developing an advanced controller to achieve an improvement of both the operational safety and energy efficiency when simultaneously controlling indoor air temperature and humidity using the experimental VS DX A/C system has been successfully carried out and is reported in this Thesis. The conclusions of the Thesis are as follows:

- 1) A study on investigating the influences of the operational characteristics of a PI controlled EEV on the operational stability of the experimental DX A/C system has been carried out and study results are reported in Chapter 5. Using the classical control theory, the influences of EEV's PI settings and time constants of EEV's temperature sensor on the system operational stability were analyzed and further experimentally verified using the experimental DX A/C system. Both the theoretical analysis and experimental results showed that EEV's PI settings and the time constant of EEV's temperature sensor which affected the rate of DS signal transfer, did impact the operational stability of the EEV-evaporator control loop, thus the DX A/C system. A larger proportional gain or integral gain of the EEV's PI controller would very likely lead to system instability. Slowing down the rate of DS signal transfer in the EEV-evaporator control loop would, on the other hand, help mitigate the hunting of the DX A/C system. The study results

also further confirmed that the operating characteristics of an EV impacted a refrigeration system operational stability and suggested an effective approach to mitigate instability problem encountered in an EEV controlled refrigeration system by incorporating a first-order transfer function in its EEV-evaporator control loop to slow down the rate of DS signal transfer.

- 2) A follow-up study on the inherent operational characteristics considering the operational stability of the experimental VS DX A/C system is reported in Chapter 6. The ICs<sub>os</sub> of the experimental VS DX A/C system at different combinations of compressor speed and supply fan speed, DS settings and inlet air states were obtained and are reported. The study results demonstrated that while different DS settings would not significantly influence output TCC and E SHR, and thus the shape of a TCC-E SHR trapezoid, they did impact the operational stability of the experimental VS DX A/C system. A lower DS setting would result in a larger unstable operating region in a TCC-E SHR trapezoid. In addition, the operational characteristics of the DX evaporator including VS operation and inlet air states also significantly impacted the operational stability. A higher compressor speed or a lower supply fan speed, and a lower inlet air temperature or RH would result in a higher possibility for the experimental VS DX A/C system to be unstably operated, which could be explained by superheat nonlinearity of an evaporator.
- 3) The development of a new capacity controller that is able to not only simultaneously control indoor air temperature and humidity using the experimental VS DX A/C system, but also select an optimized DS setting to properly balance the operational efficiency and safety is presented in Chapter 7.

Based on the known relationship between the inherent operational characteristics and operational stability of the experimental VS DX A/C system presented in Chapter 6, a DSE module was developed and added to a previous capacity control to select an optimized DS setting for the experimental VS DX A/C system when it was VS operated for simultaneously controlling indoor air temperature and humidity. Controllability tests for the new capacity controller were carried out using the experimental VS DX A/C system. The test results suggested that not only the simultaneous control over indoor air temperature and humidity was achieved, but also the hunting of the experimental VS DX A/C system was mitigated and a slight improvement in COP achieved when the system was controlled by the new capacity controller, suggesting a better control performance in terms of not only control accuracy, but also operational safety and efficiency of the DX A/C system.

The research project reported in this Thesis has provided detailed insights to the understanding of the operational stability of an EEV-controlled VS DX A/C system when it is VS operated at different inlet air states and made important contributions to the development of appropriate control strategies to ensure a safe and efficient operation when simultaneously controlling indoor air temperature and humidity using DX A/C systems. The influences of the dynamics of EEV's temperature sensor, VS operation and different inlet air states on the operational stability of an EEV-controlled VS DX A/C system are reported for the first time in the open literature, and the new capacity controller that could select an optimized DS setting to properly balance the operational safety and energy efficiency is also the first of its kind. In addition, the study results reported in this Thesis further confirmed the two views on the possible

causes for hunting in a vapor-compression refrigeration system that both the operational characteristics of an EEV and inherent operational characteristics of an evaporator impacted the operational stability of the EEV-controlled refrigeration system. The long-term significance of this research project is that it will encourage a wider application of VS DX A/C systems to achieving a better indoor thermal environment control, at a higher level of operational safety and energy efficiency, thus contributing to sustainable development.

## **8.2 Proposed future work**

A number of future studies following on the successful completion of the research project reported in this Thesis are proposed as follows:

- 1) The study results reported in Chapter 6 have been successfully used for developing a new capacity controller for improving the operational safety and efficiency of the experimental DX A/C system when it is VS operated at different inlet air states. As mentioned in Chapter 5, incorporating a first-order transfer function in an EEV-evaporator control loop to slow down the rate of DS signal transfer would also help mitigate possible system hunting. However, slowing down the rate of DS signal transfer would lead to a poor control loop sensitivity, and thus a poor control performance after experiencing certain disturbances. Therefore, a further study should be carried out to improve the control sensitivity when incorporating a first-order transfer function in an EEV-evaporator control loop for mitigating system hunting.

- 2) The influences of the operational characteristics of an EEV, including its control setting and dynamics of its temperature sensor, on the operational stability of the experimental DX A/C system have been investigated. However, as mentioned in Chapter 5, considering the limited variation range of EEV's opening during experimentation, a linear valve characteristic was assumed, and thus the influences of the nonlinear characteristics of the EEV on the operational stability were not investigated. In fact, as a control valve for regulating the refrigerant mass flow rate entering an evaporator, an EEV could also exhibit nonlinearities expressed in terms of hysteresis and deadband, and thus limiting the EEV-evaporator control loop performance, which is not discussed in this Thesis. Therefore, in order to ensure the operational safety in an EEV-controller refrigeration system, a further study should be carried out to investigate the nonlinearities of an EEV on the operational stability of an EEV-controlled refrigeration system so as to help achieve a better EEV-evaporator control loop performance.
  
- 3) The superheat nonlinearity of an evaporator expressed in terms of different evaporator gains, has been used to explain the instability problem encountered in a DX A/C system when it is VS operated at different inlet air states in Chapter 6. However, other nonlinear behaviours of the DX evaporator including different time constants and transport lags under VS operation were not discussed, which would also impact the operational stability of the VS DX A/C system. Therefore, further experimental investigations are required to provide detailed insights to the understanding of the superheat nonlinearity of a DX evaporator exhibited during

VS operation so as to provide important guides in designing adaptive control algorithms for VS DX A/C systems.

## Appendix

### Photos of the Experimental DX A/C system



Photo 1 Conditioned spaces

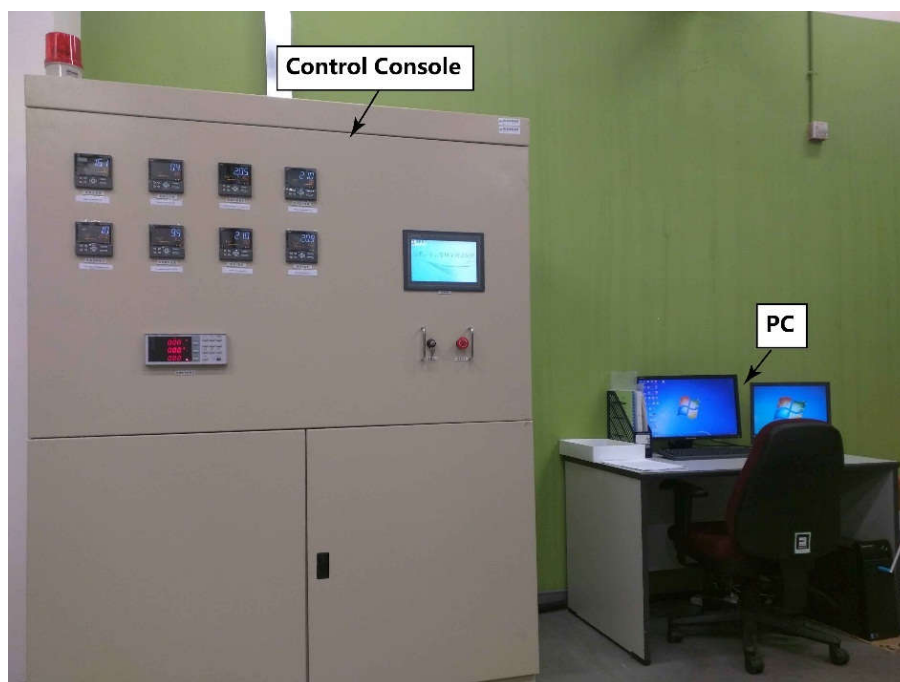


Photo 2 Control console



Photo 3 Air-distribution sub-system

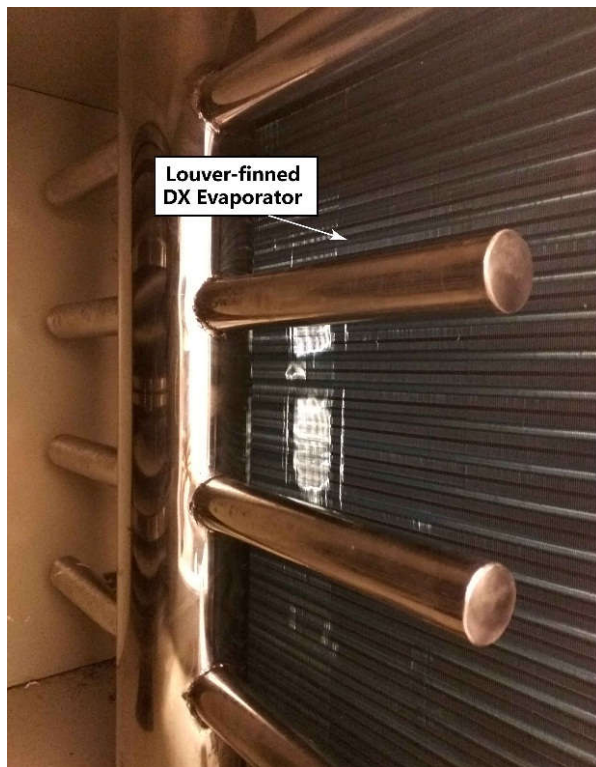


Photo 4 DX evaporator in air-distribution sub-system



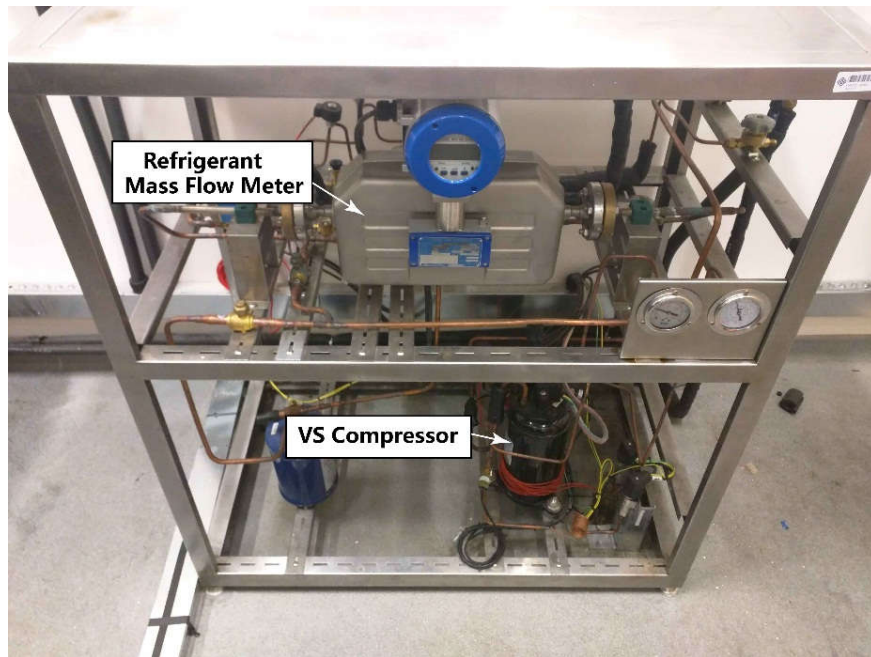


Photo 5 DX refrigeration plant



Photo 6 The EEV in the DX refrigeration plant



Photo 7 Load generation unit

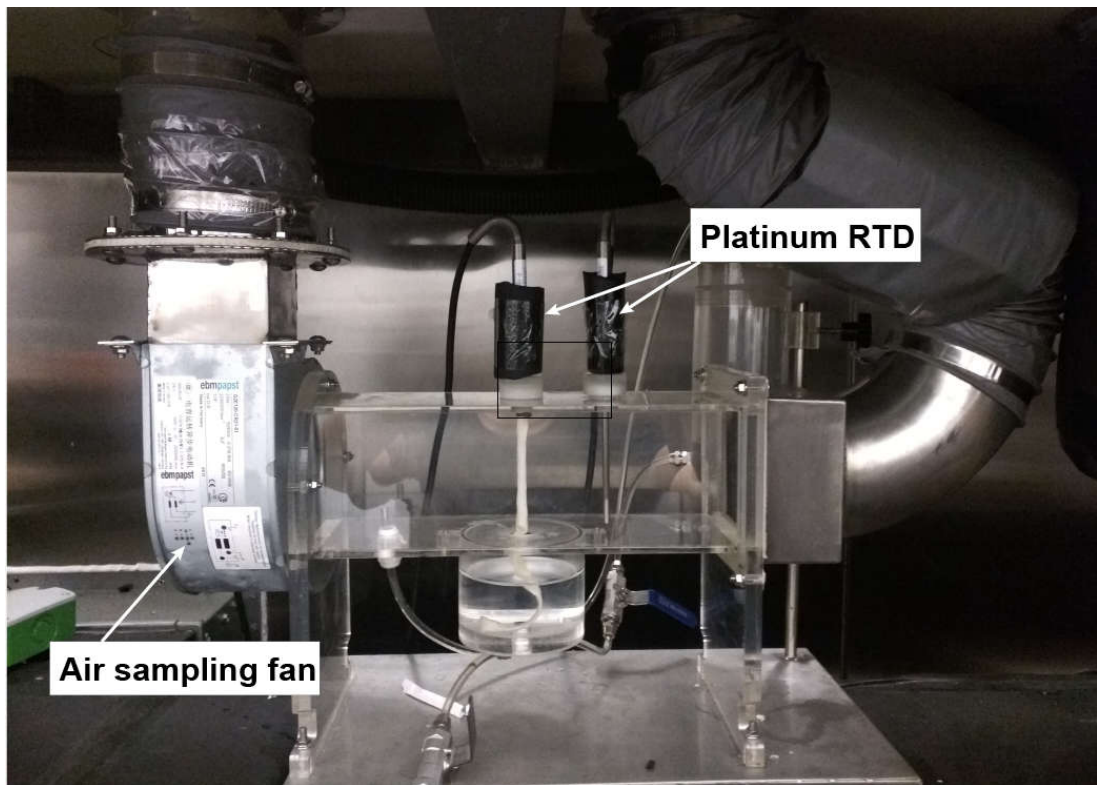


Photo 8 Air sampling device

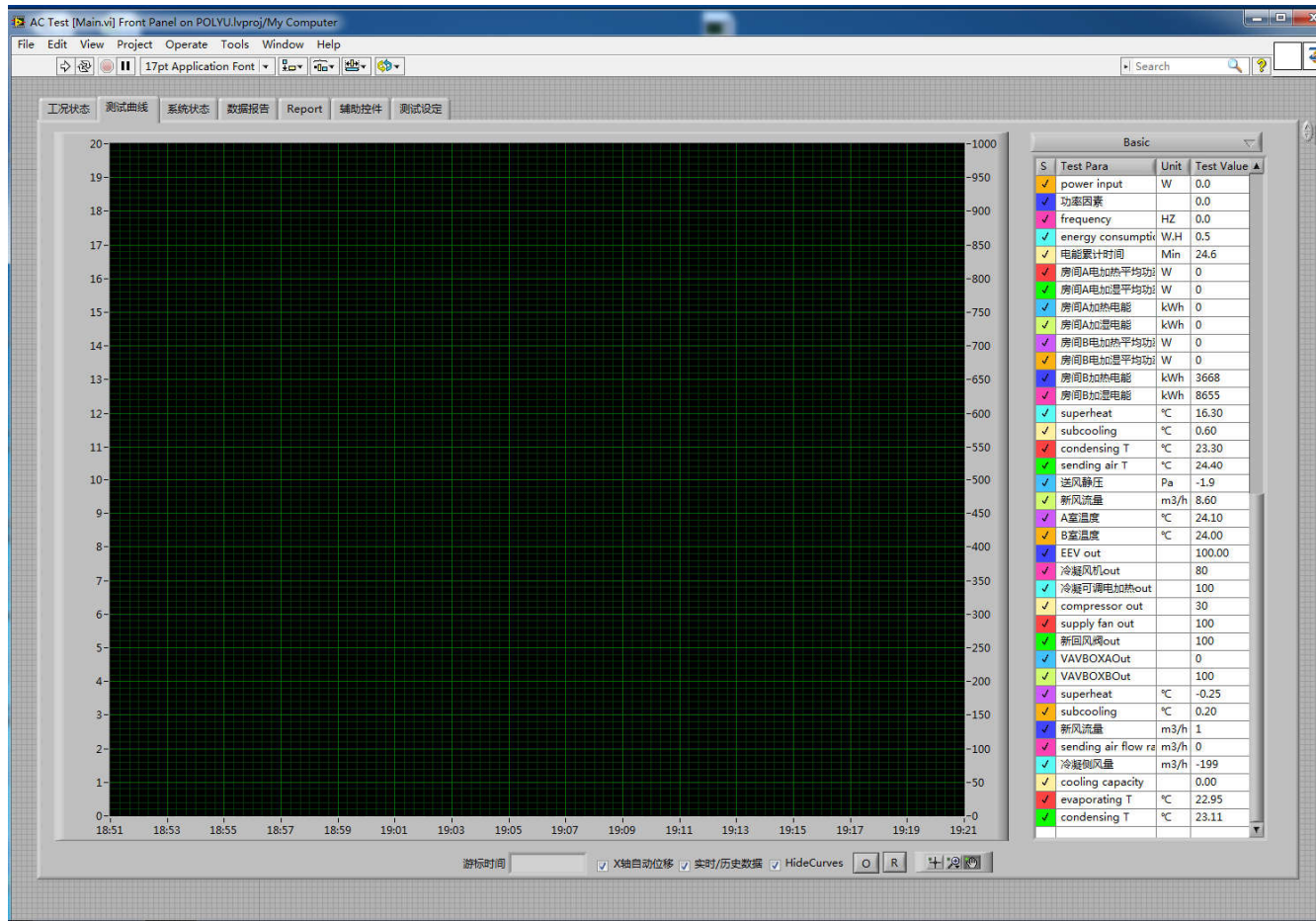


Photo 9 Logging & control supervisory program

## References

1. Andrade and Billiard 2002  
Andrade, M.A. and Billiard, C.  
Modulating blower and compressor capacities for efficient comfort control. *ASHRAE Transactions* Vol. 108, pp. 631-637 (2002)
2. Aprea et al. 2006  
Aprea, C., Mastrullo, R. and Renno, C.  
Experimental analysis of the scroll compressor performances varying its speed. *Applied Thermal Engineering* Vol. 26, pp. 983-992 (2006)
3. Aprea and Renno 2001  
Aprea, C. and Renno, C.  
Experimental analysis of a transfer function for an air cooled evaporator. *Applied Thermal Engineering* Vol. 21, pp. 481-493 (2001)
4. Aprea and Renno 2004  
Aprea, C. and Renno, C.  
An experimental analysis of a thermodynamic model of a vapour compression refrigeration plant on varying the compressor speed. *International Journal of Energy Research* Vol. 28, pp. 537-549 (2004)
5. Arens and Baughman 1996  
Arens, E.A. and Baughman, A.V.  
Indoor humidity and human health .2. Buildings and their systems. *ASHRAE Transactions* Vol. 102, pp. 212-221 (1996)
6. Armstrong and Liaw 2002  
Armstrong, S. and Liaw, J.  
The fundamentals of fungi. *ASHRAE Journal* Vol. 44, pp. 18 (2002)

7. ASHRAE 1987  
ASHRAE Standard  
Methods for Laboratory Airflow Measurement, *ASHRAE 41.2* (1987)
8. ASHRAE 2000  
ASHRAE  
Handbook-HVAC Systems and Equipment, (2000)
9. Balaras et al. 2007  
Balaras, C.A., Grossman, G., Henning, H.M., Ferreira, C.A.I., Podesser, E., Wang, L. and Wiemken, E.  
Solar air conditioning in Europe - an overview. *Renewable & Sustainable Energy Reviews* Vol. 11, pp. 299-314 (2007)
10. Bansal 2015  
Bansal, P.  
High efficiency novel window air conditioner. *Applied Energy* Vol. 156, pp. 311-320 (2015)
11. Baughman and Arens 1996  
Baughman, A.V. and Arens, E.A.  
Indoor humidity and human health .1. Literature review of health effects of humidity-influenced indoor pollutants. *ASHRAE Transactions* Vol. 102, pp. 193-211 (1996)
12. Bechtler et al. 2001  
Bechtler, H., Browne, M.W., Bansal, P.K. and Kecman, V.  
Neural networks - a new approach to model vapour-compression heat pumps. *International Journal of Energy Research* Vol. 25, pp. 591-599 (2001)
13. Beghi and Cecchinato 2009  
Beghi, A. and Cecchinato, L.  
A simulation environment for dry-expansion evaporators with application to

the design of autotuning control algorithms for electronic expansion valves. *International Journal Refrigeration* Vol. 32, pp. 1765-1775 (2009)

14. Beghi et al. 2011  
Beghi, A., Cecchinato, L. and Rampazzo, M.  
On-line, auto-tuning control of Electronic Expansion Valves. *International Journal Refrigeration* Vol. 34, pp. 1151-1161 (2011)
15. Bergles 1981  
Bergles, A.E., Collier, J., Delhaye, J.M., Hewitt, G. and Mayinger, F.  
Two-phase flow and heat transfer in the power and process industries. Hemisphere New York, (1981)
16. Berglund 1998  
Berglund, L.G.  
Comfort and humidity. *Ashrae Journal-American Society of Heating Refrigerating and Air-Conditioning Engineers* Vol. 40, pp. 35-41 (1998)
17. Bouzenada et al. 2016  
Bouzenada, S., McNevin, C., Harrison, S. and Kaabi, A.  
Performance of a liquid desiccant air-conditioner driven by evacuated-tube, flat-plate, or hybrid solar thermal arrays. *Energy and Buildings* Vol. 117, pp. 53-62 (2016)
18. Brodrick 2002  
Brodrick, J. and Gilbride, T.L.  
Focusing on Buyers' Needs: DOE's Emerging Technology Program. *Energy Engineering* Vol. 99, pp. 18-37 (2002)
19. Broersen et al. 1980  
Broersen, P.M.T. and Vanderjagt, M.F.G.  
Hunting of Evaporators Controlled by a Thermostatic Expansion Valve. *Journal of dynamic systems measurement and control transactions of the ASME* Vol. 102, pp. 130-135 (1980)



20. CABEE 2016  
CABEE  
Building energy consumption in China, China Association of Building Energy Efficiency (CABEE), 2016.
21. Chen 2005  
Chen, W.  
Modeling and control of a direct expansion (DX) variable-air-volume (VAV) air conditioning (A/C) system, *Building Service Engineering*. The Hong Kong Polytechnic University (2005)
22. Chen et al. 2002  
Chen, W., Chen, Z.J., Zhu, R.Q. and Wu, Y.Z.  
Experimental investigation of a minimum stable superheat control system of an evaporator. *International Journal of Refrigeration* Vol. 25, pp. 1137-1142 (2002)
23. Chen 2005  
Chen, W., Zhou, X.X. and Deng, S.M.  
Development of control method and dynamic model for multi-evaporator air conditioners (MEAC). *Energy Conversion and Management* Vol. 46, pp. 451-465 (2005)
24. Chen et al. 2008  
Chen, Y., Deng, S., Xu, X. and Chan, M.  
A study on the operational stability of a refrigeration system having a variable speed compressor. *International Journal of Refrigeration* Vol. 31, pp. 1368-1374 (2008)
25. Chen and Jiang 1990  
Chen, Z.J. and Jiang, W.Q.  
Stability analysis of refrigeration of evaporator and thermo expansion valve

- control loop. *Journal of Shanghai Jiaotong University* Vol. 24, pp. 58-66 (1990)
26. Chua et al. 2007  
Chua, K.J., Ho, J.C. and Chou, S.K.  
A comparative study of different control strategies for indoor air humidity. *Energy and Buildings* Vol. 39, pp. 537-545 (2007)
27. Dai et al. 2001  
Dai, Y.J., Wang, R.Z., Zhang, H.F. and Yu, J.D.  
Use of liquid desiccant cooling to improve the performance of vapor compression air conditioning. *Applied Thermal Engineering* Vol. 21, pp. 1185-1202 (2001)
28. Daninowa and Beliski 1962  
Daninowa, G. and Beliski, B.  
Experimental investigation of heat exchanger when R22 boiling. *Refrigeration Technology* Vol. 1, (1962)
29. De Bruijn et al. 1979  
De Bruijn, M., van der Jagt, M. and Machielsen, C.  
Simulation Experiments of a Compression Refrigeration System, *Proceedings IMACS Congress Simulation of Systems*, pp. 645-653 (1979)
30. De Dear et al. 1989  
De Dear, R., Knudsen, H. and Fanger, P.  
Impact of air humidity on thermal comfort during step-changes. *ASHRAE Transactions* Vol. 95, pp. 336-350 (1989)
31. Dhar 1978  
Dhar, M.  
Transient analysis of refrigeration system. Purdue University, Ann Arbor, pp. 350-350 p. (1978)



32. Dieckmann et al. 2008  
Dieckmann, J., Roth, K. and Brodrick, J.  
Liquid Desiccant Air Conditioners. *ASHRAE Journal* Vol. 50, pp. 90 (2008)
33. Domijan and Embriz-Santander 1993  
Domijan, A. and Embriz-Santander, E.  
Measurements of Electrical Power Inputs to Variable-Speed Motors and Their Solid-State Power Converters (RP-667). *ASHRAE Transactions* Vol. 99, pp. 241-241 (1993)
34. Eames et al.  
Eames, I.W., Milazzo, A. and Maidment, G.G.  
Modelling thermostatic expansion valves. *International Journal of Refrigeration* Vol. 38, pp. 189-197 (2014)
35. Elgendy 1993  
Elgendy, Y.A.M.  
Desiccant Wheel and Heat Pipes Dehumidification Technologies. *Innovative Energy & Environmental Applications*, pp. 523-527 (1993)
36. Elliott and Rasmussen 2010  
Elliott, M.S. and Rasmussen, B.P.  
On reducing evaporator superheat nonlinearity with control architecture. *International Journal of Refrigeration* Vol. 33, pp. 607-614 (2010)
37. Elliott et al. 2010  
Elliott, M.S., Shenoy, B. and Rasmussen, B.P.  
A Control Architecture Solution to Superheat Nonlinearity. *Proceedings of the American Control Conference*, pp. 5898-5903 (2010)
38. EMSD 2015  
EMSD  
Hong Kong Energy End-use Data in: Department, E.M.S. (Ed.) (2015)

39. Ertunc and Hosoz 2006  
Ertunc, H.M.and Hosoz, M.  
Artificial neural network analysis of a refrigeration system with an evaporative condenser. *Applied Thermal Engineering* Vol. 26, pp. 627-635 (2006)
40. Esen and Inalli 2009  
Esen, H.and Inalli, M.  
Modelling of a vertical ground coupled heat pump system by using artificial neural networks. *Expert Systems with Applications* Vol. 36, pp. 10229-10238 (2009)
41. Fallahsohi et al.  
Fallahsohi, H., Changenet, C., Place, S., Ligeret, C.and Lin-Shi, X.  
Predictive functional control of an expansion valve for minimizing the superheat of an evaporator. *International Journal of Refrigeration* Vol. 33, pp. 409-418 (2010)
42. Golub and Van Loan 2012  
Golub, G.H.and Van Loan, C.F.  
Matrix computations. JHU Press, (2012)
43. Grald and Macarthur 1992  
Grald, E.W.and Macarthur, J.W.  
A Moving-Boundary Formulation for Modeling Time-Dependent 2-Phase Flows. *International Journal of Heat and Fluid Flow* Vol. 13, pp. 266-272 (1992)
44. Green 1982  
Green, G.  
The positive and negative effects of building humidification. *ASHRAE Transactions* Vol. 88, (1982)
45. Gruhle and Isermann 1985  
Gruhle, W.D.and Isermann, R.

- Modeling and Control of a Refrigerant Evaporator. *Journal of Dynamic Systems Measurement and Control Transactions of the ASME* Vol. 107, pp. 235-240 (1985)
46. Harriman et al. 2001  
Harriman, L.G., Brundrett, G.W. and Kittler, R.  
Humidity control design guide for commercial and institutional buildings. (2001)
47. Harriman et al. 1999  
Harriman, L.G., Witte, M.J., Czachorski, M. and Kosar, D.R.  
Evaluating active desiccant systems for ventilating commercial buildings. *ASHRAE Journal* Vol. 41, pp. 28-37 (1999)
48. Hosoz and Ertunc 2006  
Hosoz, M. and Ertunc, H.M.  
Artificial neural network analysis of an automobile air conditioning system. *Energy Conversion and Management* Vol. 47, pp. 1574-1587 (2006)
49. Hourahan 2004  
Hourahan, G.C.  
How to properly size unitary equipment. *ASHRAE Journal* Vol. 46, pp. 15-18 (2004)
50. Huang et al. 2007  
Huang, D., He, Z.L. and Yuan, X.L.  
Dynamic characteristics of an air-to-water heat pump under frosting/defrosting conditions. *Applied Thermal Engineering* Vol. 27, pp. 1996-2002 (2007)
51. Huang et al. 2014  
Huang, D., Zhao, R.J., Gong, Q.Q. and Tang, X.Q.  
Effects of water mal-distribution on thermostatic-expansion-valve stability and its controlled two-circuit evaporator performance. *International Journal of Refrigeration* Vol. 48, pp. 38-47 (2014)

52. Huelle 1972  
Huelle, Z.  
MSS line - a new approach to hunting problem. *ASHRAE Journal* Vol. 14, pp. 43-46 (1972)
53. Huelle 1967  
Huelle, Z.R.  
Heat load influences upon evaporator parameters, *Proceedings of XII International Congress of Refrigeration Meeting*, Madrid, pp. 985-999 (1967)
54. Ibrahim 1998  
Ibrahim, G.A.  
Theoretical investigation into instability of a refrigeration system with an evaporator controlled by a thermostatic expansion valve. *Canadian Journal of Chemical Engineering* Vol. 76, pp. 722-727 (1998)
55. Ibrahim 2001  
Ibrahim, G.A.  
Effect of sudden changes in evaporator external parameters on a refrigeration system with an evaporator controlled by a thermostatic expansion valve. *International Journal of Refrigeration* Vol. 24, pp. 566-576 (2001)
56. Ilic et al. 2002  
Ilic, S., Hrnjak, P. and Bullard, C.  
Experimental comparison of continuous vs. pulsed flow modulation in vapor compression systems. *International Refrigeration and Air Conditioning Conference Paper* 541 (2002)
57. Islamoglu et al. 2005  
Islamoglu, Y., Kurt, A. and Parmaksizoglu, C.  
Performance prediction for non-adiabatic capillary tube suction line heat exchanger: an artificial neural network approach. *Energy Conversion and Management* Vol. 46, pp. 223-232 (2005)

58. ISO 2004  
ISO  
Non-ducted air conditioners and heat pumps-testing and rating for performance, *ISO 5151* (2004)
59. Jabobs 2002  
Jabobs P.C.  
Sizing single-package rooftop units for optimum performance. *HPAC Engineering*, Vol. 74, No. 8, pp. 57-60 (2002)
60. Jia et al. 1995  
Jia, X., Tso, C.P., Chia, P.K.and Jolly, P.  
A Distributed Model for Prediction of the Transient-Response of an Evaporator. *International Journal of Refrigeration* Vol. 18, pp. 336-342 (1995)
61. Jolly et al. 2000  
Jolly, P.G., Tso, C.P., Chia, P.K.and Wong, Y.W.  
Intelligent Control to Reduce Superheat Hunting and Optimize Evaporator Performance in Container Refrigeration. *HVAC&R Research* Vol. 6, pp. 243-255 (2000)
62. Karajgikar et al. 2005  
Karajgikar, S., Lakhkar, N., Agonafer, D.and Schmidt, R. I  
mpact of area contact between sensor bulb and evaporator return line on modular refrigeration unit: Computational and experimental. *Journal of Heat Transfer-Transactions of ASME* Vol. 127, pp. 95-100 (2005)
63. Kim et al. 2010  
Kim, M., Gerba, C.P.and Choi, C.Y.  
Assessment of physically-based and data-driven models to predict microbial water quality in open channels. *Journal of Environmental Sciences* Vol. 22, pp. 851-857 (2010)

64. Kenneth 1997  
Kenneth E. G.  
Rooftop HVAC. *HPAC Engineering*, Vol. 69, No. 7, pp. 51-55 (1997)
65. Kittler 1996  
Kittler, R.  
Mechanical dehumidification control strategies and psychrometrics. American Society of Heating, Refrigerating and Air-Conditioning Engineers, Inc., Atlanta, GA (United States) (1996)
66. Kosar 2006  
Kosar, D.  
Dehumidification system enhancements. *ASHRAE Journal* Vol. 48, pp. 48-58 (2006)
67. Krakow et al. 1995a  
Krakow, K.I., Lin, S. and Zeng, Z.S.  
Analytical determination of PID coefficients for temperature and humidity control during cooling and dehumidifying by compressor and evaporator fan speed variation. *ASHRAE Transactions* Vol. 101, pp. 343-354 (1995a)
68. Krakow et al. 1995b  
Krakow, K.I., Lin, S. and Zeng, Z.S.  
Temperature and humidity control during cooling and dehumidifying by compressor and evaporator fan speed variation. *ASHRAE Transactions* Vol. 101, pp. 292-304 (1995b)
69. Kulkarni et al. 2003  
Kulkarni, A., Agonafer, D. and Schmidt, R.  
Effect of the thermostatic expansion valve characteristics on the stability of a refrigeration system - Part II. *Advances in Electronic Packaging* 2003, Vol 2, pp. 613-619 (2003)

70. Kulkarni et al. 2002  
Kulkarni, A., Mulay, V., Agonafer, D. and Schmidt, R.  
Effect of the thermostatic expansion valve characteristics on the stability of a refrigeration system - Part I. *Itherm 2002: Eighth Intersociety Conference on Thermal and Thermomechanical Phenomena in Electronic Systems, Proceedings*, pp. 403-407 (2002)
71. Lakhkar et al. 2003  
Lakhkar, N., Karajgikar, S., Agonafer, D. and Schmidt, R.  
The impact of area contact between sensor bulb and evaporator return line in a modular refrigeration unit - part I, computational study. *Electronic and Photonic Packaging, Electrical Systems and Photonic Design and Nanotechnology - 2003*, pp. 651-656 (2003)
72. Lenger et al. 1998  
Lenger, M.J., Jacobi, A.M. and Hrojak, P.S.  
Superheat Stability of an Evaporator and Thermostatic Expansion Valve Air Conditioning and Refrigeration Center. College of Engineering. University of Illinois at Urbana-Champaign. (1998)
73. Li et al. 2009  
Li, H., Jeong, S.-K. and You, S.-S.  
Feedforward control of capacity and superheat for a variable speed refrigeration system. *Applied Thermal Engineering* Vol. 29, pp. 1067-1074 (2009)
74. Li et al. 2008  
Li, H., Jeong, S.K., Yoon, J.I. and You, S.S.  
An empirical model for independent control of variable speed refrigeration system. *Applied Thermal Engineering* Vol. 28, pp. 1918-1924 (2008)
75. Li et al. 2012a  
Li, N., Xia, L., Deng, S., Xu, X. and Chan, M.-Y.

- Dynamic modeling and control of a direct expansion air conditioning system using artificial neural network. *Applied Energy* Vol. 91, pp. 290-300 (2012a)
76. Li et al. 2012b  
Li, N., Xia, L., Deng, S., Xu, X. and Chan, M.-Y.  
Steady-state operating performance modelling and prediction for a direct expansion air conditioning system using artificial neural network. *Building Services Engineering Research and Technology* Vol. 33, pp. 281-292 (2012b)
77. Li et al. 2013  
Li, N., Xia, L., Deng, S.M., Xu, X.G. and Chan, M.Y.  
On-line adaptive control of a direct expansion air conditioning system using artificial neural network. *Applied Thermal Engineering* Vol. 53, pp. 96-107 (2013)
78. Li et al. 2004  
Li, X.Q., Chen, J.P., Chen, Z.J., Liu, W.H., Hu, W. and Liu, X.B.  
A new method for controlling refrigerant flow in automobile air conditioning. *Applied Thermal Engineering* Vol. 24, pp. 1073-1085 (2004)
79. Li and Deng 2007a  
Li, Z. and Deng, S.M.  
A DDC-based capacity controller of a direct expansion (DX) air conditioning (A/C) unit for simultaneous indoor air temperature and humidity control - Part I: Control algorithms and preliminary controllability tests. *International Journal of Refrigeration* Vol. 30, pp. 113-123 (2007a)
80. Li and Deng 2007b  
Li, Z. and Deng, S.M.  
A DDC-based capacity controller of a direct expansion (DX) air conditioning (A/C) unit for simultaneous indoor air temperature and humidity control - Part II: Further development of the controller to improve control sensitivity. *International Journal of Refrigeration* Vol. 30, pp. 124-133 (2007b)



81. Li and Deng 2007c  
Li, Z. and Deng, S.M.  
An experimental study on the inherent operational characteristics of a direct expansion (DX) air conditioning (A/C) unit. *Building and Environment* Vol. 42, pp. 1-10 (2007c)
82. Li et al. 2014  
Li, Z., Xu, X., Deng, S. and Pan, D.  
Further study on the inherent operating characteristics of a variable speed direct expansion air conditioning system. *Applied Thermal Engineering* Vol. 66, pp. 206-215 (2014)
83. Li et al. 2015a  
Li, Z., Xu, X., Deng, S. and Pan, D.  
A novel proportional-derivative (PD) law based fuzzy logic principles assisted controller for simultaneously controlling indoor temperature and humidity using a direct expansion (DX) air conditioning (A/C) system. *International Journal of Refrigeration* Vol. 57, pp. 239-256 (2015a)
84. Li et al. 2015b  
Li, Z., Xu, X.G., Deng, S.M. and Pan, D.M.  
A novel neural network aided fuzzy logic controller for a variable speed (VS) direct expansion (DX) air conditioning (A/C) system. *Applied Thermal Engineering* Vol. 78, pp. 9-23 (2015b)
85. Liang et al. 2011  
Liang, N., Shao, S.Q., Tian, C.Q. and Yan, Y.Y.  
Two-phase flow instabilities in horizontal straight tube evaporator. *Applied Thermal Engineering* Vol. 31, pp. 181-187 (2011)
86. Liang et al. 2010  
Liang, N., Shao, S.Q., Xu, H.B. and Tian, C.Q.  
Instability of refrigeration system - A review. *Energy Conversion and Management* Vol. 51, pp. 2169-2178 (2010)

87. Lienhard 2013  
Lienhard, J.H.  
A heat transfer textbook. Courier Corporation, (2013)
88. Liang et al. 2010  
Ling, J.Z., Hwang, Y. and Radermacher, R.  
Theoretical study on separate sensible and latent cooling air-conditioning system. *International Journal of Refrigeration* Vol. 33, pp. 510-520 (2010)
89. Looney 1997  
Looney, C.G.  
Pattern recognition using neural networks: theory and algorithms for engineers and scientists. Oxford University Press, Inc., (1997)
90. Maia et al. 2014  
Maia, A.A.T., Horta-Gutierrez, J.C., Koury, R.N.N. and Machado, L.  
Superheating control using an adaptive PID controller. *HVAC&R Research* Vol. 20, pp. 424-434 (2014)
91. Maia et al. 2013  
Maia, A.A.T., Koury, R.N.N. and Machado, L.  
Development of a control algorithm employing data generated by a white box mathematical model. *Applied Thermal Engineering* Vol. 54, pp. 120-130 (2013)
92. Miro 2005  
Miro, C.  
ASHRAE issues guidance on minimizing mold, mildew. *ASHRAE Journal* Vol. 47, pp. 86-86 (2005)
93. Mithraratne and Wijesundera 2001  
Mithraratne, P. and Wijesundera, N.E.  
An experimental and numerical study of the dynamic behaviour of a counter-

- flow evaporator. *International Journal of Refrigeration* Vol. 24, pp. 554-565 (2001)
94. Mithraratne and Wijesundera 2002  
Mithraratne, P. and Wijesundera, N.E.  
An experimental and numerical study of hunting in thermostatic-expansion-valve-controlled evaporators. *International Journal of Refrigeration* Vol. 25, pp. 992-998 (2002)
95. Mithraratne et al. 2000  
Mithraratne, P., Wijesundera, N.E. and Bong, T.Y.  
Dynamic simulation of a thermostatically controlled counter-flow evaporator. *International Journal of Refrigeration* Vol. 23, pp. 174-189 (2000)
96. Mulay et al. 2005  
Mulay, V., Kulkarni, A. and Agonafer, D.  
Effect of the location and the properties of thermostatic expansion valve sensor bulb on the stability of a refrigeration system. *Journal of Heat Transfer-Transactions of ASME* Vol. 127, pp. 85-94 (2005)
97. Nagaya et al. 2006  
Nagaya, K., Senbongi, T., Li, Y., Zheng, J. and Murakami, I.  
High energy efficiency desiccant assisted automobile air-conditioner and its temperature and humidity control system. *Applied Thermal Engineering* Vol. 26, pp. 1545-1551 (2006)
98. Otten 2010  
Otten, R.J.  
Superheat control for air conditioning and refrigeration systems: Simulation and experiments, *Mechanical Sci & Engineering*. University of Illinois at Urbana-Champaign (2010)
99. Outtagarts et al. 1997  
Outtagarts, A., Haberschill, P. and Lallemand, M.

The transient response of an evaporator fed through an electronic expansion valve. *International Journal of Energy Research* Vol. 21, pp. 793-807 (1997)

100. Poort and Bullard 2006  
Poort, M.J.and Bullard, C.W.  
Applications and control of air conditioning systems using rapid cycling to modulate capacity. *International Journal of Refrigeration* Vol. 29, pp. 683-691 (2006)
101. Qi and Deng 2008  
Qi, Q.and Deng, S.  
Multivariable control-oriented modeling of a direct expansion (DX) air conditioning (A/C) system. *International Journal of Refrigeration* Vol. 31, pp. 841-849 (2008)
102. Qi and Deng 2009  
Qi, Q.and Deng, S.  
Multivariable control of indoor air temperature and humidity in a direct expansion (DX) air conditioning (A/C) system. *Building and Environment* Vol. 44, pp. 1659-1667 (2009)
103. Qi et al. 2010  
Qi, Q., Deng, S., Xu, X.and Chan, M.Y.  
Improving degree of superheat control in a direct expansion (DX) air conditioning (A/C) system. *International Journal of Refrigeration* Vol. 33, pp. 125-134 (2010)
104. Qureshi and Tassou 1996  
Qureshi, T.Q.and Tassou, S.A.  
Variable-speed capacity control in refrigeration systems. *Applied Thermal Engineering* Vol. 16, pp. 103-113 (1996)
105. Scalabrin and Bianco 1994  
Scalabrin, G.and Bianco, G.

- Experimental Thermodynamic Analysis of a Variable-Speed Open Reciprocating Refrigeration Compressor. *International Journal of Refrigeration* Vol. 17, pp. 68-75 (1994)
106. Schoen 1990  
Schoen, A.  
Resolving TEV hunting problems. *Heating, Piping and Air Conditioning* Vol. 62, pp. 69-72 (1990)
107. Shang et al. 2015  
Shang, Y.J., Wu, A.G. and Fang, X.  
A study on the modeling of the minimal stable superheat for a variable speed refrigeration system. *International Journal of Refrigeration* Vol. 59, pp. 182-189 (2015)
108. Shang et al. 2016  
Shang, Y.J., Wu, A.G., Fang, X. and You, Y.W.  
Dynamic simulation of electronic expansion valve controlled refrigeration system under different heat transfer conditions. *International Journal of Refrigeration* Vol. 72, pp. 41-52 (2016)
109. Shaw and Luxton 1988  
Shaw, A. and Luxton, R.  
A comprehensive method of improving part load air conditioning performance. *ASHRAE Transactions* Vol. 94, pp. 442-457 (1988)
110. Shirey and Henderson 2004  
Shirey III, D.B. and Henderson Jr, H.I.  
Dehumidification at Part Load. *ASHRAE Journal* Vol. 46, pp. 42 (2004)
111. Silver et al. 1990  
Silver, S., Fine, P. and Rose, F.  
Performance monitoring of DX rooftop cooling equipment. *Energy engineering* Vol. 87, pp. 32-41 (1990)

112. Singhal and Salsbury 2007  
Singhal, A. and Salsbury, T.I.  
Characterization and Cancellation of Static Nonlinearity in HVAC Systems.  
*ASHRAE Transactions* Vol. 113, (2007)
113. Sozen et al. 2003  
Sozen, A., Arcaklioglu, E. and Ozalp, M.  
A new approach to thermodynamic analysis of ejector-absorption cycle:  
artificial neural networks. *Applied Thermal Engineering* Vol. 23, pp. 937-952  
(2003)
114. Steiner and Taborek 1992  
Steiner, D. and Taborek, J.  
Flow Boiling Heat-Transfer in Vertical Tubes Correlated by an Asymptotic  
Model. *Heat Transfer Engineering* Vol. 13, pp. 43-69 (1992)
115. Sterling et al. 1985  
Sterling, E., Arundel, A. and Sterling, T.  
Criteria for human exposure to humidity in occupied buildings. *ASHRAE  
Transactions* Vol. 91, pp. 611-622 (1985)
116. Stoecker 1966  
Stoecker, W.F.  
Stability of an Evaporator-Expansion Valve Control Loop *ASHRAE  
Transactions* Vol. 72, pp. IV.3.1-IV.3.8. (1966)
117. Tahat et al. 2001  
Tahat, M.A., Ibrahim, G.A. and Probert, S.D.  
Performance instability of a refrigerator with its evaporator controlled by a  
thermostatic expansion-valve. *Applied Energy* Vol. 70, pp. 233-249 (2001)
118. Tanabe and Kimura 1994  
Tanabe, S. and Kimura, K.

Effects of air temperature, humidity, and air movement on thermal comfort under hot and humid conditions. American Society of Heating, Refrigerating and Air-Conditioning Engineers, Inc., Atlanta, GA (United States) (1994)

119. Tassou and Al-Nizari 1993a  
Tassou, S.A. and Al-Nizari, H.O.  
Effect of refrigerant flow control on the thermodynamic performances of reciprocating chillers. *Applied Energy* Vol. 45, pp. 101-116 (1993a)
120. Tassou and Al-Nizari 1993b  
Tassou, S.A. and Al-Nizari, H.O.  
Investigation of the effects of thermostatic and electronic expansion valves on the steady-state and transient performance of commercial chillers. *International Journal of Refrigeration* Vol. 16, pp. 49-56 (1993b)
121. Tian et al. 2005a  
Tian, C.Q., Dou, C.P., Yang, X.J. and Li, X.T.  
Instability of automotive air conditioning system with a variable displacement compressor. Part 1. Experimental investigation. *International Journal of Refrigeration* Vol. 28, pp. 1102-1110 (2005a)
122. Tian et al. 2005b  
Tian, C.Q., Dou, C.P., Yang, X.J. and Li, X.T.  
Instability of automotive air conditioning system with a variable displacement compressor. Part 2. Numerical simulation. *International Journal of Refrigeration* Vol. 28, pp. 1111-1123 (2005b)
123. Tian and Li 2005  
Tian, C.Q. and Li, X.T.  
Transient behavior evaluation of an automotive air conditioning system with a variable displacement compressor. *Applied Thermal Engineering* Vol. 25, pp. 1922-1948 (2005)

124. Tso et al. 2001  
Tso, C.P., Wong, Y.W., Jolly, P.G. and Ng, S.M.  
A comparison of hot-gas by-pass and suction modulation method for partial load control in refrigerated shipping containers. *International Journal of Refrigeration* Vol. 24, pp. 544-553 (2001)
125. USDOE 2012  
USDOE  
Annual energy review 2011, in: Energy, D.O. (Ed.) (2012)
126. Vargas and Parise 1995  
Vargas, J.V.C. and Parise, J.A.R.  
Simulation in Transient Regime of a Heat-Pump with Closed-Loop and on Off Control. *International Journal of Refrigeration* Vol. 18, pp. 235-243 (1995)
127. Visioli 2006  
Visioli,  
A. Practical PID control. Springer Science & Business Media, (2006)
128. Wedekind 1971  
Wedekind, G.  
An experimental investigation into the oscillatory motion of the mixture-vapor transition point in horizontal evaporating flow. *Journal of Heat Transfer* Vol. 93, pp. 47-54 (1971)
129. Wedekind 1965  
Wedekind, G.L.  
Transient Response of the Mixture-vapor Transition Point in Two-phase Horizontal Evaporating Flow. University of Illinois at Urbana-Champaign, (1965)
130. Wedekind and Beck 1974  
Wedekind, G.L. and Beck, B.T.  
Theoretical Model of the Mixture-Vapor Transition Point Oscillations



Associated With Two-Phase Evaporating Flow Instabilities. *Journal of Heat Transfer* Vol. 96, pp. 138-144 (1974)

131. Wedekind and Stoecker 1968  
Wedekind, G.L. and Stoecker, W.F.  
Theoretical Model for Predicting the Transient Response of the Mixture-Vapor Transition Point in Horizontal Evaporating Flow. *Journal of Heat Transfer* Vol. 90, pp. 165-174 (1968)
132. Xie et al. 2007  
Xie, G.N., Wang, Q.W., Zeng, M. and Luo, L.Q.  
Heat transfer analysis for shell-and-tube heat exchangers with experimental data by artificial neural networks approach. *Applied Thermal Engineering* Vol. 27, pp. 1096-1104 (2007)
133. Xu et al. 2008  
Xu, X.G., Deng, S.M. and Chan, M.Y.  
A new control algorithm for direct expansion air conditioning systems for improved indoor humidity control and energy efficiency. *Energy Conversion and Management* Vol. 49, pp. 578-586 (2008)
134. Xu et al. 2010  
Xu, X.G., Xia, L.A., Chan, M.Y. and Deng, S.M.  
Inherent correlation between the total output cooling capacity and equipment sensible heat ratio of a direct expansion air conditioning system under variable-speed operation *Applied Thermal Engineering* Vol. 30, pp. 1601-1607 (2010)
135. Yamamoto et al. 1982  
Yamamoto, T., Hibi, H. and Kuroda, T.  
Development of an energy-saving-oriented variable capacity system heat pump. *ASHRAE Transactions* Vol. 88, (1982)
136. Yang and Lee 1991  
Yang, K.H. and Lee, M.L.

Analysis of an Inverter-Driven Air-Conditioning System and Its Application in a Hot and Humid Area. *International Journal of Energy Research* Vol. 15, pp. 357-365 (1991)

137. Yang et al. 2011a  
Yang, Z.Y., Andersen, C. and Izadi-Zamanabadi, R.  
On-line Auto-Tuning of PI Control of the Superheat for a Supermarket Refrigeration System. *IEEE International Conference on Control Applications*, pp. 792-797 (2011a)
138. Yang et al. 2011b  
Yang, Z.Y., Sun, Z. and Andersen, C.  
Nonlinear FOPDT Model Identification for the Superheat Dynamic in a Refrigeration System. *37th Annual Conference of the IEEE Industrial Electronics Society*, (2011b)
139. Yao and Chen 2010  
Yao, Y. and Chen, J.  
Global optimization of a central air-conditioning system using decomposition-coordination method. *Energy and Buildings* Vol. 42, pp. 570-583 (2010)
140. Yaqub and Zubair 1996  
Yaqub, M. and Zubair, S.M.  
Thermodynamic analysis of capacity-control schemes for refrigeration and air-conditioning systems. *Energy* Vol. 21, pp. 463-472 (1996)
141. Yaqub and Zubair 2001  
Yaqub, M. and Zubair, S.M.  
Capacity control for refrigeration and air-conditioning systems: A comparative study. *Journal of Energy Resources Technology -ASME* Vol. 123, pp. 92-99 (2001)
142. Yaqub et al. 1995  
Yaqub, M., Zubair, S.M. and Khan, S.H.

- 2nd-Law-Based Thermodynamic Analysis of Hot-Gas, Bypass, Capacity-Control Schemes for Refrigeration and Air-Conditioning Systems. *Energy* Vol. 20, pp. 483-493 (1995)
143. Yasuda et al. 1983  
Yasuda, H., Toubert, S. and Machielsen, C.  
Simulation-Model of a Vapor Compression Refrigeration System. *ASHRAE Journal* Vol. 39, pp. 408-425 (1983)
144. Yau 2007  
Yau, Y.H.  
Application of a heat pipe heat exchanger to dehumidification enhancement in a HVAC system for tropical climates - a baseline performance characteristics study. *International Journal of Thermal Science* Vol. 46, pp. 164-171 (2007)
145. Yuan and Riffat 2010  
Yuan, Y.J. and Riffat, S.  
A Mini Thermal Liquid Desiccant Air Conditioner for Residential Application. *Proceedings of the First International Conference on Sustainable Urbanization (Icsu 2010)*, pp. 782-787 (2010)
146. Zahn 1964  
Zahn, W.R.  
A Visual Study of Two-Phase Flow While Evaporating in Horizontal Tubes. *Journal of Heat Transfer* Vol. 86, pp. 417-429 (1964)
147. Zhang 2002  
Zhang, G.Q.  
China HVACR Annual Business Volume II. Chinese Construction Industry Press, (2002)